NASA Technical Memorandum 110351

Investigation of Wing Upper Surface Flow-Field Disturbance Due to NASA DC-8-72 In-flight Inboard Thrust-Reverser Deployment

Hedayat U. Hamid, Richard J. Margason, and Gordon Hardy

June 1995

National Aeronautics and Space Administration

NASA Technical Memorandum 110351

Investigation of Wing Upper Surface Flow-Field Disturbance Due to NASA DC-8-72 In-flight Inboard Thrust-Reverser Deployment

Hedayat U. Hamid, Richard J. Margason, and Gordon Hardy
Ames Research Center, Moffett Field, California

June 1995

National Aeronautics and
Space Administration

Ames Research Center
Moffett Field, California 94035-1000

Contents

Nomenclature

d	diameter, ft
M	Mach number
N_F	engine fan rpm in percent of rated rpm
N_R	engine rated rpm
R	air gas constant, Joules/(Kilogram*Kelvin)
t	time, sec
T	static temperature, deg Celsius
T_o	total temperature, deg Celsius
V_∞	free-stream velocity
V_j	exhaust-jet velocity
V_{RT}	thrust-reverser exit velocity
w	vertical speed, ft/min
z	altitude, ft
ϕ	roll angle, deg
γ	air specific heat ratio
η	wing semispan station, percent
θ	pitch angle, deg

Abbreviations

AIA	Aerospace Industry Association
DADS	Data Acquisition Distribution System
FAA	Federal Aviation Administration
FADEC	Full Authority Digital Electronic Control
rpm	Revolutions Per Minute
STOVL	Short Take-Off and Vertical Landing

Investigation of Wing Upper Surface Flow-Field Disturbance Due to NASA DC-8-72 In-flight Inboard Thrust-Reverser Deployment

HEDAYAT U. HAMID, RICHARD J. MARGASON, AND GORDON HARDY

Ames Research Center

Summary

An investigation of the wing upper surface flow-field disturbance due to in-flight inboard thrust reverser deployment on the NASA DC-8-72, which was conducted cooperatively by NASA Ames, the Federal Aviation Administration (FAA), McDonnell Douglas, and the Aerospace Industry Association (AIA), is outlined and discussed in detail. The purpose of this flight test was to obtain tufted flow visualization data which demonstrates the effect of thrust reverser deployment on the wing upper surface flow field to determine if the disturbed flow regions could be modeled by computational methods. A total of six symmetric thrust reversals of the two inboard engines were performed to monitor tuft and flow cone patterns as well as the character of their movement at the nominal Mach numbers of 0.55, 0.70, and 0.85. The tufts and flow cones were photographed and video-taped to determine the type of flow field that occurs with and without the thrust reversers deployed. In addition, the normal NASA DC-8 onboard Data Acquisition Distribution System (DADS) was used to synchronize the cameras.

Results of this flight test will be presented in two parts. First, three distinct flow patterns associated with the above Mach numbers were sketched from the motion videos and discussed in detail. Second, other relevant aircraft parameters, such as aircraft's angular orientation, altitude, vertical descent, and Mach number, are discussed. The flight test participants' comments were recorded on the videos and the interested reader is referred to the video supplement section of this report for that information.

Introduction

The development and use of engine thrust reversers have become widely accepted on military and civilian aircraft. Thrust reversers are mechanical devices which primarily decelerate the aircraft during flight (DC-8-72 and C-5B are the only aircraft certified for in-flight thrust-reverser deployment) or augment their braking system after landing. Independent from wheel brakes, thrust reversers have the ability to significantly reduce stopping distances and increase safety levels on wet or icy runways when wheel braking is less effective. A significant additional benefit for military aircraft is the resulting decreased ground roll which will allow operations from airfields with reduced runway lengths. A thrust reverser also increases safety during an aborted takeoff. Minimizing operating costs of transport aircraft has also been a major concern in the airline industry. One possible saving may be achieved by the implementation and the usage of thrust reversers during landing rollout. The use of thrust reversers can minimize operating costs by reducing wear on the aircraft brakes and tires.

The most commonly used thrust reverser design solutions are shown in figures 1 and 2 (figure obtained from Rohr interdepartment memorandum dated June 1992). The target- or clamshell-type thrust reverser, figure 1, is used mainly on low bypass ratio engines. On low bypass ratio engines, fan mass flow makes up a smaller portion of the total flow and both core and fan flow must be diverted to produce significant reverse thrust. With this design two buckets are deployed into the exhaust jet to produce reverse thrust.

The second commonly used design is the integrated- or cascade-type reverser, figure 2. It incorporates mechanical blocker doors with turning vanes or deflectors to redirect the fan flow radially outward in a desired direction. High bypass ratio power plants use cascade reversers effectively. Since fan mass flow can be as much as seven times the core flow, only the air passing through the fan need to be turned to achieve braking (ref. 1). In addition to large braking effects, thrust reverser deflectors on high bypass ratio power plants are also designed such that they meet two more conditions: (1) minimize thrust reverser exhaust interference with the fuselage on landing roll out; and (2) reduce the interference on the pylon and wing. Figure 3 schematically shows a cutaway rear view of the thrust reverser deflector configuration for the NASA DC-8 SNECMA-GE CFM-56 high bypass ratio turbofan for engines 2 and 3 (figure obtained from CFM-56 Service Bulletin 78-033, dated August 30, 1982). This figure shows where and how the thrust reverser deflectors are configured on engines 2 and 3. Those deflectors which are

situated near the top half of engines are turned in various directions so that most of the thrust reverser exhaust goes over the wing. This achieves large deceleration after landing and, at the same time, the exhaust efflux does not impinge on the fuselage, wing, and the pylon. In some instances, the deflectors which are situated near the lower half of engines and those directly across from the fuselage are simply blocked off to improve vehicle ride quality (passenger comfort) and to reduce excessive noise.

Thrust reversers have proven to be very effective in stopping aircraft on landing. However, a large percentage of aircraft types equipped with thrust reversers have had several incidents of unplanned reverser deployments. Of these, at least one in-flight reverser deployment incident has been implicated as a possible cause of an accident. In May of 1991, an accident involving the Lauda Airlines Boeing 767, was suspected to have been caused in part by the inadvertent in-flight deployment of a thrust reverser. Climbing at a Mach number of 0.78–0.80 and just moments before establishing its cruise configuration, the airplane departed from its normal flightpath and crashed. The crash took place on a remote jungle hillside northwest of Bangkok. The tail had separated from the aircraft and both engines were found within a comparatively short distance from one another. The flight was en route from Hong Kong to Vienna, via Bangkok when the incident occurred.

Subsequent investigation showed that the thrust reverser on one of the engines had apparently unlatched and deployed causing a loss of lift on the affected wing and inducing a rolling motion. A reading of the Full Authority Digital Electronic Control (FADEC) memory from one engine by Pratt and Whitney indicated that there may have been a maintenance problem associated with the thrust reverser. The FADEC is a doubly redundant system that electronically controls the operation of the engines from the flight deck. The system also monitors and records engine parameters, such as speed, temperatures, pressures and the status of engine components (ref. 2).

The Lauda Airlines accident prompted the Federal Aviation Administration (FAA) and Aerospace Industry Association (AIA) to form a Thrust Reverser Task Force to evaluate inadvertent thrust reverser deployments. One part of this task force involved a Controllability Team to evaluate methods for avoiding adverse thrust reverser deployment effects on the aircraft controllability. As part of this activity NASA, in cooperation with the FAA, McDonnell Douglas, and the AIA, planned and conducted an in-flight thrust reverser deployment test flight on a NASA DC-8-72. The DC-8-72 was selected for the investigation because the inboard thrust reversers are certified for in-flight deployment at speeds above 190 knots. This aircraft, stationed at Ames Research Center in Moffett Field, California, has been at NASA since August 1987. This airplane, which is extensively modified as a flying laboratory, is mainly used as an instrumentation platform for research activities that range from atmospheric and space sciences applications, climatology, Earth resources, and aeronautics. The purpose of the present flight test was to obtain flow visualization data to document the effect of thrust reverser deployment on the wing upper surface flow field in order to determine if the disturbed flow regions could be modeled by computational methods. Data was gathered photographically using tufts and cones to determine the direction and character of the local flow on the wing upper surface with and without thrust reversers deployed. In addition, other relevant aircraft parameters, such as aircraft's angular orientation, altitude, vertical descent, and Mach number, were recorded using the normal NASA DC-8 onboard Data Acquisition Distribution System (DADS).

Aircraft Description

The DC-8 is a four-engine aircraft with wing mounted nacelles which was designed and developed during the mid 1950s. When Douglas decided on June 7, 1955, to proceed with construction of the DC-8, they announced that all projected versions would have the same standardized airframe and overall dimensions. The first five versions of the DC-8 (Series 10, 20, 30, 40, and 50) have identical airframes, with common electrical, hydraulic, control, and air-conditioning system. The Super Sixty (Series 60) versions of DC-8 were, however, a departure from the standardized airframe and overall dimensions policy.

The Super 62 is an ultra-long range version which has an extended wing span and a fuselage 6 ft 8 in. longer than that of the standard DC-8. A 3 ft 4 in. cabin section is inserted both fore and aft of the wing, giving accommodation for up to 189 passengers. Each wing tip is fitted with a 3 ft extension which significantly reduces drag under cruise conditions and increases fuel capacity. Engine pods of a new design augment thrust and reduce drag by ducting by-pass air through the entire length of each nacelle.

A final 70 Series of DC-8 four-turbofan transports were announced by Douglas in the Spring of 1979. The DC-8-72 series is a re-engined Series 62 aircraft. The original JT3D-3B/7 engines were replaced by the new high bypass ratio turbofan (maximum thrust = 22,000 lb each and bypass ratio of 6:1), CFM International, SNECMA-GE CFM-56 engines (ref. 3).

The NASA DC-8-72 (fig. 4) used in the present experiment is capable of a maximum take-off weight of 330,000 lb (ref. 4). Since the runway load bearing capacity limits all flight out of NASA Ames to a maximum take-off weight of 270,000 lb, the aircraft was flown at this reduced weight.

As discussed earlier in the text, the primary experimental data for the flight test used tufts and cones situated spanwise to capture the type of flow field over the left wing. Rows of double-tufts as well as flow cones were installed on the wing upper surface. A black tape was laid along the inboard engine center line on the wing to visually identify its location on the video. The flow cones are hollow, about 2.5 in. long and a maximum diameter of 0.35 in. The tips of the flow cones are tethered using a nylon string, which in turn is taped onto the wing surface. As can be seen from figure 5, there were a total of 17 rows of tuft/cone combination along the span of the left wing. Since the thrust reversals were performed on the inboard engines, 9 of the 17 rows of tufts were in the proximity of the number 2 engine to acquire detailed effects of thrust reversers on the wing flow field. The distance between the rows within this vicinity was about 24 in., and this distance increased with increasing distance from the center line of the inboard engine to the tip of the wing.

The tufts and flow cones, as described above, were photographed and visually evaluated to determine the character of the flow with thrust reversers deployed. Photography consisted of one cockpit camera to record the instrumentation panel, a high speed black and white camera to record the overall tuft movement at about 500 frames per second, two color cameras to record tuft patterns near the leading and the trailing edges of the left wing, and a 35 mm still camera. In addition, the normal NASA DC-8 onboard DADS was turned on for the duration of the flight to synchronize all cameras. DADS is a central computer system on the NASA DC-8 that gathers input from both Standard Aircraft and Research Support Systems. DADS then processes the raw input into engineering units, records, displays the data, and distributes it to individual experimenters.

Flight Profile

Prior to the flight all of the participants attended a safety and flight plan discussion. The test periods were chosen so that the weather at the test altitudes was clear and that the air was smooth. The flight included six symmetric thrust reversals at a target altitude of 28,000 ft. The first deployment was at the center of the Mach range at 0.70, three deployments were at Mach 0.85, and two deployments were at Mach 0.55. The flight test at Mach number of 0.55 was repeated because the high speed video of the earlier run had been accidentally erased. The flight test at Mach number of 0.85 was repeated twice to, first, capture the shock position and its movement on the videos and, second, to see if there was any correlation between the engine power level and the movement of the wing shock waves.

The procedure used for each test point involved three distinct phases. They are:

1. The pre-deployment phase. This phase of the experiment comprised two different periods and they are:

    a. The steady state period. The procedure utilized for this period was to cruise with normal forward thrust and with no angular variations at an altitude just above the desired altitude of 28,000 ft and slightly above the desired Mach number.

    b. The preparation period. Maximum continuous power was steadily added on the outboard engines during the preparation period. The numbers 2 and 3 engines were then throttled back to the idle position to permit reverser deployment on the inboard engines. To maintain the desired Mach number a gentle descent was initiated just prior to the inboard engine reversals.

2. The reverse thrust phase. Once the thrust reversers were deployed, the inboard engines were placed at the maximum reverse power lever stop for the duration of reverse thrust flight. As in the preparation period of the pre-deployment phase, maximum continuous power was steadily added on the outboard engines to minimize loss of airspeed of the aircraft during the reverse thrust phase. Near the end of each run, the inboard engines were returned to the idle position to enable stowing the thrust reverser system.

3. The post-deployment phase. Normal flight was resumed at the end of each run with forward thrust on all four engines and with possible angular motion. Changes in the pitch and roll angles were required to bring the aircraft back to its prescribed flight envelope in preparation for the next run.

The first test point, Mach number of 0.70, was initiated at Mach number of 0.74 and required only a small pitch down and descent rate. The buffet at this condition was light to moderate. The entry for the test point at Mach 0.85 was initiated with a gentle descent with maximum continuous power on all four engines to Mach 0.88 before bringing numbers 2 and 3 engines to the idle position and starting the reverse procedure. The buffet at this

condition was slightly higher than Mach 0.70 and about 10 deg of pitch down was required to hold the aircraft at a Mach number of 0.85. The entry to the last test point was made at a Mach number of 0.57. Only a small descent was required to hold the target Mach number of 0.55 just before the inboard engine reversals. The buffet was fairly heavy with large low frequency content. For all three Mach numbers, only small lateral control inputs were required during the maneuvers except when the reverser initially deployed. It was found that deployment tended to cause a momentary roll transient due to slight differences in reverser deployment timing between engines 2 and 3. Fan speed, N_F, for all test points on engines 2 and 3 at the reverse thrust position were about 72 to 74 percent of rated Revolutions Per Minute (rpm), N_R. Graphical representations of the test procedure involving fan rpm (fan speed) for all Mach cases can be found in figures 6–8. Note that fan rpm, N_F, is being plotted as function of the three phases of the experiment described above.

Table 1 below summarizes the Mach number variations of the aircraft during the reverse thrust phase at t = 0 (onset of reverse thrust flight), t = 15 sec (an intermediate point), and at t_{max} (termination point) for each of the six runs.

The day ended with a post flight debrief. The aircraft was thoroughly inspected for any external damages, such as cracks or fuel leaks. Minor fuel leaks in the number 3 engine pylon area and minor damage on the reverser blocker doors on the same engine were found.

Results and Discussion

Tuft and Flow Cone Visualization and Analysis

Figures 10–16 have been prepared from the videos and illustrate regions of the flow field on the upper surface of the left wing affected by reverse thrust flight (figs. 10–13) and forward thrust flight (figs. 14–16). As can be seen on the video supplement, three distinct flow types on the wing were associated for reverse thrust flight and for forward thrust flight. They are:

1. Fully attached flow. In this pattern, there were negligible changes in directions of motion of the tufts and flow cones from those expected in a typical cruise condition. The tuft/cone combination situated further away from the inboard engine was not disturbed by the presence of reverse thrust, hence characterizes attached flow. Figure 17, which is a still photograph taken just prior to the inboard engine thrust reversals, shows the tufts and flow cones aligned in the local flow direction on the left wing upper surface and thereby indicates fully attached flow.

2. Reverse flow. Tufts which point into the local free stream direction represents reverse flow. During reverse thrust flight at lower speeds, the tuft/cone combination situated on and around the flap near the trailing edge of the wing pointed upstream to the free stream flow and formed a small triangularly shaped region of steady reverse flow.

3. Separated flow. The tuft/cone combination that appeared to move in circular and swirling motion for the duration of reverse thrust represents an unsteady separated flow.

As can be seen from figures 10–16, the vertical bars represent separated flow while the boxed region in figure 10 illustrates reverse flow. The procedure for determining whether reverse or separated flow regions required repeated attempts to capture each individual tuft and cone flow directions of movement from the motion videos. Figure 9, which shows a typical procedure for determining reverse and separated flow regions as seen from the videotapes, supplements figures 10–16. Figure 9 illustrates how and where the above three flow patterns on the wing upper surface were captured. An "x" mark was

Table 1. Nominal and actual Mach number variations of the aircraft during the reverse thrust phase in each of the six runs

Run	Nominal Mach number	Actual Mach number			Reverse thrust duration time, sec
		t = 0	t = 15	t_{max}	
1	0.70	0.768	0.736	0.702	58
2	0.85	0.878	0.843	0.772	46
3	0.85	0.883	0.851	0.790	37
4	0.55	0.604	0.608	0.546	69
5	0.85	0.885	0.852	0.793	35
6	0.55	0.565	0.546	0.555	33

placed at each individual tuft/cone combination representing separated flow. As discussed above, the combination that appeared to move in circular or swirling motion is representative of separated flow. Similarly, the letter "o" representing reverse flow was placed at each individual tuft/cone combination that pointed upstream to the flow. Regions of the upper surface of the wing where the tuft/cone combination was unaffected by the presence of reverse thrust were left untouched. Once the procedure was completed for all Mach cases, a smooth curve was drawn through the boundary of the points, marked with x's and o's, to show the region of the flow field affected by reverse thrust within the wing planform.

At lower speeds, particularly Mach number 0.55, (run number 4 which lasted 69 sec), it is seen from figure 10 that a somewhat elliptical, divergent-convergent separated flow region was formed as a result of deployment of the inboard thrust reversers. This separated flow region is an average flow field representation at Mach number 0.55 over the entire 69 sec of the reverse thrust flight. The separated flow region, nearly symmetrical with respect to the inboard engine centerline, occupies nearly 37 percent of the total planform area of the left wing upper surface. The separated flow field area does not include the small separated region seen on the Yehudi portion of the wing in figure 10. The Yehudi is the nonswept portion of the planform on the inboard trailing edge of a wing and is typically not included in the reference area used for aerodynamic lift and drag coefficients. The foregoing separated flow region caused by reverse thrust extends from about $\eta = 18$ percent to $\eta = 48$ percent of the wing semispan on the trailing edge and at about $\eta = 22$ percent to $\eta = 45$ percent of the wing semispan on the leading edge of the wing. In addition to the figure above, figure 18 is a photograph taken during reverse thrust at Mach number 0.55 and shows the swirling motions of the tufts and cones on the left-wing upper surface.

In addition to developing a large area of separated flow at lower speeds, the aircraft also experienced reverse flow behind the inboard engine and near the flap on the trailing edge. As figure 10 shows, the small triangularly shaped region which represents reverse flow resides within the larger separated region and occupies an average of 3 percent of the total planform area of the left wing. This reverse flow region has its boundary coordinates at about $\eta = 27$ percent to $\eta = 39$ percent of the wing semispan along the trailing edge. The two points then converge at $\eta = 35$ percent in the semispan direction just ahead of the flap leading edge and 6.5 ft forward of the trailing edge.

As the aircraft entered the flight test run at Mach number 0.70 (first test run for 58 sec), it is seen from figure 11 that a hyperbolic, divergent separated flow region was formed. This separated flow region as a result of reverse thrust flight is an average flow field representation for the duration of 58 sec. The separated flow region boundary starts close to the inboard engine nacelles and diverges out in both directions along the wing chord. In contrast to the previous test run at Mach 0.55, this run did not experience any reverse flow on any part of the wing. The separated region occupies nearly 20 percent of the total planform area of the left wing. The calculations in determining the separated flow field area does not take into account the small separated region that is present on the Yehudi portion of the wing in figure 11. The separated flow region boundaries are at about $\eta = 18$ percent to $\eta = 46$ percent along the semispan on the trailing edge and are at about $\eta = 32$ percent to $\eta = 40$ percent along the semispan on leading edge. Figure 19 is a photograph that shows the disturbed flow field regions taken at Mach number 0.70 during reverse thrust flight. The photograph shows that the tufts situated near the leading edge of the wing on either side of the inboard engine centerline (marked with a black tape) being affected by the presence of reverse thrust. It can also be seen that the separated flow region which starts out close to the nacelle increases in width on both sides as the flow gets near the trailing edge of the wing.

The entry to the flight test run at Mach number 0.85, (run number 2 which lasted 46 sec), was the fastest flight speed tested. Graphical representations for this part is presented in two parts; namely, the results will be broken down to two time segments: a time segment for 15 sec into the reverse thrust flight ($0 \le t \le 15$) and the time increment following 15 sec of reverse thrust flight ($15 \le t \le 46$). The separated flow region for the first 15 sec as a result of reverser deployment, figure 12, reveals a narrow hyperbolic flow-field shape. The separated flow region starts at a single point at the inboard engine centerline on the leading edge of the wing and diverges out in the chordwise direction ending at points $\eta = 32$ percent and $\eta = 40$ percent along the wing semispan on the trailing edge. The above separated flow field occupies nearly 8.5 percent of the total planform area of the left wing. It should be noted that at the onset of the inboard engine reversal, no separations of the tufts and cones were noticed for about the initial 4 sec. As the reverse thrust duration time progressed forward, the Mach number stabilized near 0.78 and separations of the tufts and cones began to occur. Therefore, figure 12 is an average separated flow field representation for the first 15 sec.

The separated flow region for the final time segment ($15 \le t \le 46$) looks similar to Mach 0.70 case except that the overall separated flow shape for this run, figure 13, is narrower than the Mach 0.70 run. The separated flow

region for this time increment is again a time-averaged flow-field representation. The separated flow region maintains its boundaries at about $\eta = 27$ percent to $\eta = 45$ percent along the semispan on the trailing edge and at about $\eta = 33$ percent to $\eta = 38$ percent along the semispan on the leading edge of the left wing. Figure 20 presents a photograph of the tufts and cones during reverse thrust flight at Mach number of 0.85. The trend seen in the motions of the tufts and cones looks identical to the Mach 0.70 case except that the entire separated flow region is notably narrower than the Mach 0.70 run. The separated flow region for the Mach number 0.85 for the second time increment also starts out close to the nacelle and diverges out in the chordwise direction of the wing. The separated region for this time increment occupies an average 11.5 percent of the area on the left side of the wing.

For the duration of reverse thrust flight at the three Mach cases, it was found that the tufts and cones showed no separations near Mach number of 0.88 and the separated flow regions became notably wider as the Mach number decreased. At higher speeds, the separated flow regions tend to start close to the engine nacelle and increase in width as the flow reaches the trailing edge of the wing. The reverse flow region present for the Mach number of 0.55 did not occur at the two higher speeds.

In addition to presenting regions of reverse and separated flow field (figs. 10–13) for reverse thrust flight, figures 14–16 reveal regions of the separated flow on left wing at forward thrust (steady state) conditions. The latter figures are included to show the wing flow patterns for both reverse thrust and steady-state flight. For the reverse thrust flight phase, it is seen that the separated flow regions starts close to the inboard engine nacelle and occupies a large area of separated flow. For the steady-state period of the aircraft, however, the separated flow regions reside entirely on the flap and on the Yehudi portions at the trailing edge of the wing. The separated flow regions for the steady-state flight for all Mach numbers look similar in shape. The separated flow region at Mach number 0.55 has its boundary coordinates at the intersection of the Yehudi on the trailing edge of the wing and the left side of the fuselage ($\eta = 10$ percent) and at about $\eta = 38$ percent of the semispan. The flight test run at Mach number 0.70 maintains its separated flow region boundary coordinates during steady state flight at about $\eta = 11$ percent to about $\eta = 36$ percent (inboard engine center line) on the trailing edge of the wing. Similarly, the separated flow region at Mach number 0.85 keeps its boundary coordinates at about $\eta = 15$ percent to about $\eta = 32$ percent along the semispan on the trailing edge of the wing. Note that for all Mach numbers, the three points on the trailing edge of the wing converge at $\eta = 23$ percent in the semispan direction at or just below the flap leading edge and about 5 ft forward of the trailing edge.

Standard Aircraft Research Data Analysis

In order to investigate how other major aircraft parameters were affected by the presence of reverse thrust, data acquired using the DC-8 central computer system was analyzed. Data acquisition using the central computer system was discussed earlier in the text. Of major importance are the aircraft's angular orientation, altitude, vertical speed, Mach number, and the total and static temperatures of the air outside of the aircraft as a function of the three phases of the experiment. Table 2 below lists these variations and their figure numbers in the order of flight test runs.

It should be noted that in the figures listed in the above table the pre-deployment phase occurs at $t < 0$, reverse thrust phase occurs at $t = 0$ and the termination times are different for each run, and the post-deployment phase

Table 2. Figure numbers for the angular, altitude, vertical speed, Mach number, and temperature variations of the aircraft during the reverse thrust phase for each of the six runs

Run	Nominal Mach number	Figures for θ, ϕ vs. t	z vs. t	w vs. t	M vs. t	To, T. vs. t
1	0.70	21	27	33	39	45
2	0.85	22	28	34	40	46
3	0.85	23	29	35	41	47
4	0.55	24	30	36	42	48
5	0.85	25	31	37	43	49
6	0.55	26	32	38	44	50

immediately follows the reverse thrust phase The above aircraft parametric variations in the order of flight-test runs, as a function of all three test phases, are discussed in more details below:

Variations of pitch and roll angles– Because the thrust reversers were deployed symmetrically in all six runs, figures 21–26 show minimal changes in the roll angles during the duration of reverse thrust phase. These figures, however, show significant negative pitch angles just prior to the inboard engine thrust reversals and during the duration of reverse thrust phase. A significant change in the elevator was required on all six deployments to keep the aircraft at the desired Mach number prior to the reversals and to minimize loss of air speed throughout the duration of reverse thrust phase.

As will be discussed later in the text, the aircraft steadily lost altitude at the reverse thrust configuration, therefore, it was necessary to climb back to the desired altitude of 28,000 ft in preparation for the next flight test. As a result, figures 21–26 show positive pitch angles immediately following each run. These figures also indicate large changes in the roll angles immediately following each run. Large changes in the ailerons were necessary to bring the aircraft to within the prescribed flight envelope.

The reader should note that a few of the figures above show high frequency oscillations in with the data traces. High frequent oscillations will occur whenever any single experiment, including the present investigation, undergoes frequent and abrupt changes in the motion of the experiment being tested. As the NASA DC-8 deviated from its established cruise configuration into the reverse thrust mode, it experienced a large change of kinetic and potential energy. The vehicle was no longer able to maintain attached flow over the entire wing. The lack of attached flow over the entire wing and the introduction of turbulence induced by reverse thrust caused an unsteady motion of the vehicle, and contributed to small inconsistencies in data acquisition. In addition, the central computer system that gathers data is also sensitive to aircraft motion. This sensitivity in data collection, in turn, contributes to noise in the data.

Figure 21 shows angular variations of the aircraft for run number 1 as a function of the three phases of the experiment at Mach number of 0.70 and at an altitude of 30,000 ft. Prior to reverser deployment, the aircraft experienced only minimal variations in the roll and pitch angles. As the aircraft entered the reverse thrust phase, figure 21 indicates an initial roll in the left wing down direction. This initial roll occurred because the reversers on the two inboard engines on the DC-8 do not deploy simultaneously. The aircraft's pitch angle is shown to be in the negative direction (nose down) throughout the reverse thrust duration. This was done in an attempt to minimize loss of air speed, as stated above.

Figure 22 illustrates angular variations of the aircraft for run number 2 as a function of the three phases of the experiment at Mach number 0.85 and at an altitude of 31,500 ft. As was discussed earlier, this figure illustrates only minimal variations in the roll angle of the aircraft prior to and during the duration of reverse thrust phase. This figure also shows 4 deg of negative pitch angle prior to reverser deployment and as much as 14 deg of negative pitch angle as the lowest value during the duration of reverse thrust phase. Consistent with the discussions earlier in the text, a negative pitch angle was required to minimize loss of airspeed. Figure 22, however, shows a positive pitch angle while the aircraft is still in reverse thrust mode almost halfway through the reverse thrust phase. As will be discussed later, it will be shown that the aircraft descended at a rate of almost 9000 ft per minute for the higher Mach numbers tested. This descent rate was too rapid to maintain for a longer reverse thrust duration and catastrophic failures and destruction of the aircraft would have been unavoidable.

Figure 23 represents angular variations of the aircraft for run number 3 as a function of the three phases of the experiment at Mach number of 0.85 and at an altitude of 31,000 ft. This was a repetition to the previous run that was performed to capture the shock position and its movement on the videos. The angular orientation of the aircraft for run number three resembles the results for run number two flown at the same Mach number. Note, the small levels of noise in the data described above also pertains to this particular test run.

Figure 24 presents angular variations of the aircraft for run number 4 as a function of the three phases of the experiment at Mach number 0.55 and at an altitude of 31,000 ft. Except for minimal fluctuations in roll angle with respect to the centerline of the fuselage, shown as line 0 on the ordinate in figure 24, the aircraft prior to and during reverse thrust phase is shown to have flown with negligible bank angle. The figure, however, shows 5 deg of positive pitch angle but it is further decreased just prior to reversal deployment. The noise in the data can be seen to be an inherent part of the general data representation.

Figure 25 is another graphical illustration of angular variations of the aircraft as a function of the three phases of the experiment performed at Mach number of 0.85 and at an altitude of 31,000 ft. This test condition was repeated to see if there was any correlation between the engine power level and the movement of the wing shock waves. Prior to deployment, a verbal description of the shock indicated its position to be about 2 ft forward of the aft spoiler line. When the aircraft entered reverse thrust phase, the

position of the shock wave was noticed to be near the wing leading edge. DADS data representation for this run is similar to the previous runs tested at Mach number 0.85.

Figure 26 is a final representation of the angular variations of the aircraft as a function of the three phases of the experiment performed at Mach number of 0.55 and at an altitude of little over 29,000 ft. This test point was repeated because the high-speed video of the earlier run had been accidentally erased. DADS data representation patterns generally agree with the previous run tested at Mach number of 0.55 which was discussed above.

Variation of altitude– Figures 27–32 are graphical representations of the altitude variations of the aircraft as a function of the three phases of the experiment. For the steady-state period of the experiment, these figures show constant altitude for the aircraft just above the desired altitude for each of the six runs performed. Because the numbers 2 and 3 engines were placed to the idle position in preparation for thrust reverser deployment (discussed in Flight Profile section), it is seen from these figures that the aircraft lost altitude just prior to reversal deployment. The instant the thrust reversers were deployed, shown as line zero on the abscissa in the above figures, the aircraft descent increased to a much higher rate. Except for the test runs at Mach 0.85, the rest of the above figures show a steady descent rate throughout the reverse thrust phase. For Mach number 0.85, however, figures 28, 29, and 31 show a steady descent for most of the reverse thrust phase but then the aircraft gained altitude towards the end of each run. Because the aircraft lost altitude at these higher Mach numbers more rapidly than the other Mach numbers, it was necessary to recover from any additional loss of altitude below 25,000 ft to arrest the descent to maintain a safe altitude.

Figures 27–29 show increasing increments in the aircraft's altitude immediately following the first three runs. Since the aircraft lost altitude during the duration of reverse thrust phase, the aircraft altitude was increased to just over 28,000 ft prior to the next run. Figures 30–32, however, show continued decreasing increments in the aircraft's altitude well after the inboard engine thrust reversers were stowed. The recovery or the post-deployment phase for the last three runs took place about 60–70 sec after closing the inboard engine reversers.

Descent rate variations– Figures 33–38 are graphical illustrations of the aircraft descent rate as a function of the three phases of the experiment for the present investigation. Data plotted in these figures were acquired using the aircraft's central computer system. The vertical speed or the descent rate of the aircraft in these figures appear to be related to the pitch angle variation and altitude variation of the aircraft. Angular and altitude variation of the aircraft as a function of the three phases of the experiment was discussed in some detail above. It should be noted from figures 33, 36, and 38 that the aircraft descended at a steady rate throughout the reverse thrust phase at the nominal Mach numbers of 0.55 (two runs) and 0.70. These figures exhibit the same type of trend seen in figures 21, 24, and 26 for the pitch angle variations of the aircraft and figures 27, 30, and 32 for altitude variations of the aircraft. At the nominal Mach number of 0.85, however, it is seen from figures 34, 35, and 37 that the aircraft descended at a steady rate approximately halfway through reverse thrust phase but then ascended at a steady rate prior to the inboard engine reversals being stowed. This trend is shown in these figures and is consistent with the discussion of aircraft's angular and altitude variations. As a precautionary measure, because the aircraft at these higher speeds descended at a steeper rate, any additional loss in the vehicle's altitude had to be prevented below 25,000 ft.

Mach number variations– Figures 39–44 are Mach number variations of the aircraft as a function of all three phases of the experiment. As was discussed above in the text (Flight Profile), an attempt was made to maintain the desired Mach number during the preparation period and to keep the loss of airspeed of the aircraft to a minimum during the reverse thrust phase. Consistent with the discussion above, figures 39–44 show a slight gain in aircraft Mach number just above the desired Mach number prior to the inboard engine reversals. The above figures, however, reveal a steady decrease in Mach number for the entire reverse thrust duration phase for runs number 1 (M = 0.70), 2, 3, and 5 (M = 0.85). For the remaining two runs (runs number 4 and 6, M = 0.55), increasing as well as decreasing increments in the aircraft airspeed during reverse thrust phase can be seen from figures 42 and 44.

It is shown from reference 5 that the local Mach number of the aircraft during flight is directly proportional to the local airspeed of the aircraft and inversely proportional to the square root of the absolute static temperature of the aircraft. Specifically, local Mach number of the aircraft is

$$M = \frac{V_\infty}{\sqrt{\gamma R T}} \qquad (1)$$

where V_∞ is true airspeed of the aircraft, γ is the air specific heat ratio, R is the air gas constant, and T is the absolute static temperature of the aircraft. Evidently from equation (1), a decrease in the aircraft airspeed and an increase in the static temperature will indeed lower the Mach number. As stated in the text above (Flight Profile), the procedure used for each test point was to start at an altitude just above 28,000 ft. This region of the Earth's

atmosphere, the troposphere, is characterized by increasing temperature gradients with decreasing altitude. The aircraft in all test points experienced increasing temperature gradients during reverse thrust phase due to altitude change. This increase in temperature is one reason for the declining Mach number during the reverse thrust phase.

Another and more important reason for the declining Mach number is a steady decrease of the aircraft airspeed during reverse thrust flight. This decrease in the aircraft airspeed is largely due to the fan airflow being deflected out normal both from the top and from the sides of the inboard engine nacelle during reverse thrust flight (refer to figs. 2 and 3). As was discussed earlier (Introduction), this type of airflow deflection reduces thrust to produce great deceleration. The deceleration of the aircraft at each test point, however, was kept to a minimum due to a steady increase in the thrust on the outboard engines prior to and during reverse thrust phase (discussed earlier in the Flight Profile Section of the text).

In contrast to the reverse thrust phase, the post-deployment flight phase, figures 39–44, reveal a sudden increase in Mach number at the instant when the inboard engine reversals were stowed. Because the aircraft thrust increased rapidly during this phase, it was able to accelerate and attach the flow everywhere except for a small region on flaps and on the nonswept portion at the trailing edge on the wing.

Variations of temperatures– Figures 45–50 represent total and static (measured and calculated) temperatures of the aircraft as function of the three phases of the experiment. These figures are presented here to identify flight test conditions and to validate data gathered by the NASA DC-8 central computer system. Total and static temperatures were both measured directly by the NASA DC-8 central computer system. These figures exhibit a constant temperature profile during steady state motion of the aircraft, but then reveal increasing temperature gradients during reverse thrust phase. Since all six in-flight thrust reversals took place at about 30,000 ft of altitude, this lower region of the Earth's atmosphere, the troposphere, is characterized by increasing temperature with decreasing altitude. As the inboard engine reversals were stowed and as the aircraft ascended back to its desired altitude of 28,000 ft, it can be seen from figures 45–47 that the aircraft experienced lower temperature gradients because of gain in altitude. Figures 48–50, however, reveal higher temperature gradients during the post-deployment phase because the recovery phase for the last three runs took place about 60–70 sec after the end of these runs.

To validate data presented in the current section and in all previous sections, static temperature will be calculated using the steady, one dimensional flow of a perfect gas equation and will be compared with the measured value. The equation obtained from reference 5 is of the form

$$T = \frac{T_o}{1 + \frac{\gamma - 1}{2} M^2} \qquad (2)$$

where T_o is the total temperature, M is the Mach number, and γ is the air specific heat ratio. A value of 1.4 was used for γ in calculating equations 1 and 2. Values obtained for static air temperature in using equation 2 agrees well with the measured values. Calculated values for static air temperature fall to within a maximum of 7 percent of the measured values.

Concluding Remarks

The investigation of the wing upper surface flow field disturbance due to in-flight inboard thrust reverser deployment on the NASA DC-8-72, which was conducted cooperatively by NASA Ames, the Federal Aviation Administration (FAA), McDonnell Douglas, and the Aerospace Industry Association (AIA), was outlined and discussed in detail. The purpose of this flight test was to obtain tufted flow visualization data to determine the effect of thrust reverser deployment on the wing upper surface flow field in order to determine if the disturbed flow regions could be modeled by computational methods. A total of six symmetric thrust reversals in the two inboard engines were performed to monitor tuft and flow cone patterns, as well as, the character of their movement at Mach numbers of 0.55, 0.70, and 0.85. The tufts and flow cones were photographed and video taped to determine the type and extent of flow field with and without the thrust reversers deployed. In addition, other relevant aircraft parameters, such as aircraft's angular orientation, altitude, vertical descent, and Mach number, were recorded using the normal NASA DC-8 onboard Data Acquisition Distribution System (DADS).

Results of this investigation were presented in two parts. First, three distinct flow patterns associated with the above Mach numbers, which were prepared and sketched from the motion videos, were discussed. In general, for the duration of the reverse thrust phase at the three Mach cases, there were no separations of the tufts and cones near Mach number of 0.88. The separated flow regions just below Mach number of 0.88 became notably wider as the Mach number decreased. At higher speeds, the separated flow regions tended to start close to the engine nacelle and increase in width as the flow approached the wing trailing edge. The reverse flow region present for the Mach number of 0.55 did not occur at the two higher speeds.

Second, other aircraft parameters, such as the aircraft's angular orientation, altitude, vertical descent, and Mach number, were also discussed. The aircraft's angular motion was minimal in each of six test points. During reverse thrust phase, the aircraft descended steadily throughout the reverse thrust duration at the lower speeds. At higher speeds, however, the aircraft descended at a much faster rate. There was a steady decrease in the aircraft's Mach number for the entire reverse thrust duration for the two higher air speeds. At a Mach number 0.55, there were both increasing and decreasing increments in the Mach number during reverse thrust flight.

Finally, to validate data acquired by NASA DC-8 central computer system, static air temperature was calculated and graphically presented by using the steady, one-dimensional flow, perfect gas equation and was compared with the measured values. Calculated values for static air temperature fell to within a maximum of 7 percent of the measured values.

References

1. Harford, James J.: Thrust Reversing Too Complex for Computers. Aerospace America, vol. 22, no. 11, Nov. 1984, pp. 30–33.
2. Ott, James; and Mecham, Michael: Lauda Crash Probers Focus on Midair Thrust Reversal. Aviation Week and Space Technology, June 10, 1991, pp. 28–29.
3. Jane's All The World's Aircraft 1979-80. McDonnell Douglas DC-8 SRS 71, 72, 73. p. 387.
4. Medium Altitude Missions Branch: NASA DC 8-72 Airborne Laboratory Experimenters Handbook. NASA Ames Research Center, May 11, 1990.
5. Hill, Philip; and Peterson, Carl: Steady One Dimensional Flow of a Perfect Gas. Mechanics and Thermodynamics of Propulsion, second edition, 1992, p. 70.

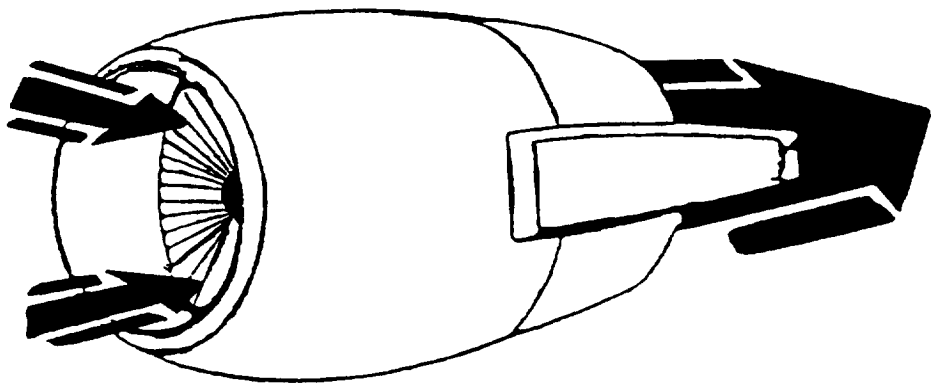

(a)

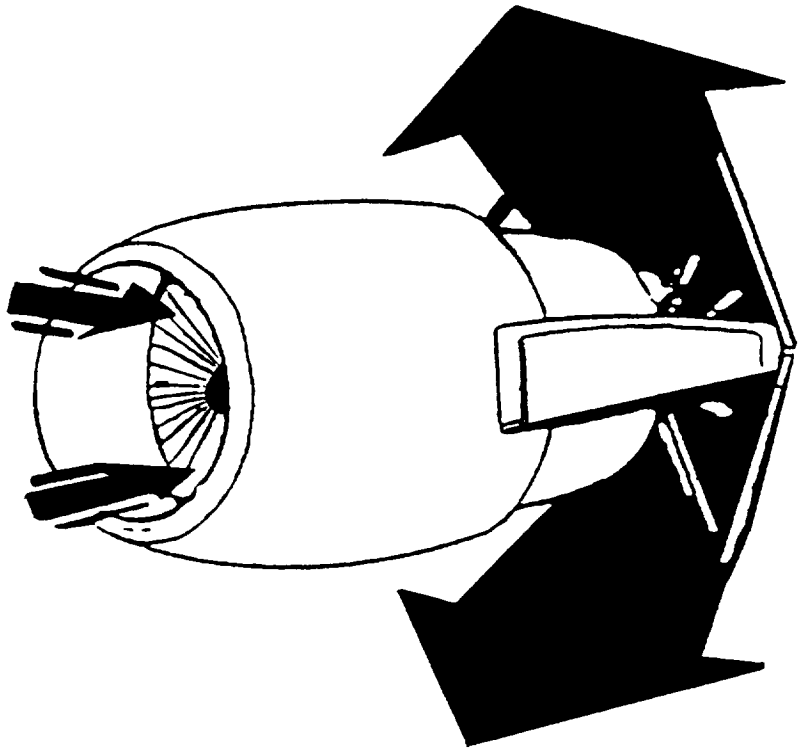

(b)

Figure 1. A typical target- or clamshell-type thrust reverser. (a) Stowed position, (b) deployed position.

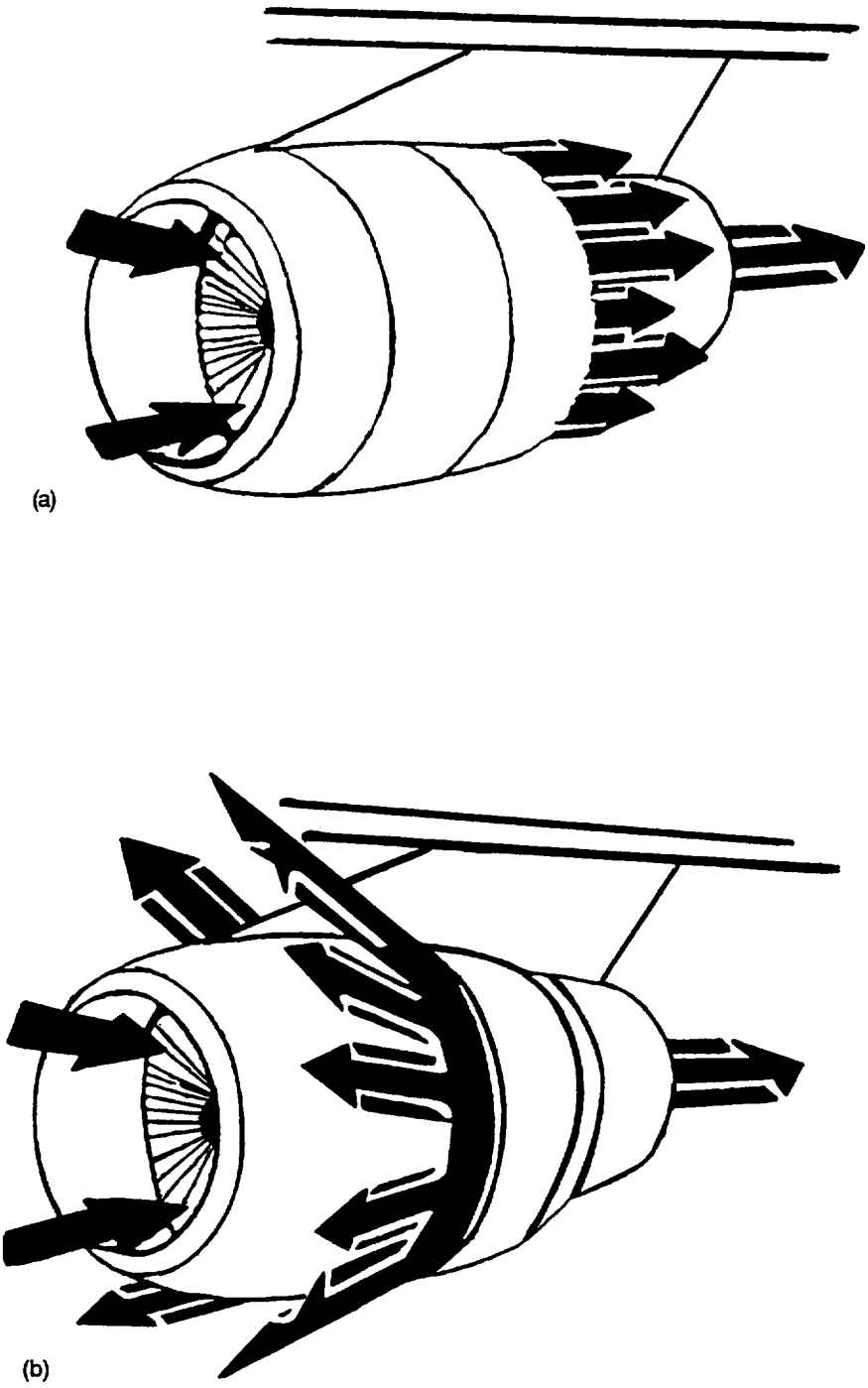

Figure 2. A typical integrated- or cascade-type thrust reverser. (a) Stowed position, (b) deployed position.

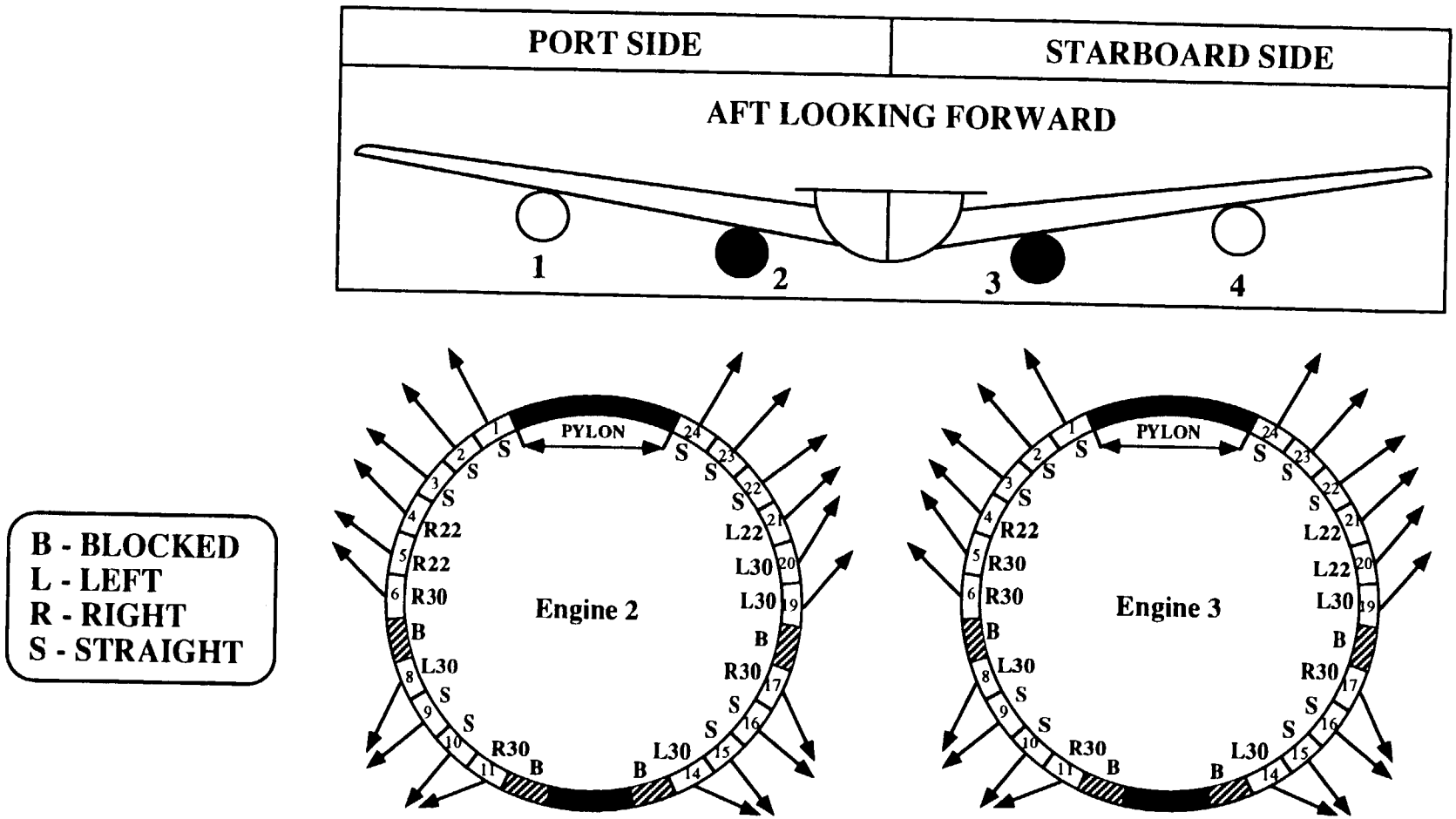

Figure 3. SNECMA-GE CFM-56 thrust reverser deflector configuration.

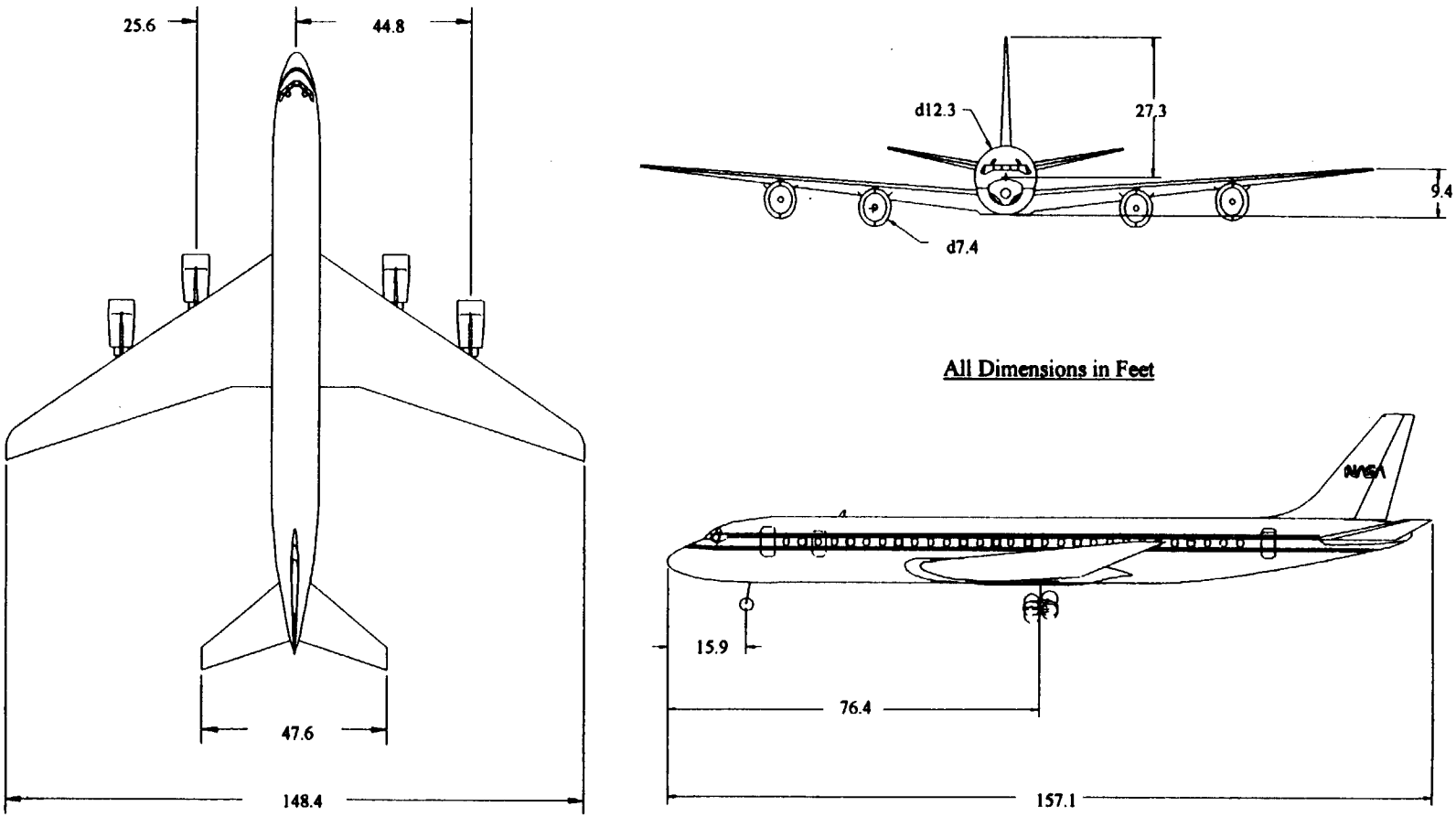

Figure 4. NASA DC-8-72.

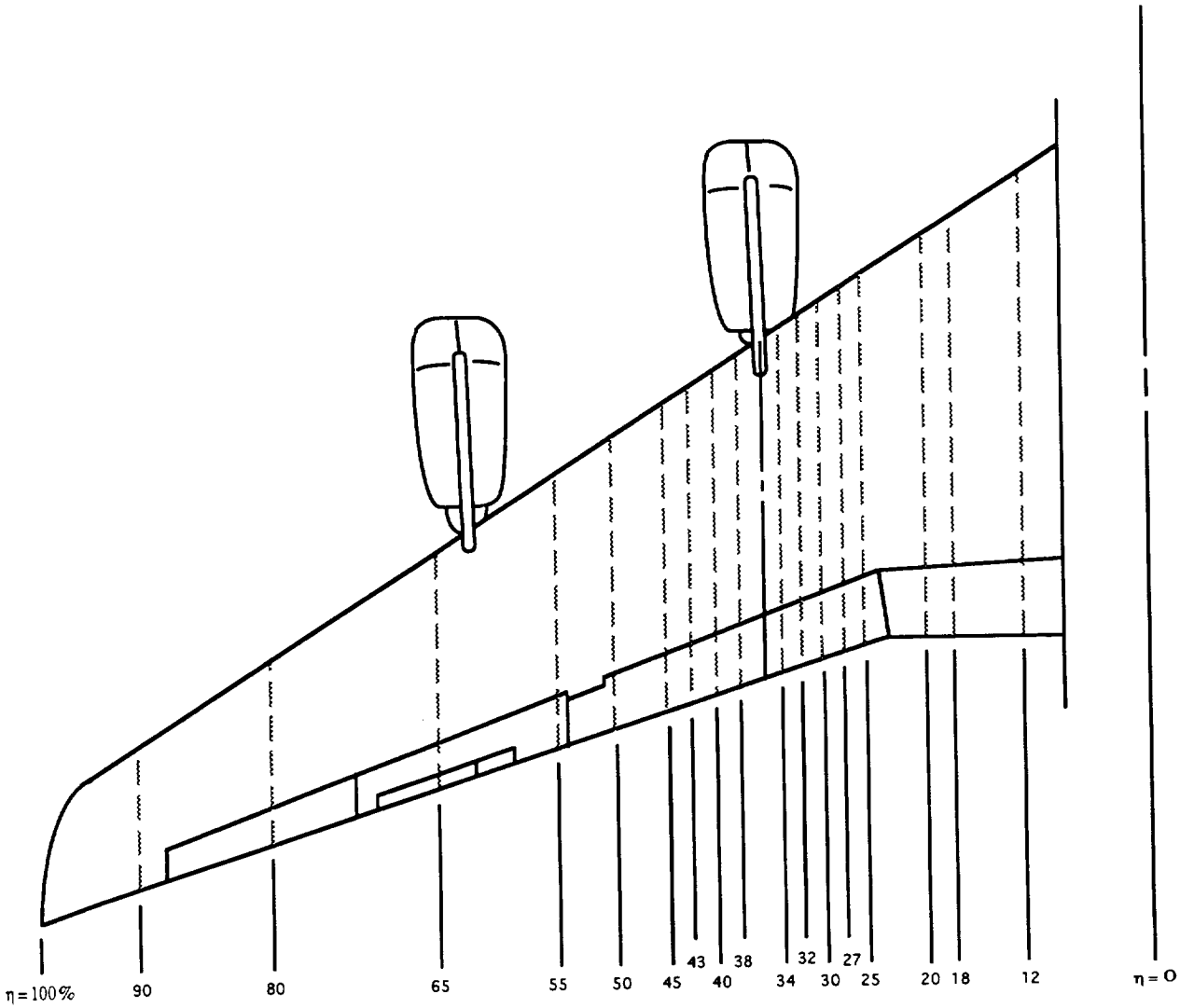

Figure 5. Tuft and flow cone locations along the chord and the semispan of the left-wing upper surface.

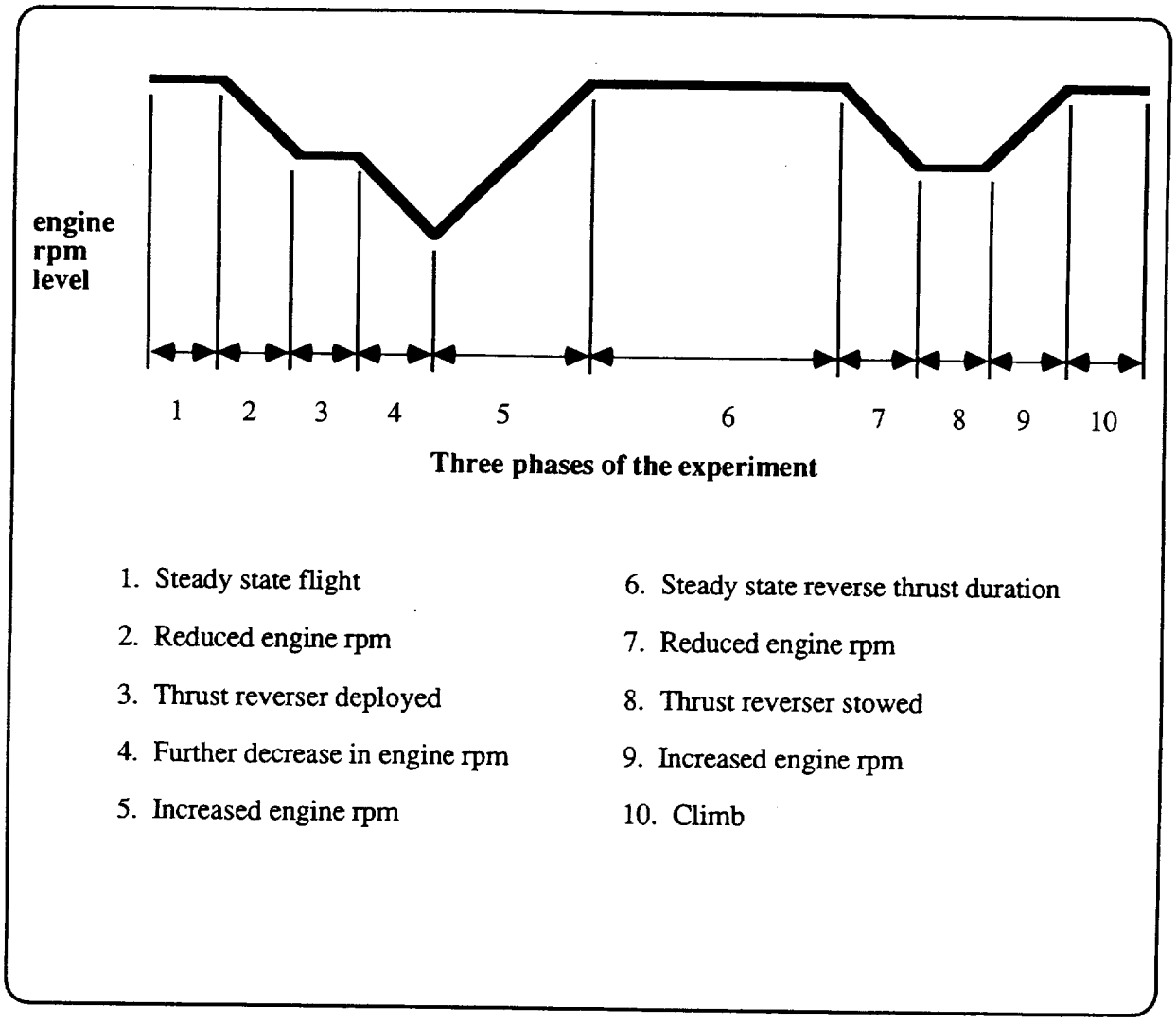

Figure 6. A typical NASA DC-8 flight thrust reverser deployment profile characterized by pilot's controlled engine rpm variation as a function of the three phases of the experiment for the two inboard engines. Note that regions number 1 and 2 above involve the pre-deployment phase, regions number 3–8 present the reverse thrust phase, and regions number 9 and 10 indicate the post-deployment phase.

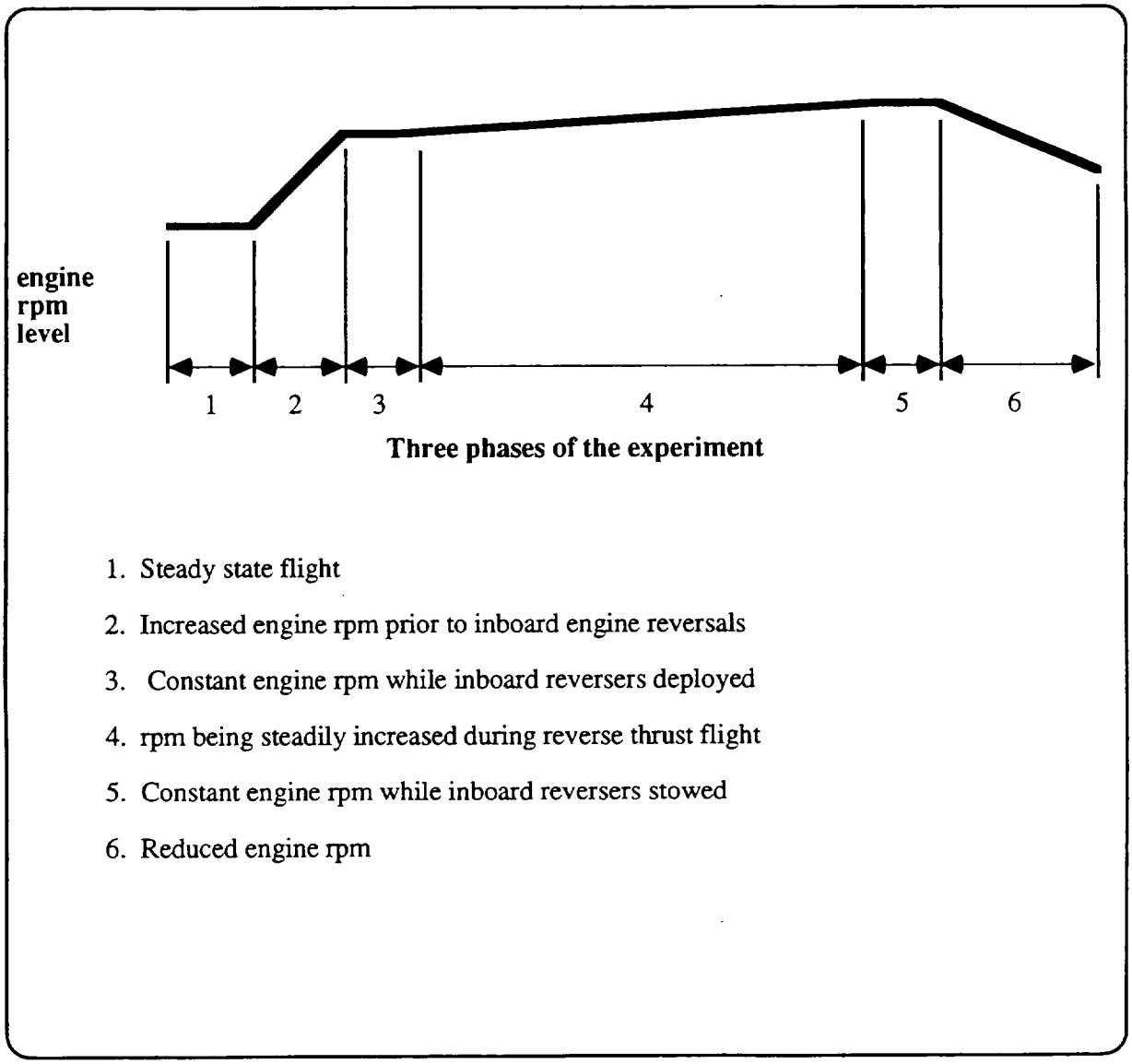

Figure 7. A typical NASA DC-8 flight thrust-reverser deployment profile characterized by pilot's controlled engine rpm variation as a function of the three phases of the experiment for the two outboard engines at M = 0.55 and 0.70. Note that regions number 1 and 2 above involve the pre-deployment phase, regions number 3–5 present the reverse thrust phase, and region number 6 indicates the post-deployment phase.

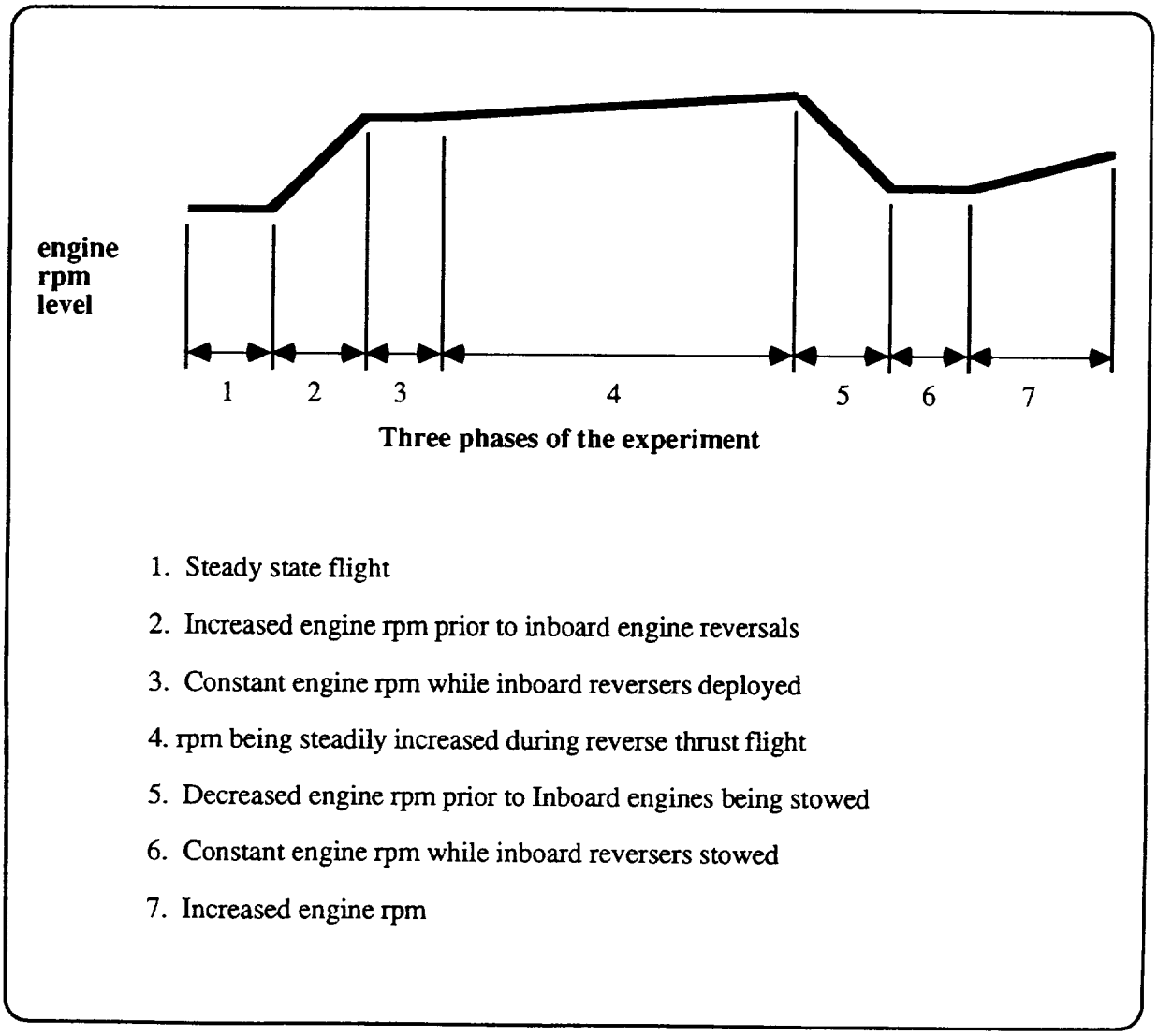

Figure 8. A typical NASA DC-8 flight thrust-reverser deployment profile characterized by pilot's controlled engine rpm variation as a function of the three phases of the experiment for the two outboard engines at M = 0.85. Note that regions number 1 and 2 above involve the pre-deployment phase, regions number 3–6 present the reverse thrust phase, and region 7 indicates the post-deployment phase.

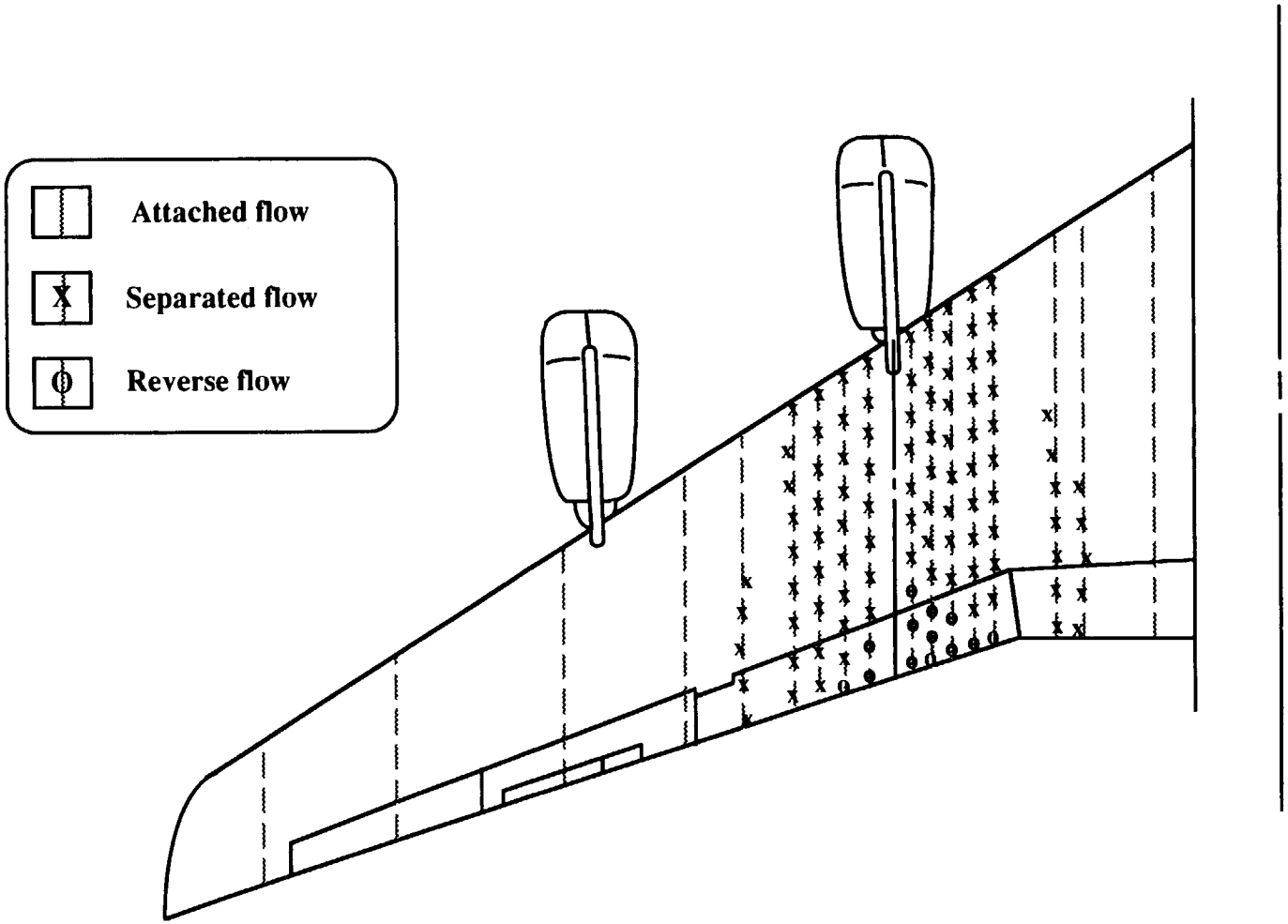

Figure 9. A typical procedure for determining reverse and separated flow regions.

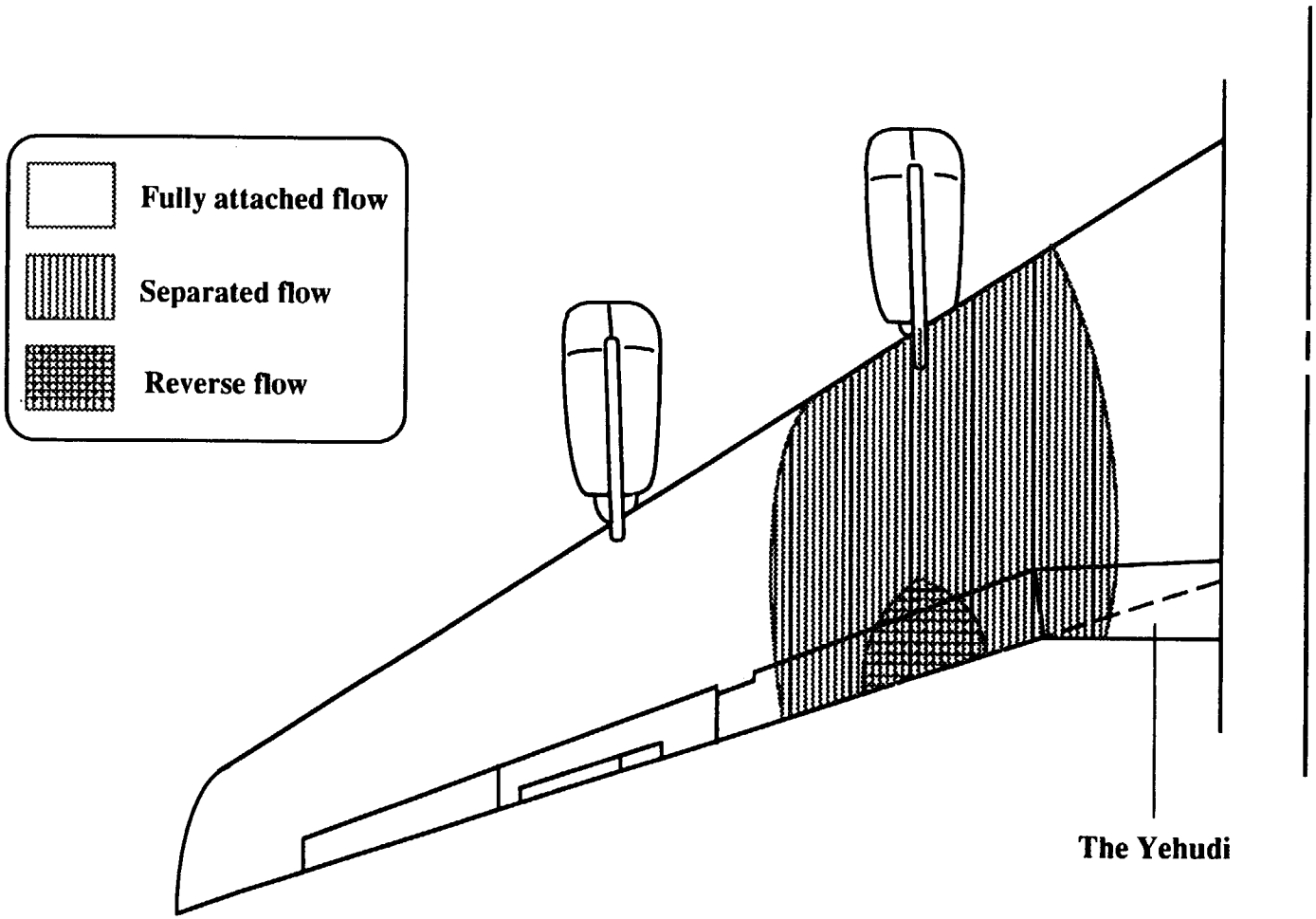

Figure 10. Regions of separated and reverse flow of the aircraft averaged over 69 sec of reverse-thrust flight at M = 0.55.

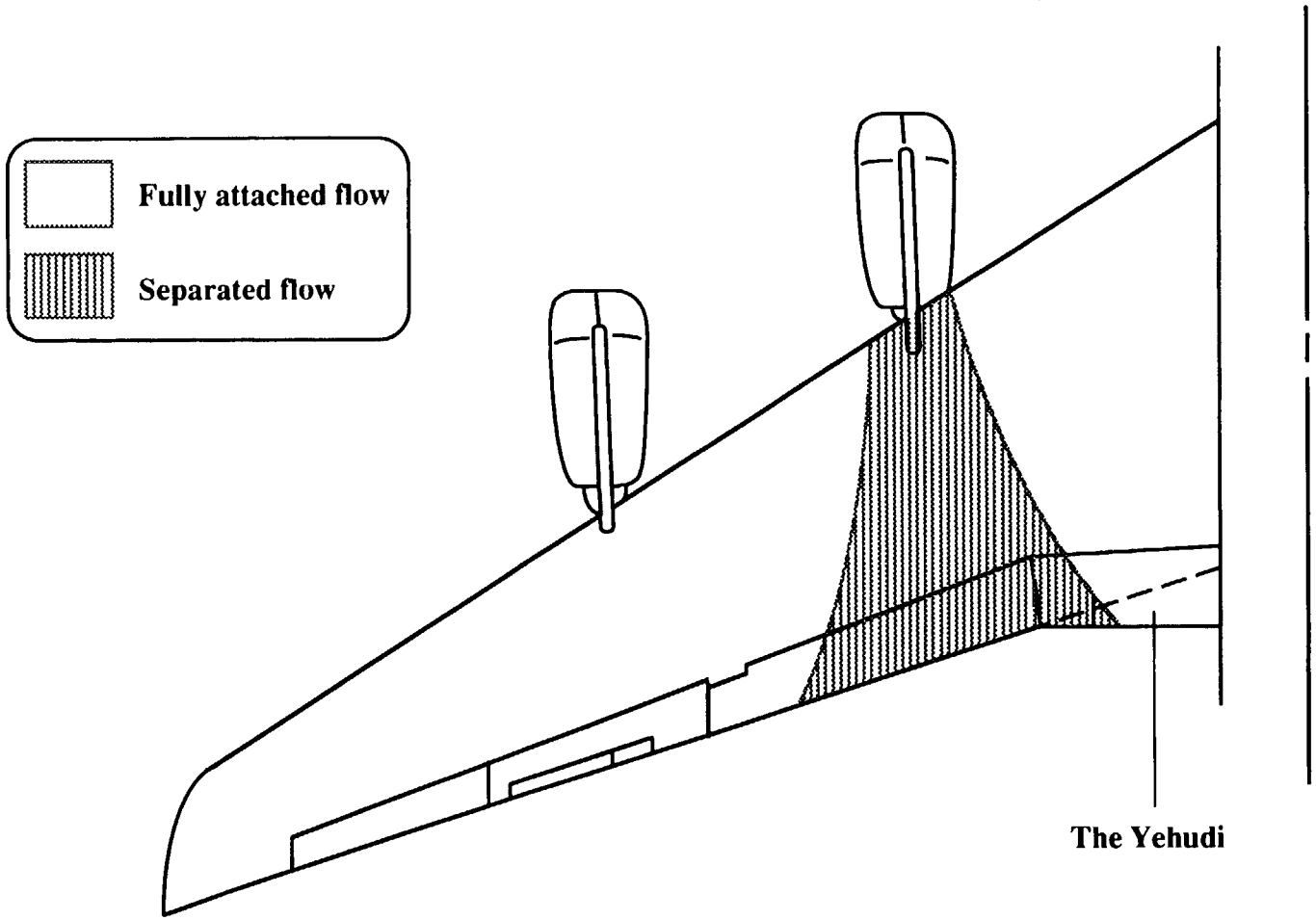

Figure 11. Region of separated flow of the aircraft averaged for the entire 58 sec of reverse-thrust flight at M = 0.70.

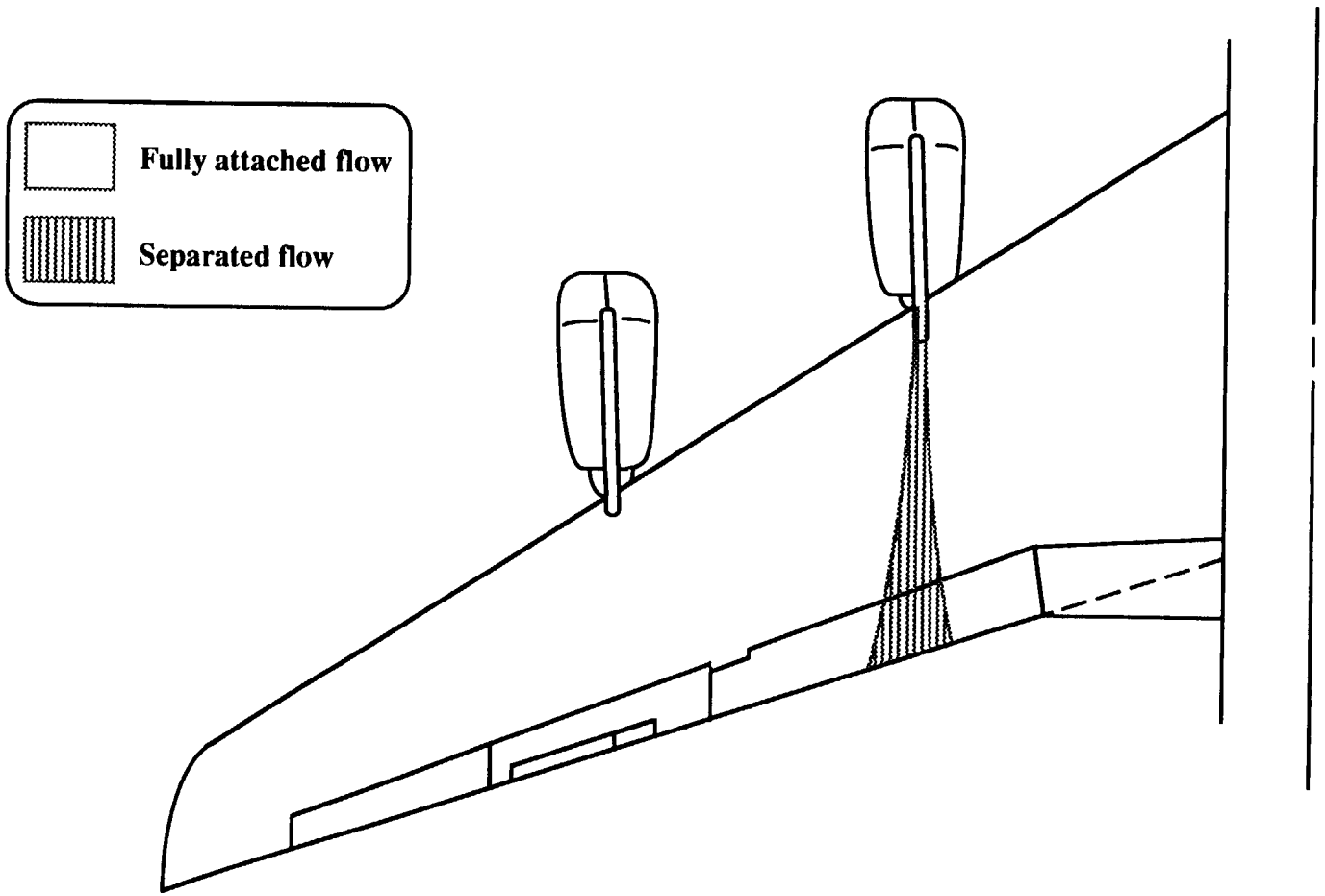

Figure 12. Region of separated flow of the aircraft average at $0 \leq t \leq 15$ sec ($0.82 \leq M \leq 0.88$) into the reverse-thrust flight at $M = 0.85$.

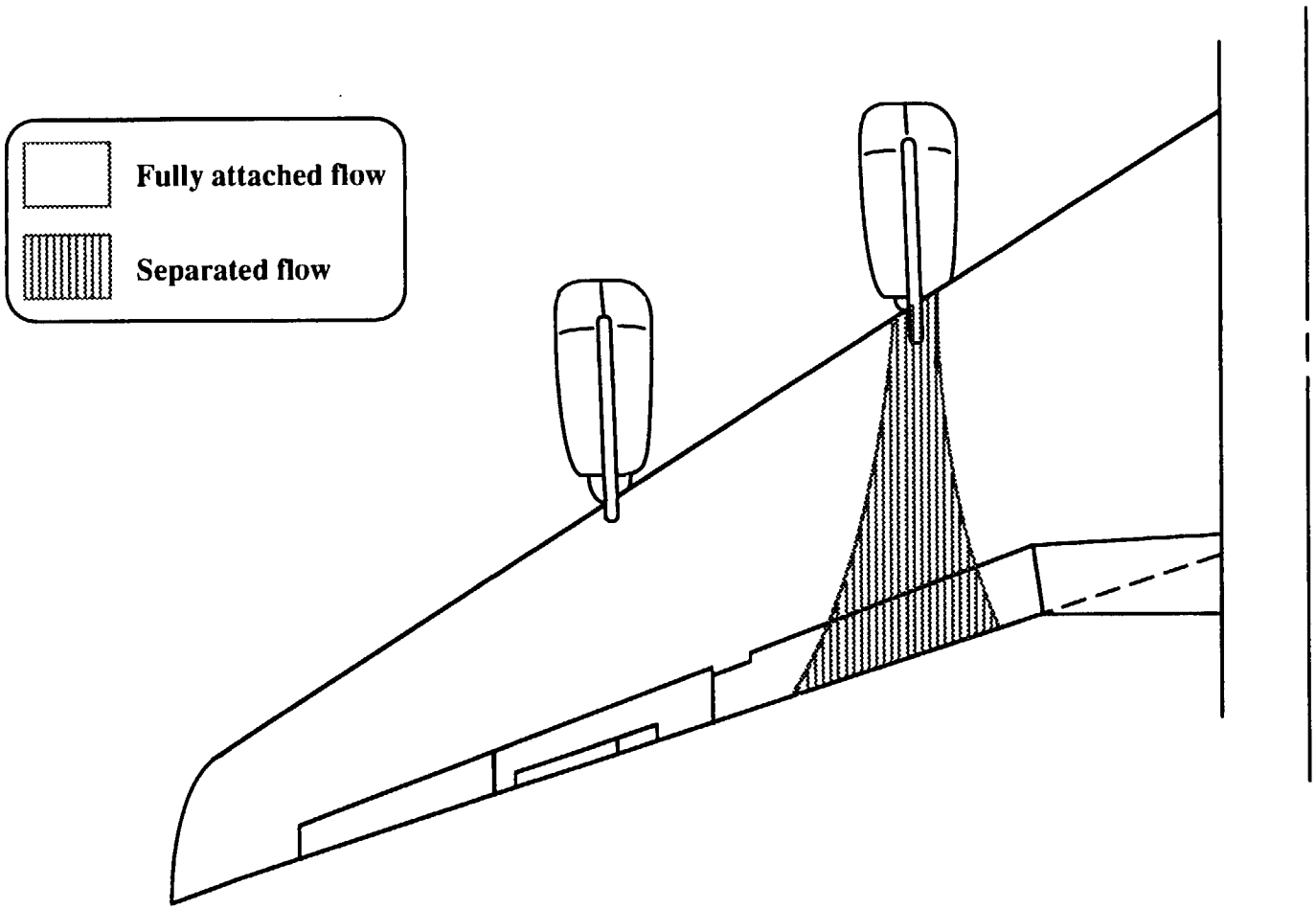

Figure 13. Region of separated flow of the aircraft average at 15 ≤ t ≤ 46 sec (0.72 ≤ M ≤ 0.82) during reverse-thrust flight at M = 0.85.

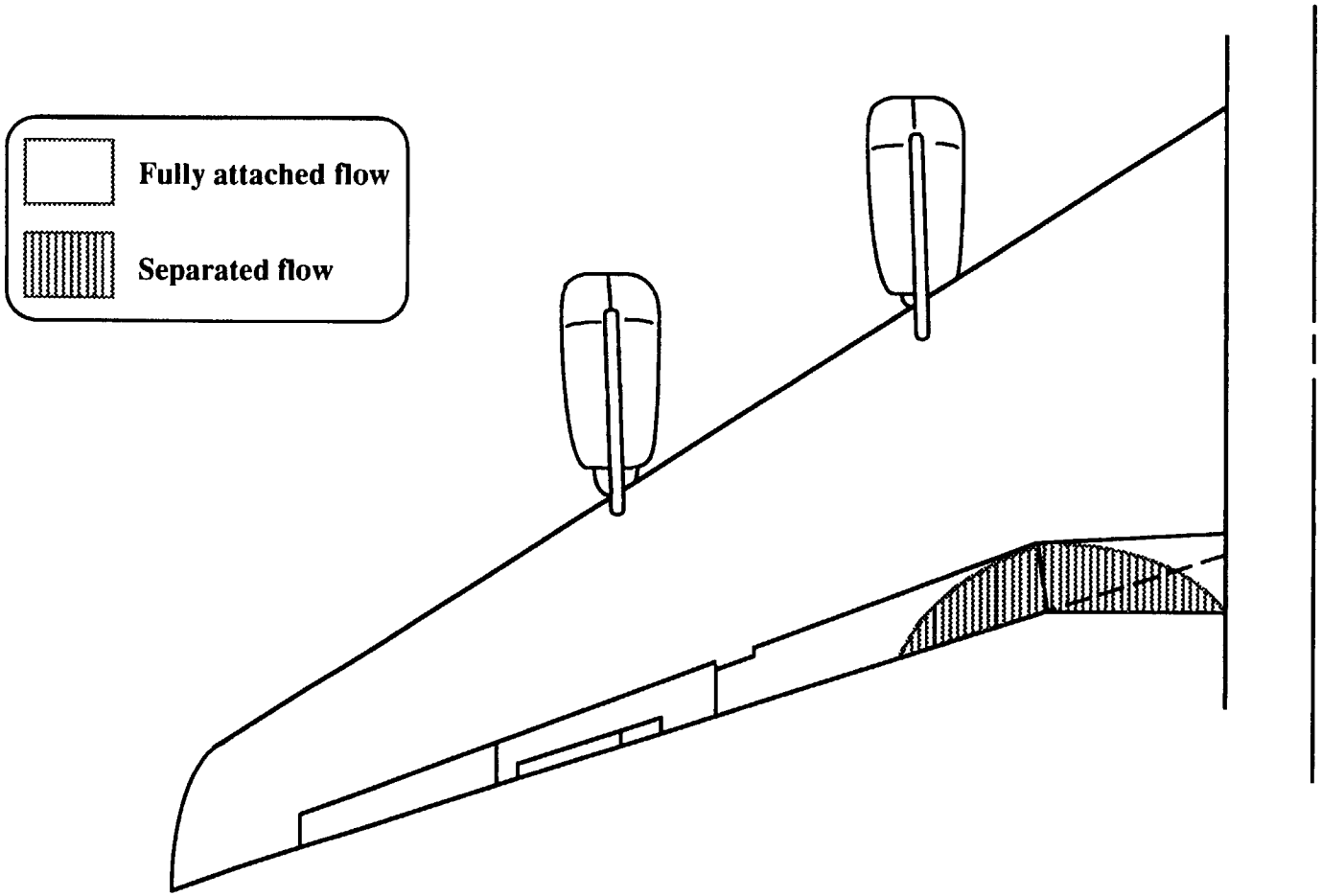

Figure 14. Region of separated flow of the aircraft during steady-state flight at M = 0.55.

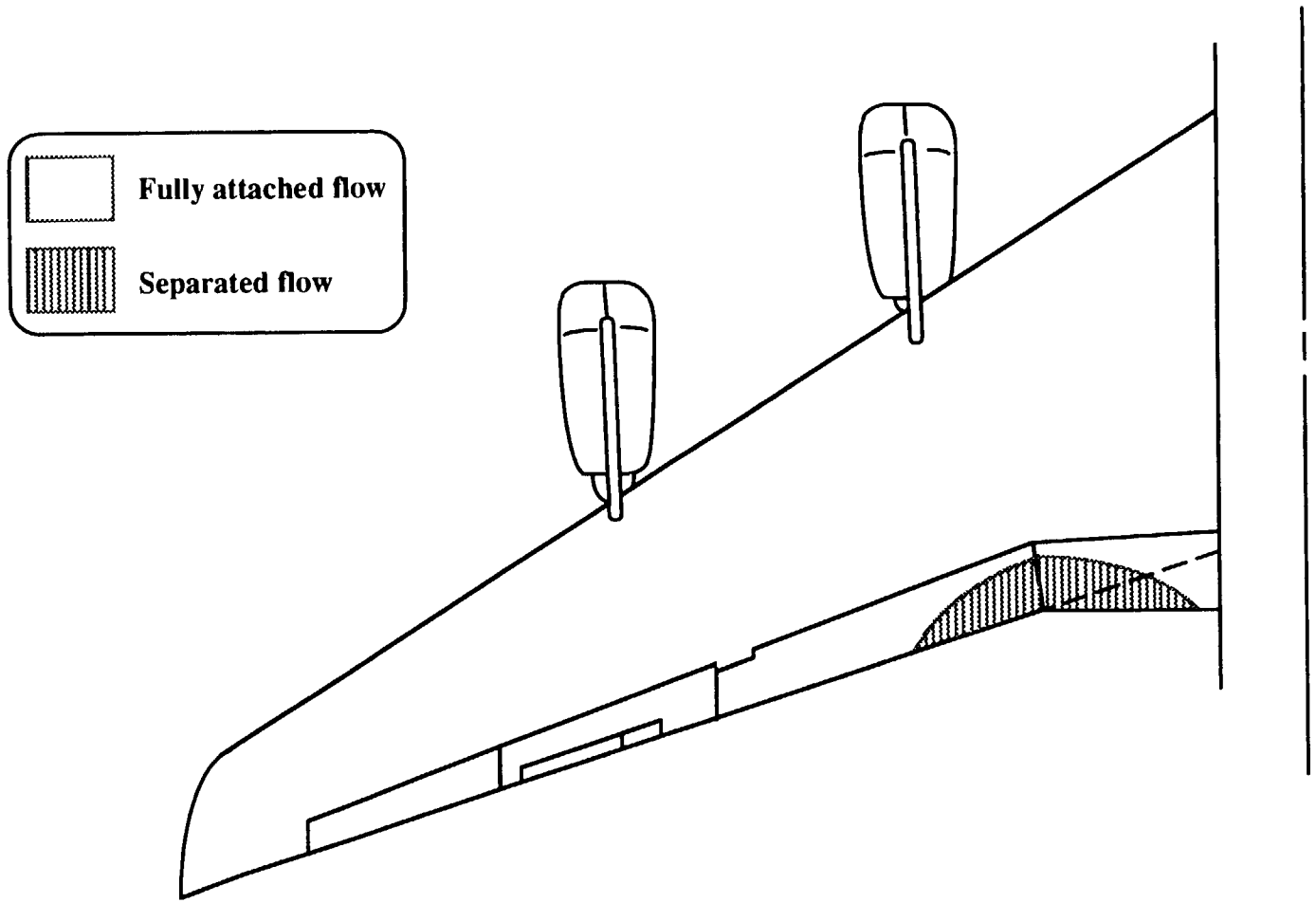

Figure 15. Region of separated flow of the aircraft during steady-state flight at M = 0.70.

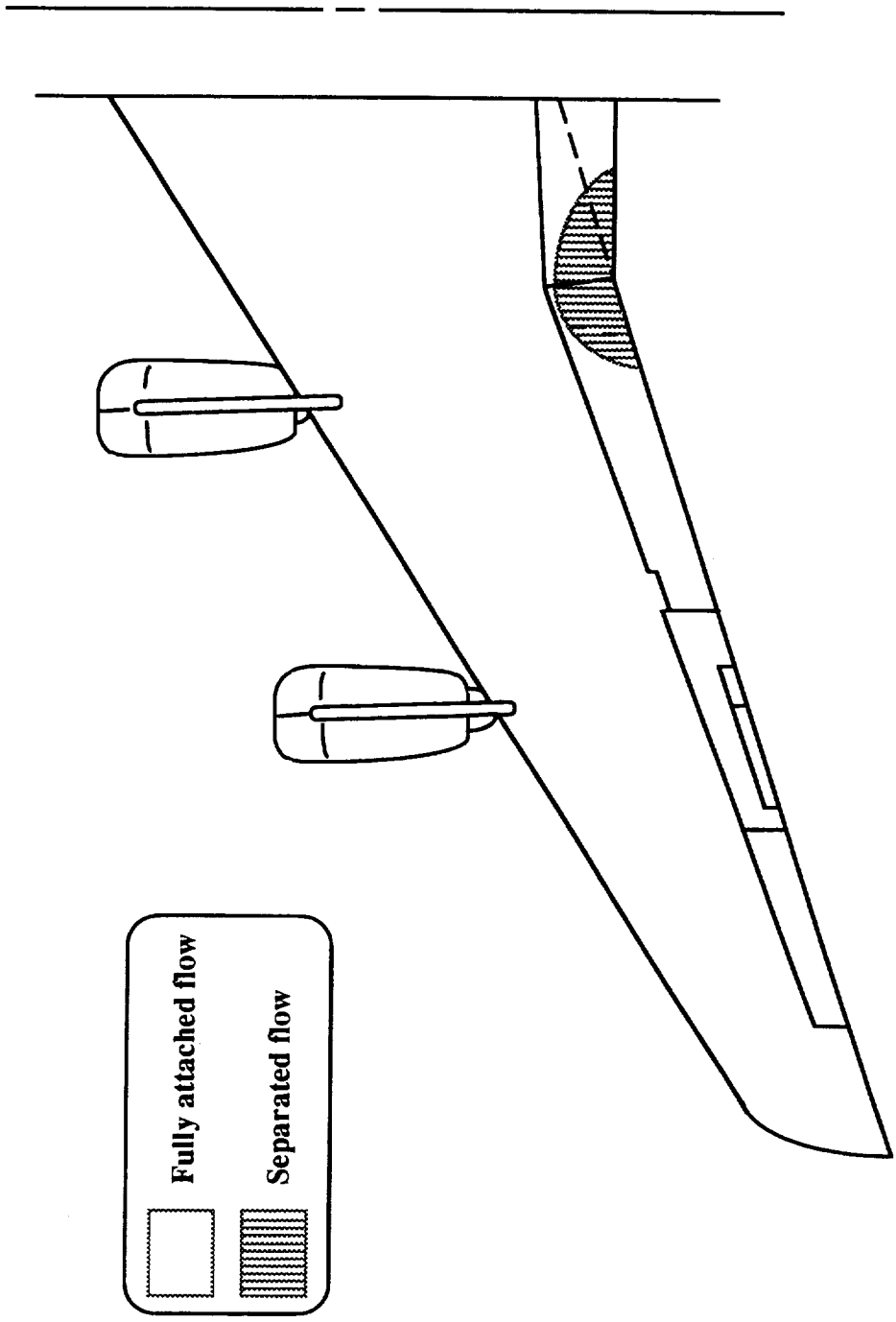

Figure 16. Region of separated flow of the aircraft during steady-state flight at M = 0.85.

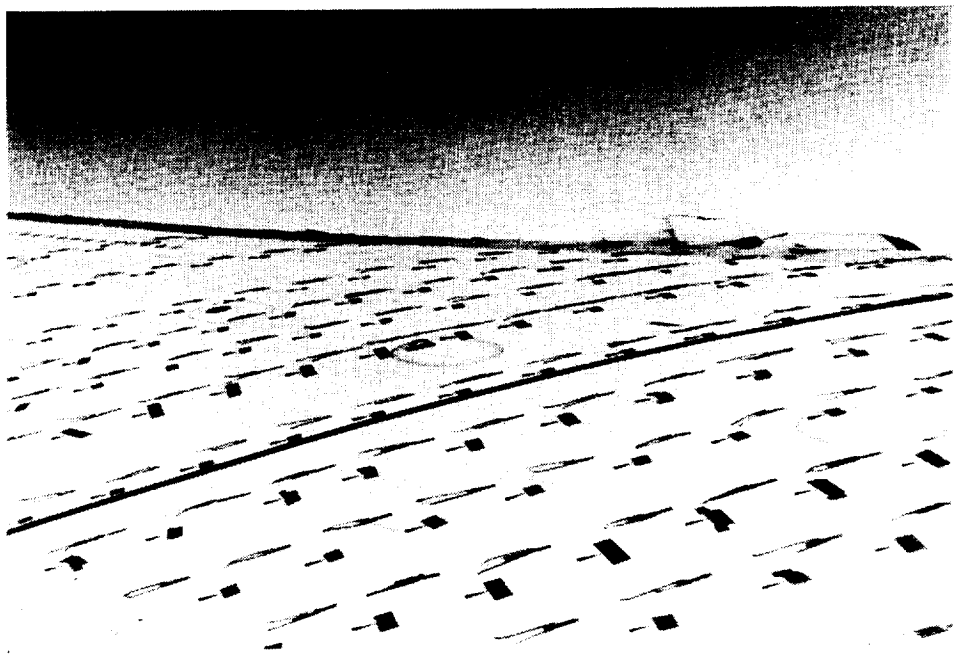

Figure 17. Still photograph showing the tufts and cones on the left wing during steady-state flight.

Figure 18. Still photograph showing tufts and cones during reverse-thrust flight at M = 0.55.

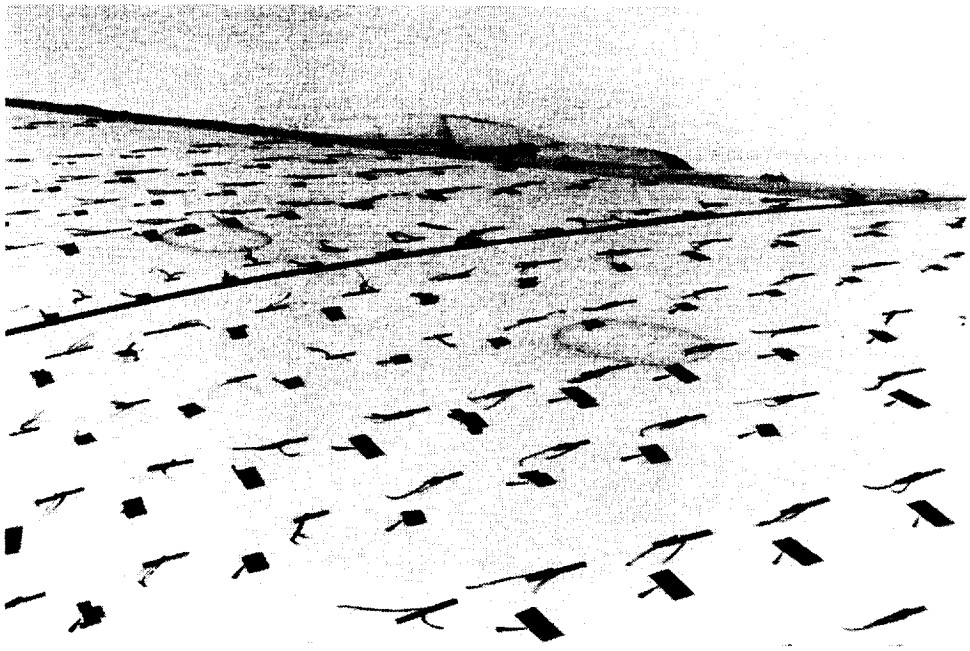

Figure 19. Still photograph showing the tufts and cones during reverse-thrust flight at M = 0.70.

Figure 20. Still photograph showing tufts and cones during reverse-thrust flight at M = 0.85.

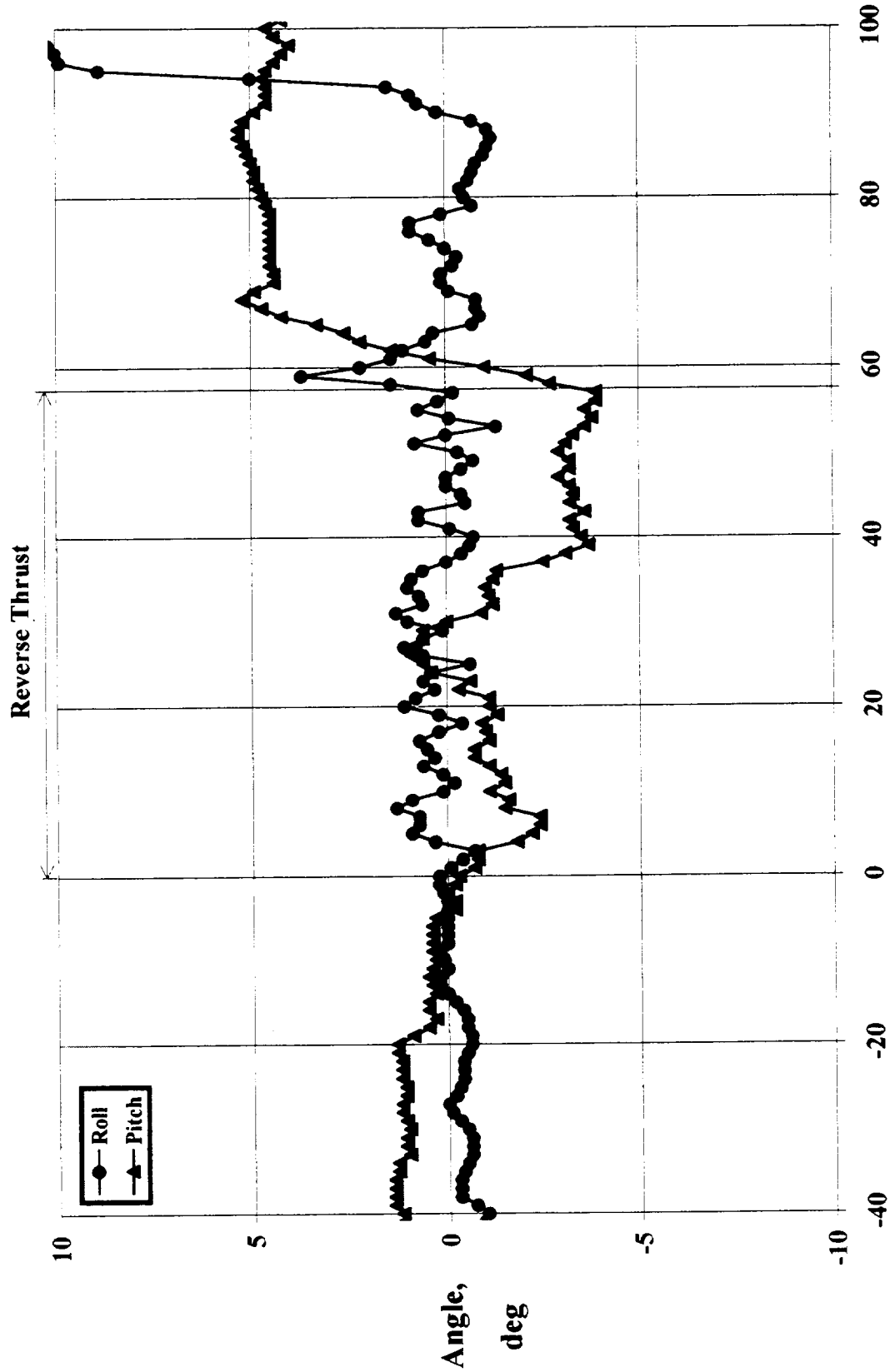

Figure 21. Angular variations during the three phases of the experiment at the nominal Mach number of 0.70.

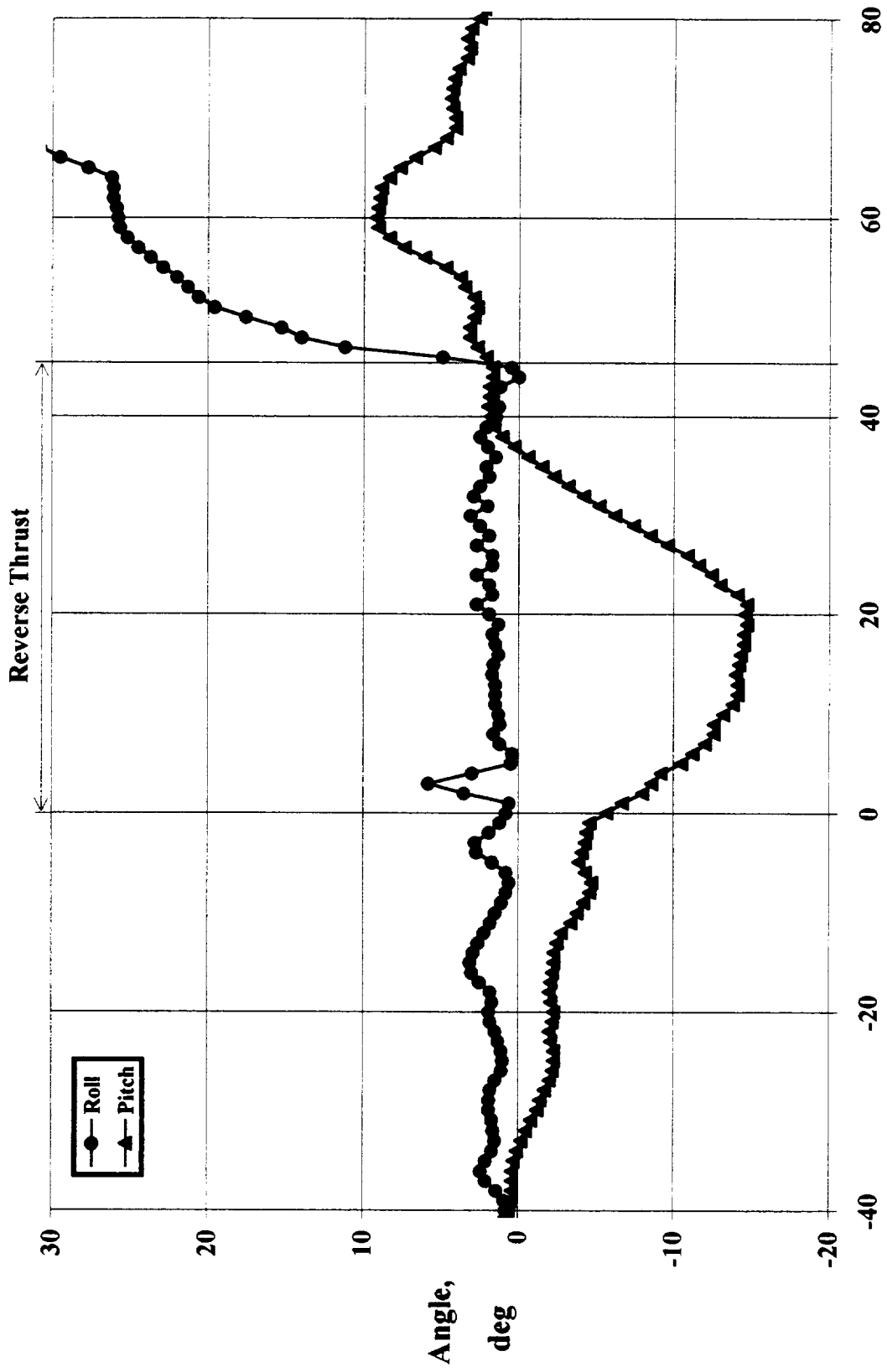

Figure 22. Angular variations during the three phases of the experiment at the nominal Mach number of 0.85.

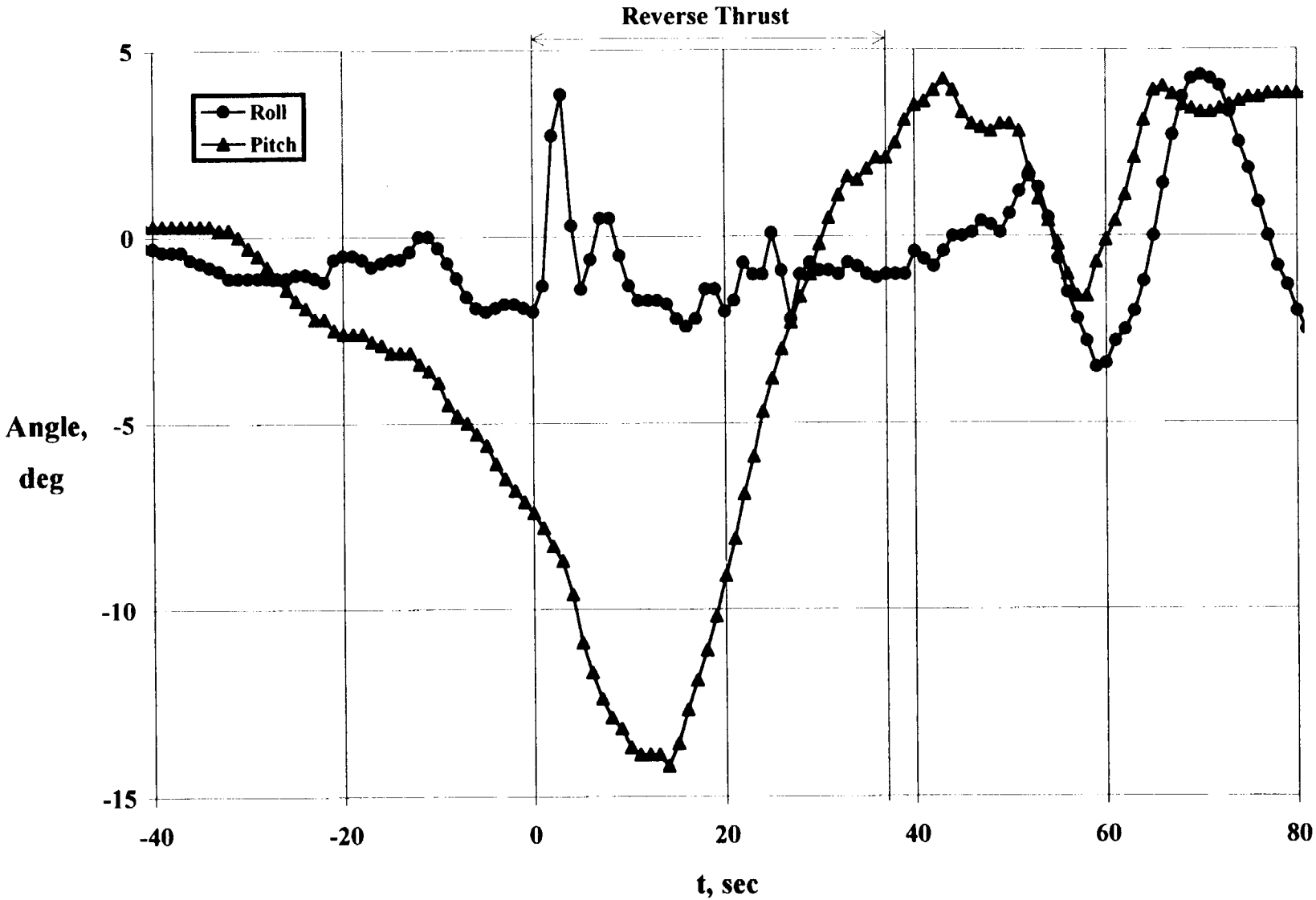

Figure 23. Angular variations during the three phases of the experiment at the nominal Mach number of 0.85.

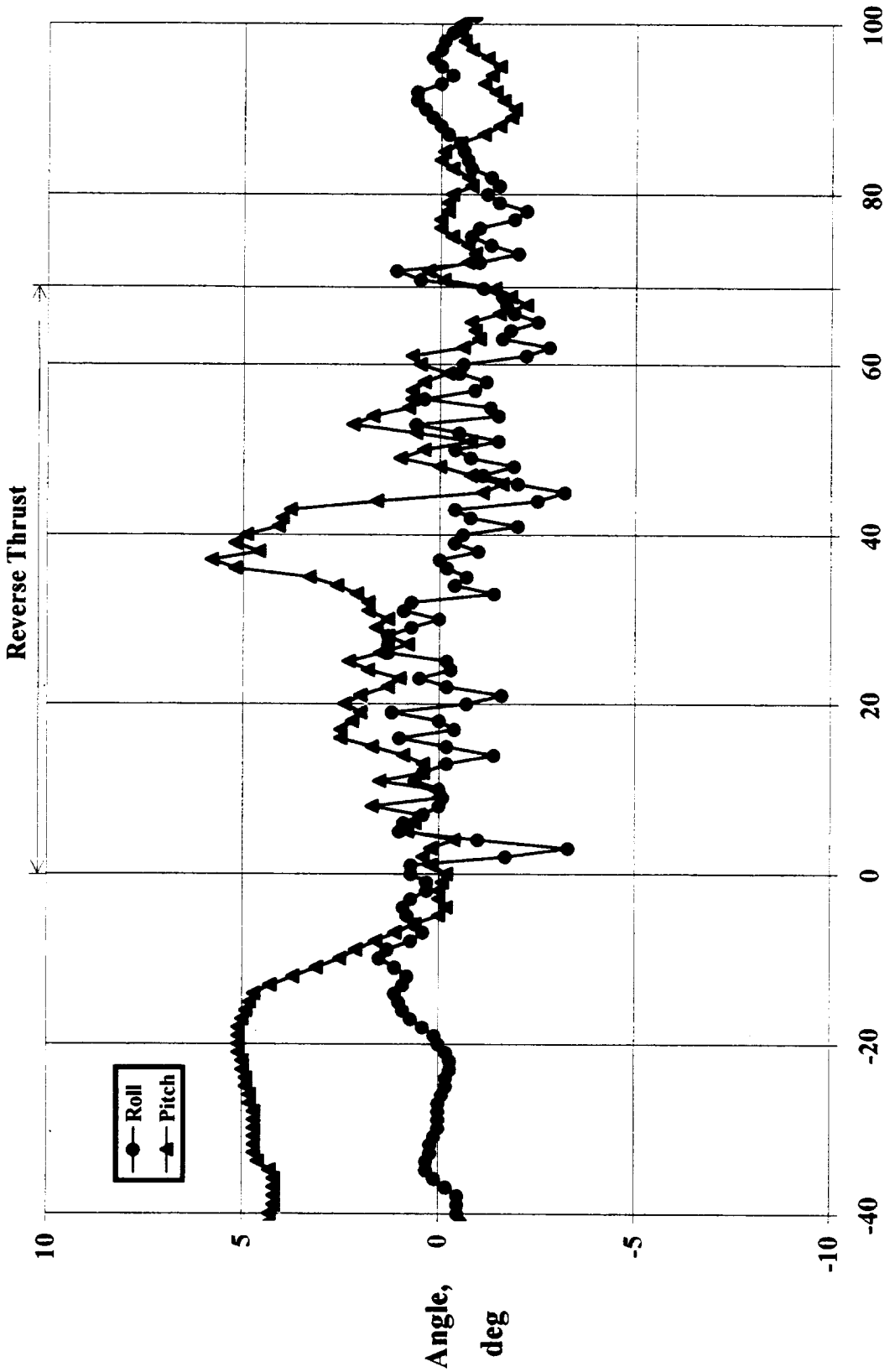

Figure 24. Angular variations during the three phases of the experiment at the nominal Mach number of 0.55.

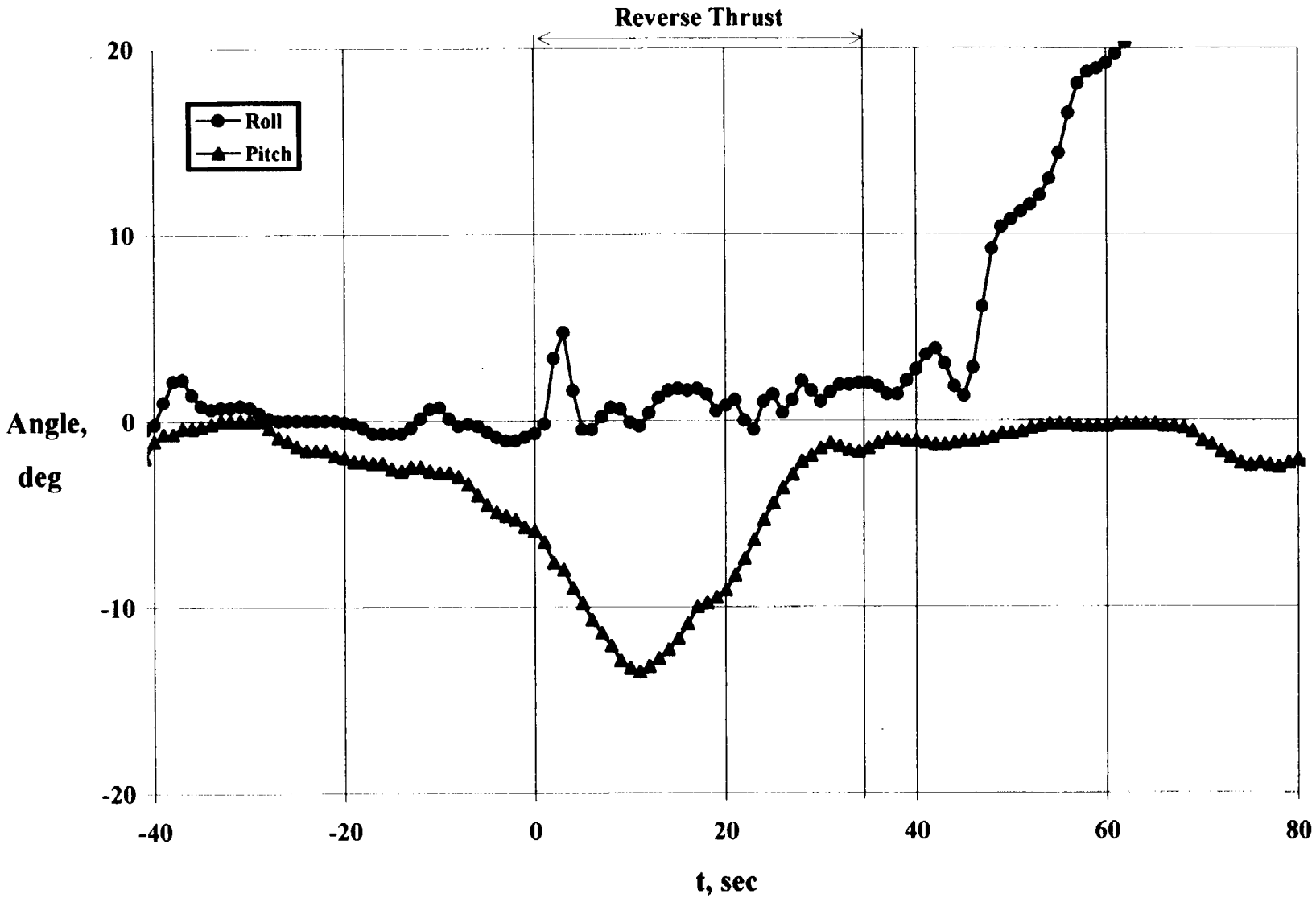

Figure 25. Angular variations during the three phases of the experiment at the nominal Mach number of 0.85.

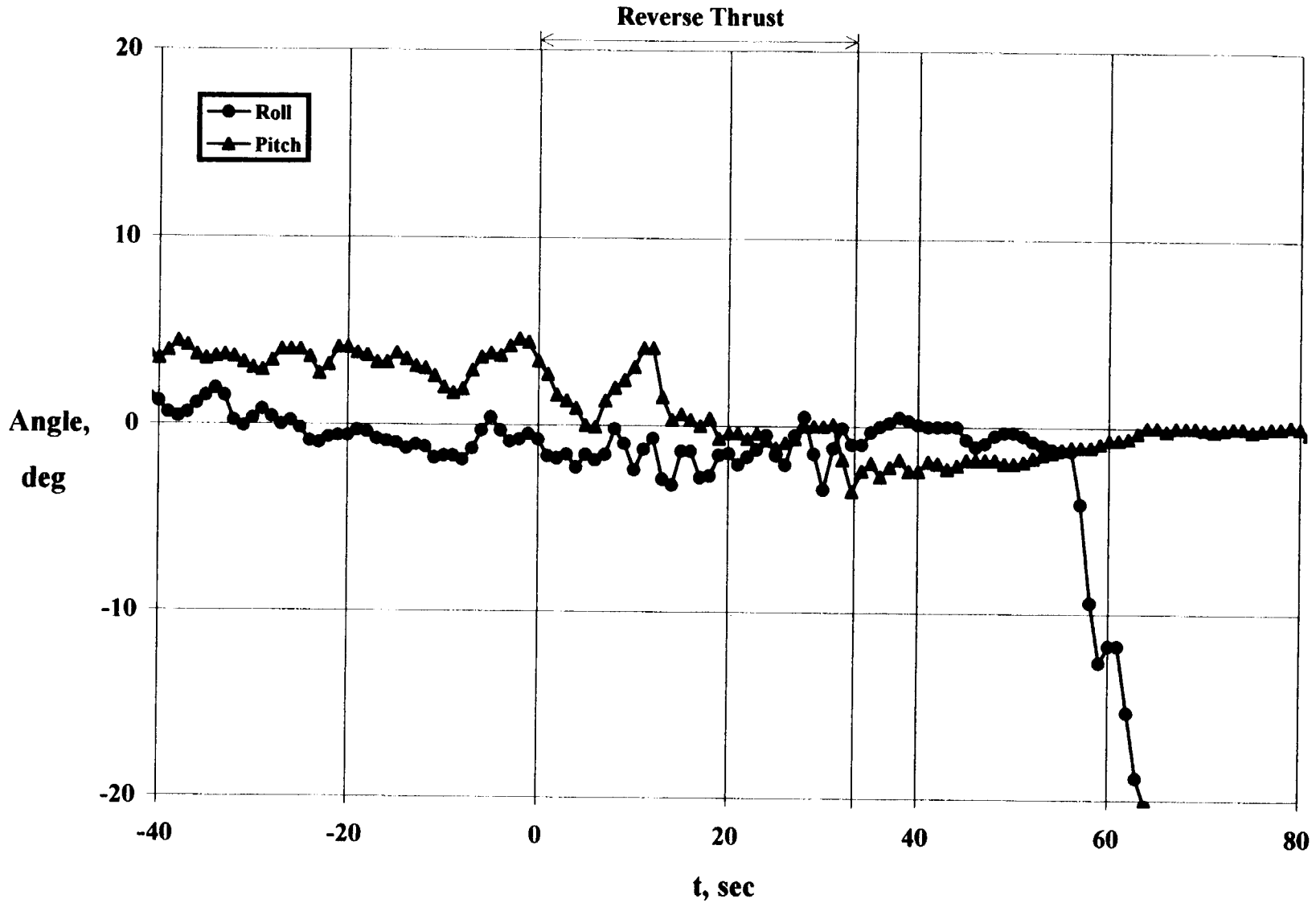

Figure 26. Angular variations during the three phases of the experiment at the nominal Mach number of 0.55.

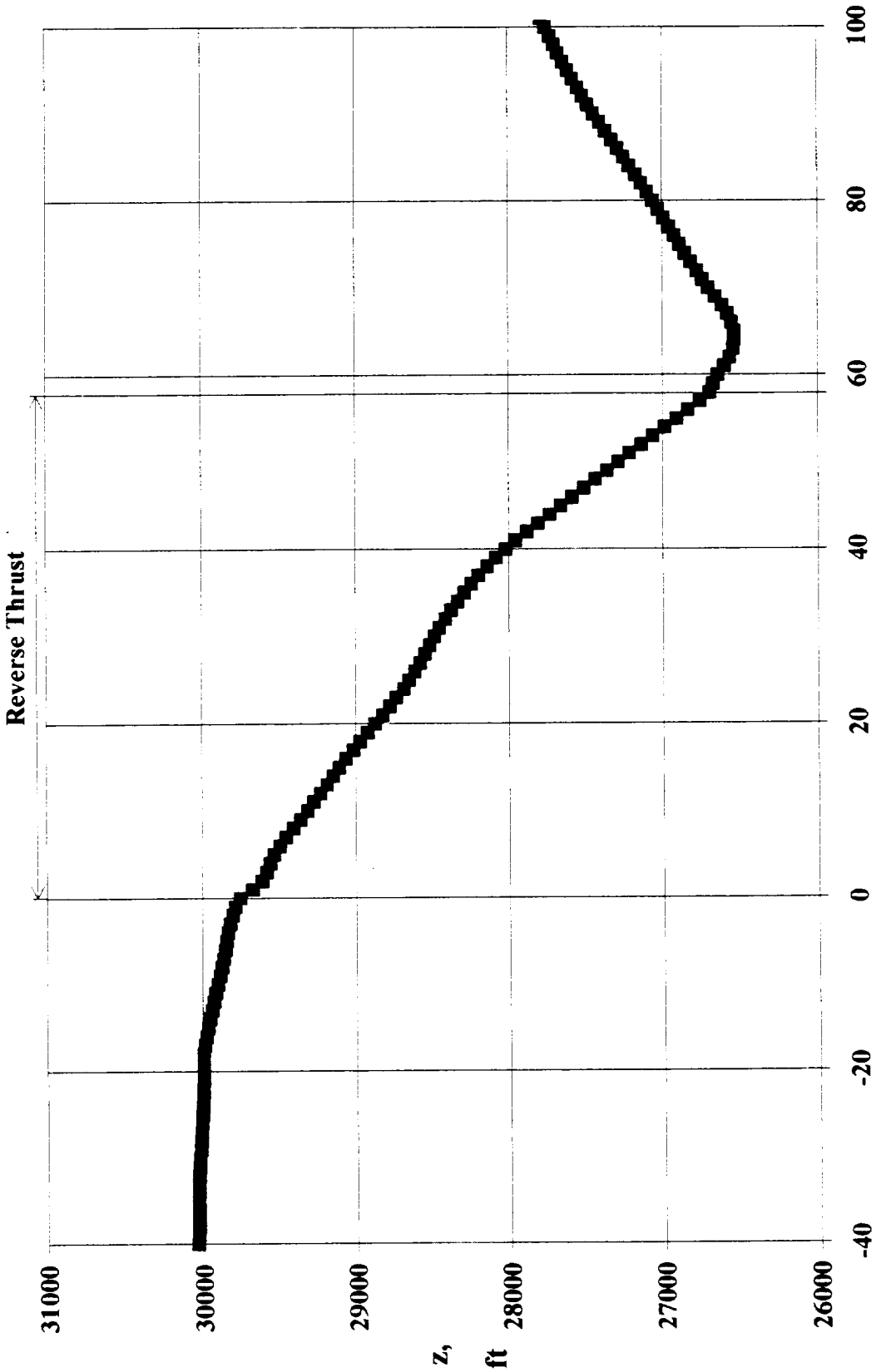

Figure 27. Altitude variations during the three phases of the experiment at the nominal Mach number of 0.70.

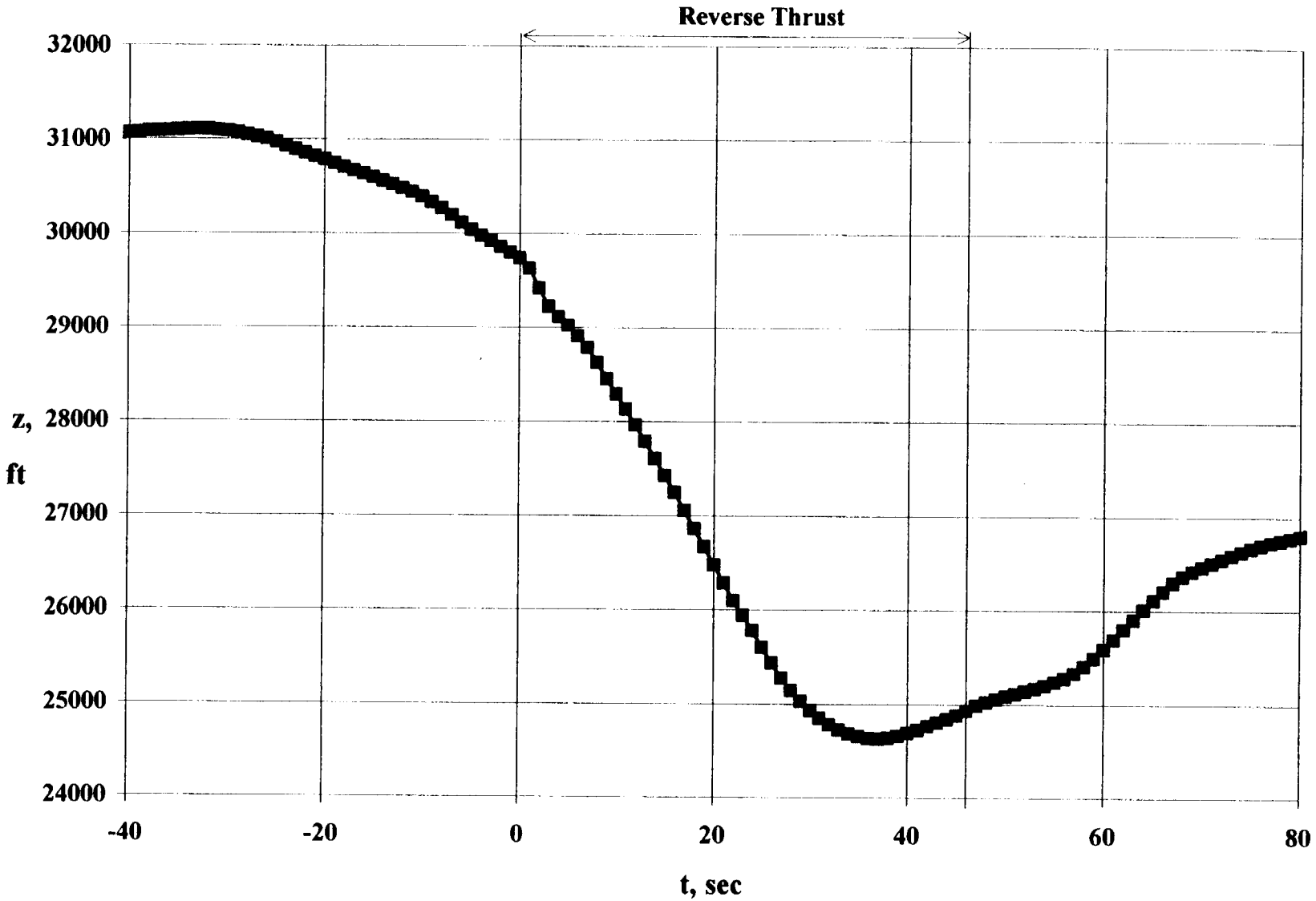

Figure 28. Altitude variations during the three phases of the experiment at the nominal Mach number of 0.85.

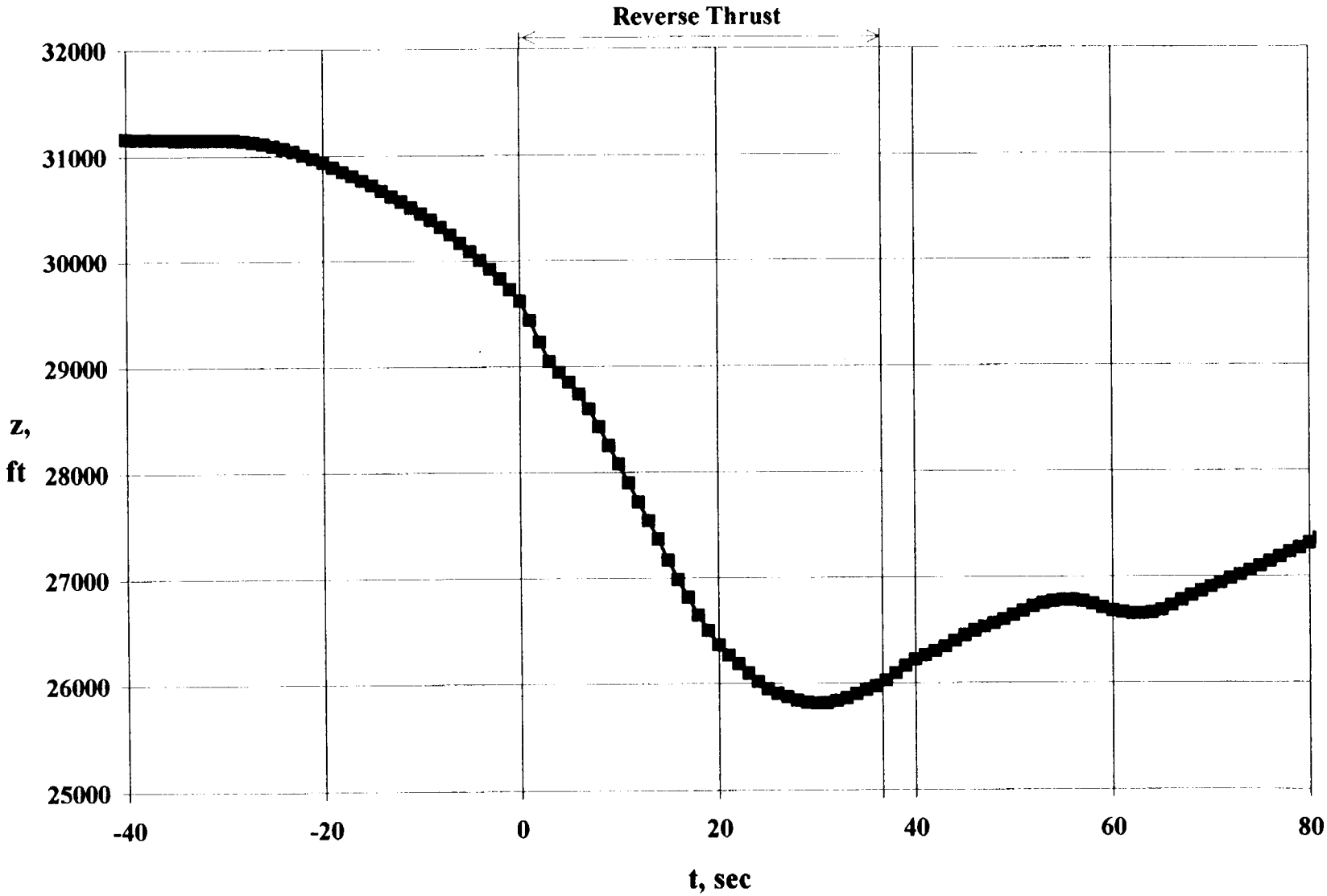

Figure 29. Altitude variations during the three phases of the experiment at the nominal Mach number of 0.85.

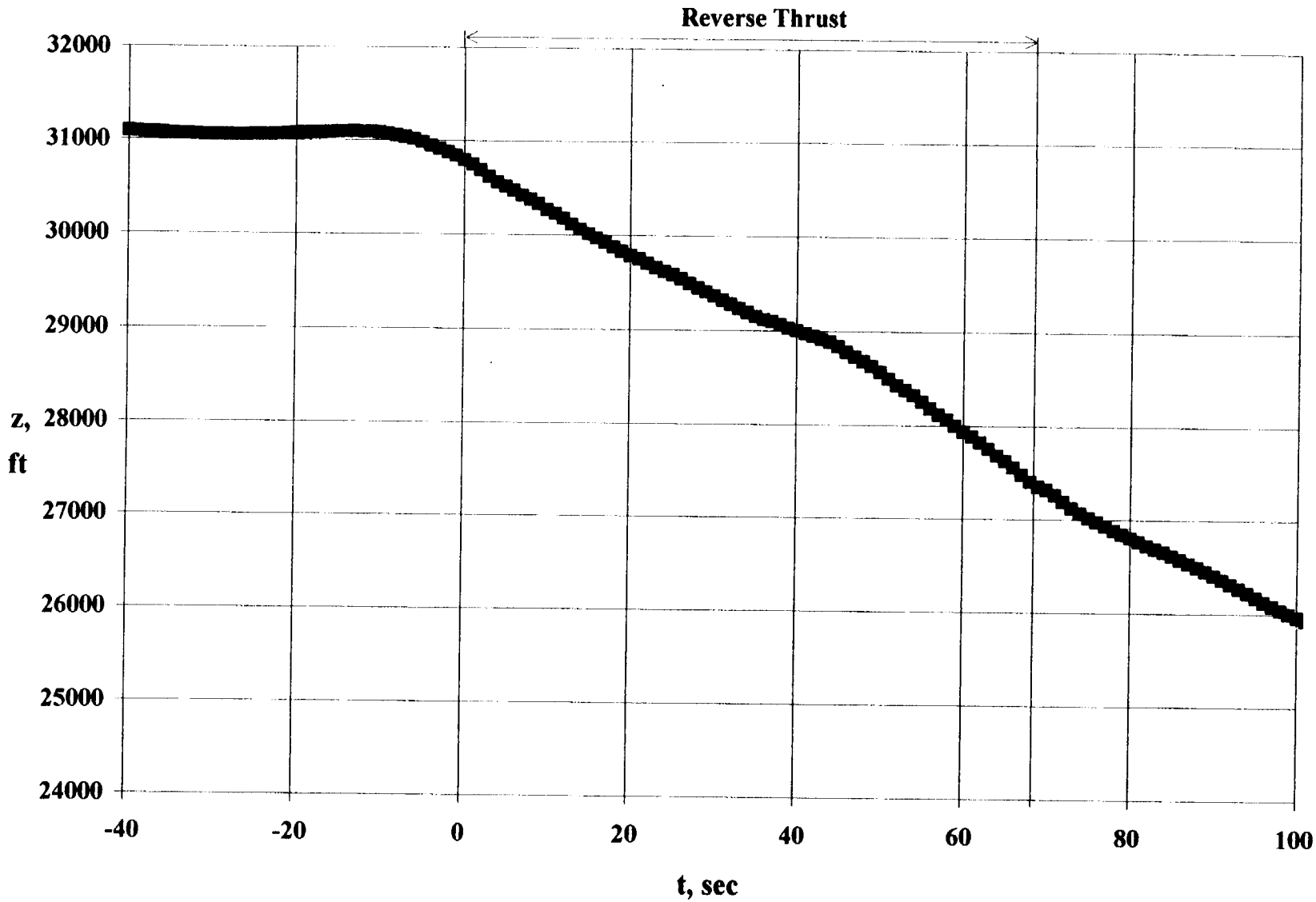

Figure 30. Altitude variations during the three phases of the experiment at the nominal Mach number of 0.55.

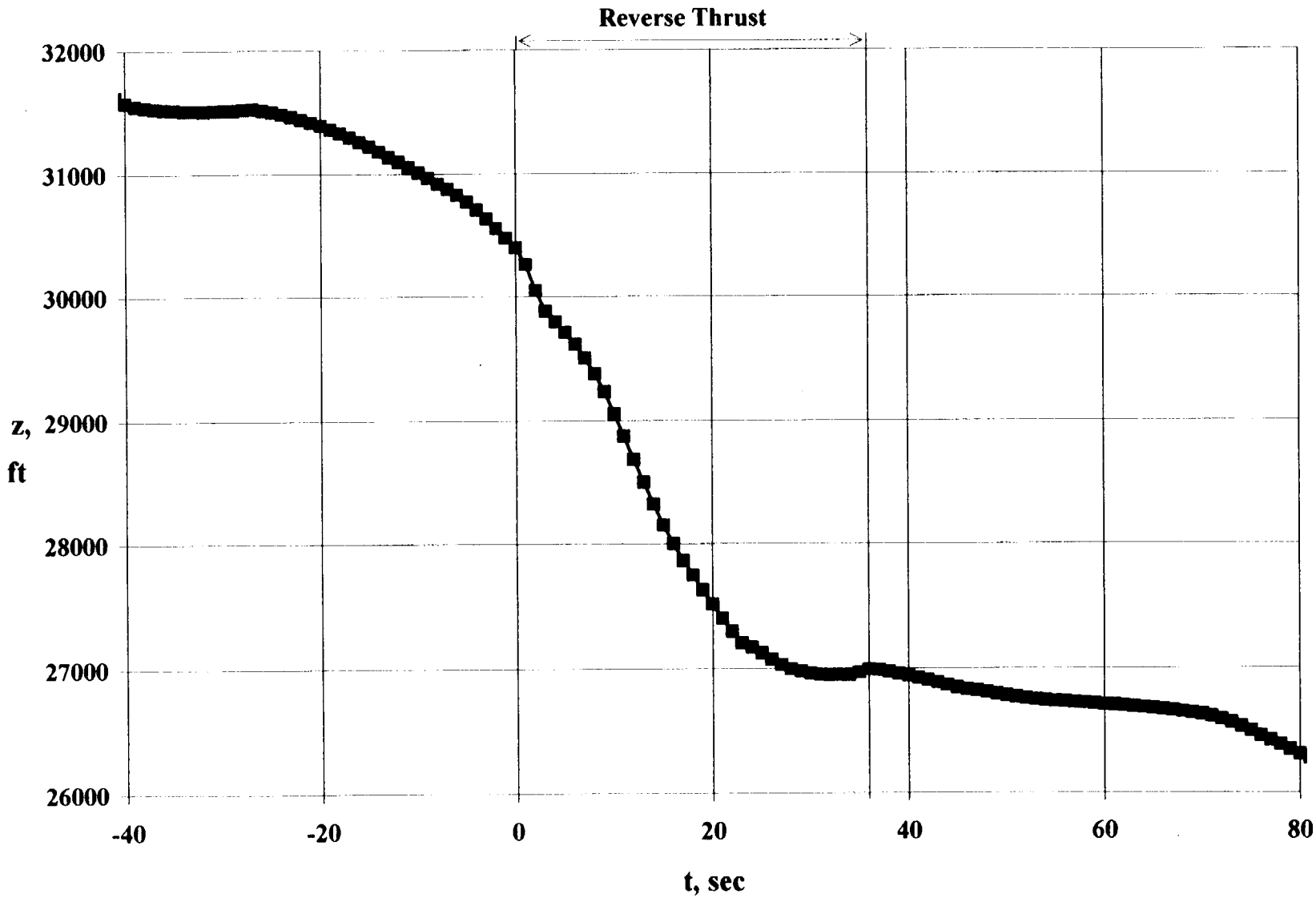

Figure 31. Altitude variations during the three phases of the experiment at the nominal Mach number of 0.85.

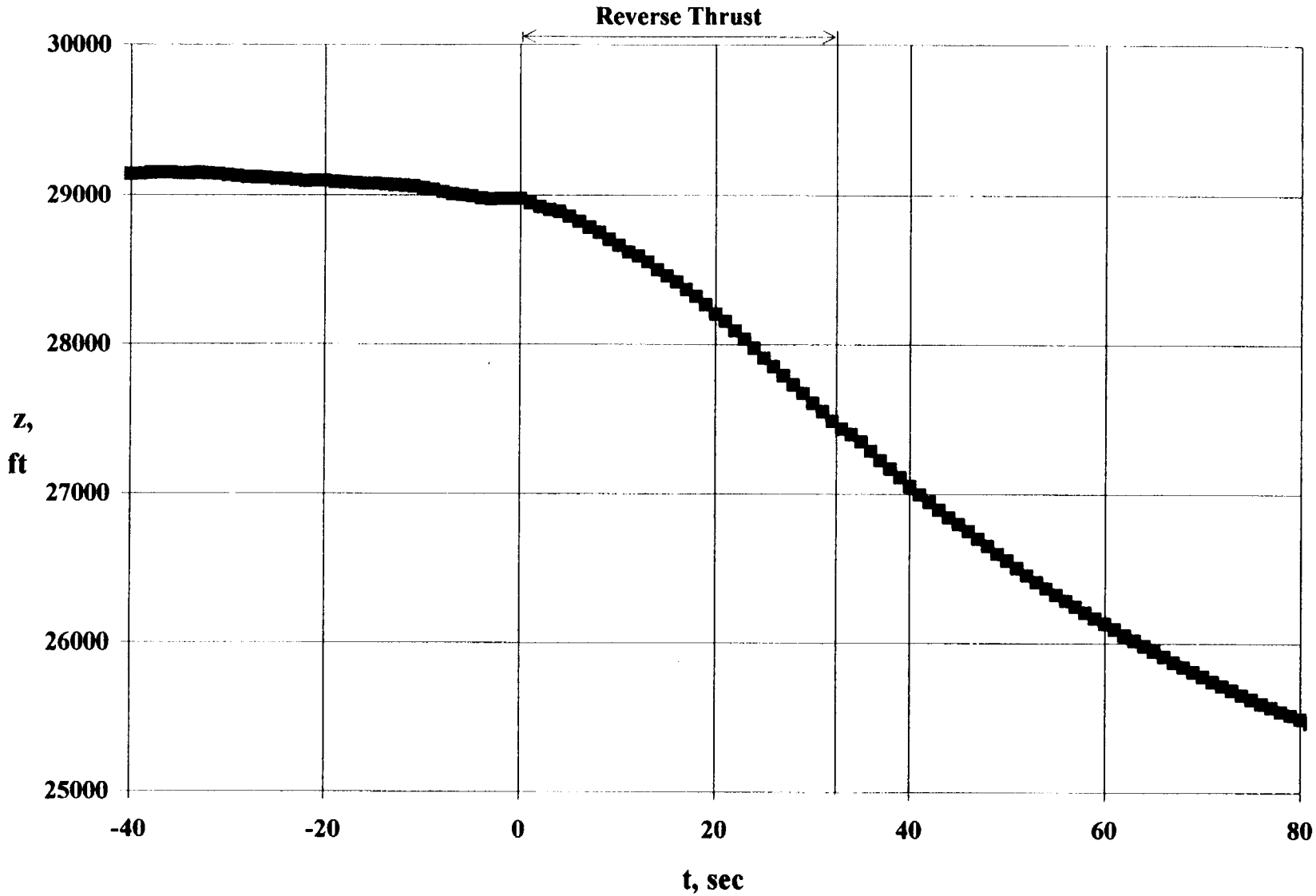

Figure 32. Altitude variations during the three phases of the experiment at the nominal Mach number of 0.55.

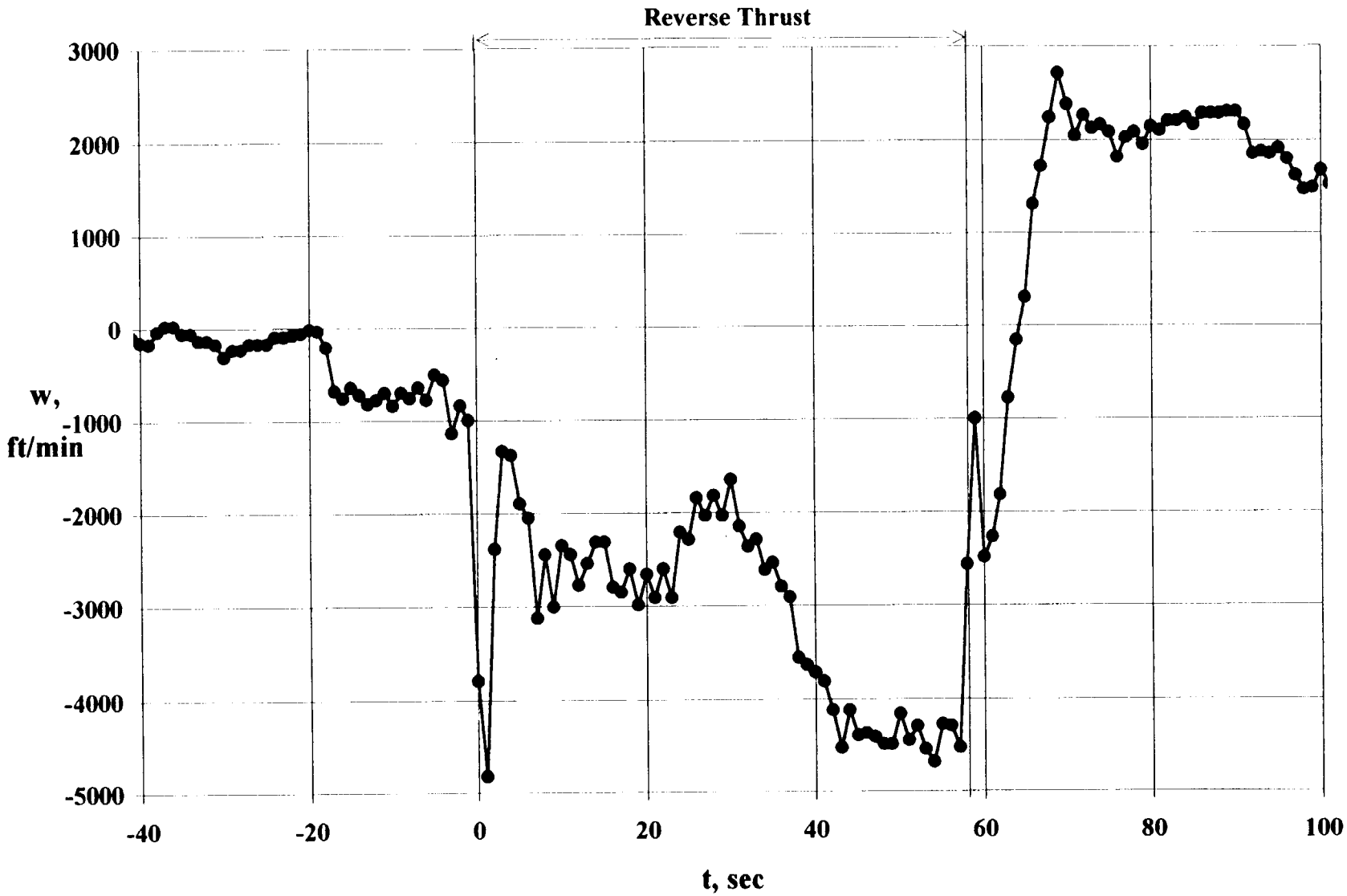

Figure 33. Vertical descent of the aircraft during the three phases of the experiment at the nominal Mach number of 0.70.

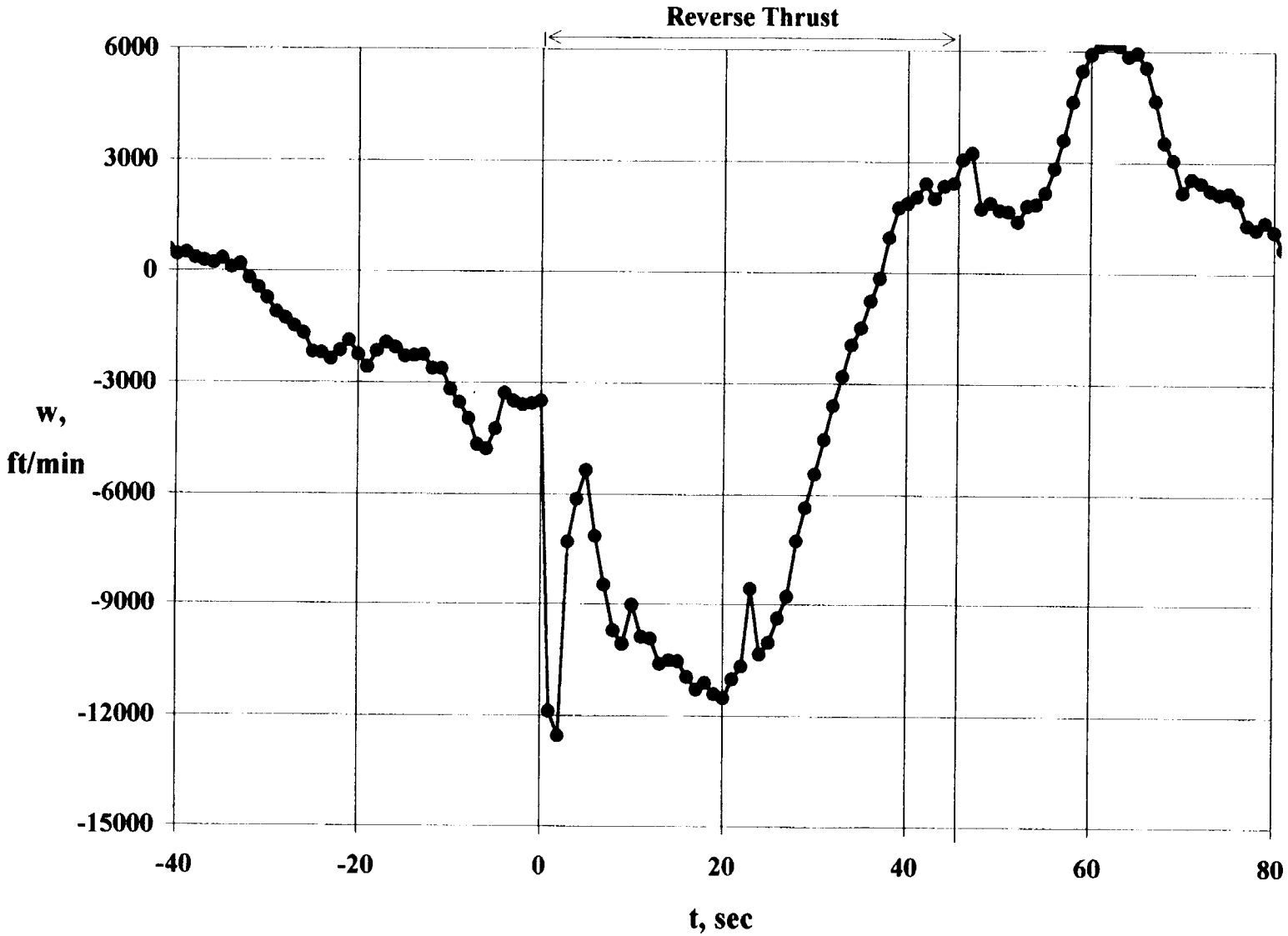

Figure 34. Vertical descent of the aircraft during the three phases of the experiment at the nominal Mach number of 0.85.

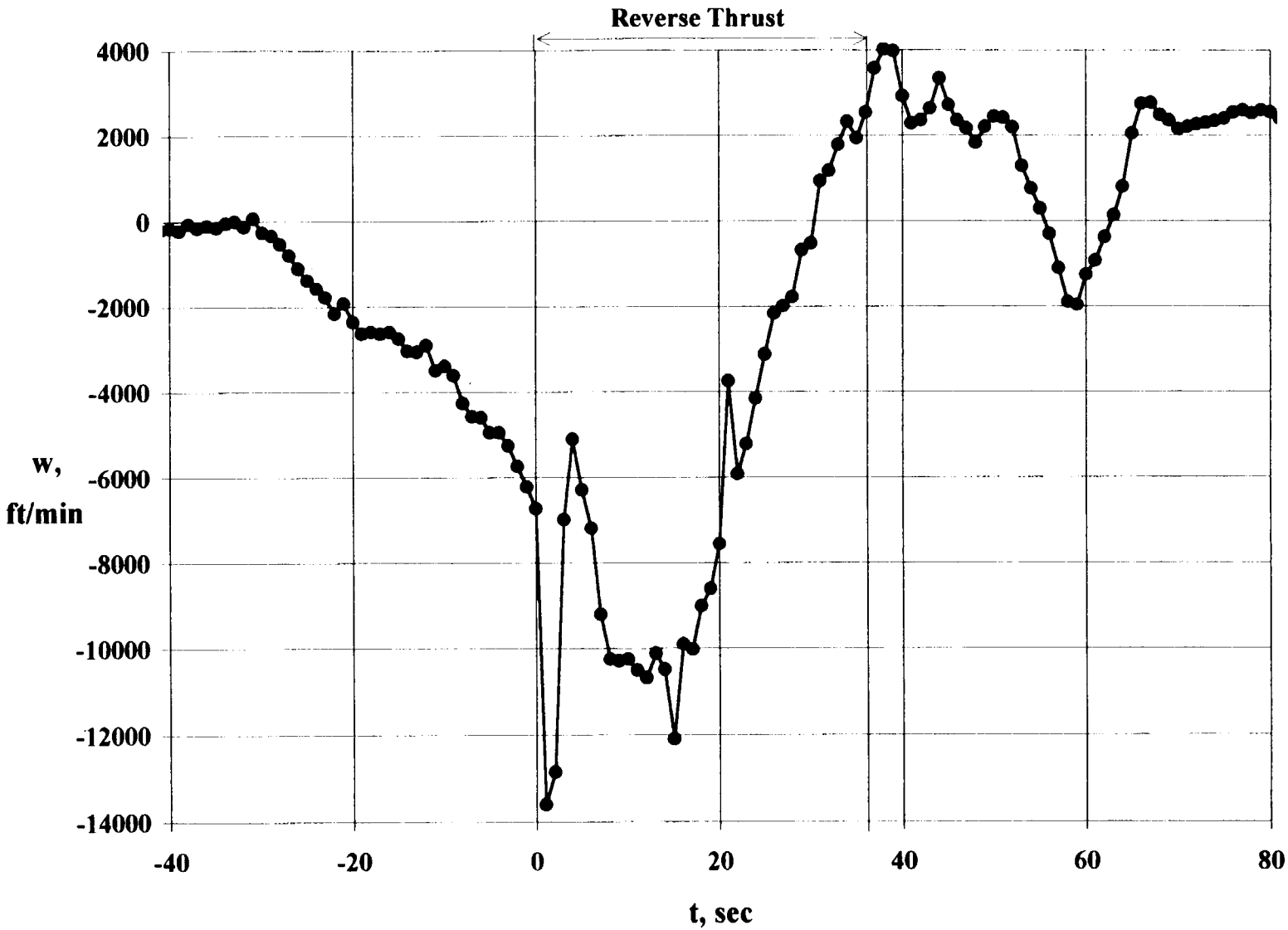

Figure 35. Vertical descent of the aircraft during the three phases of the experiment at the nominal Mach number of 0.85.

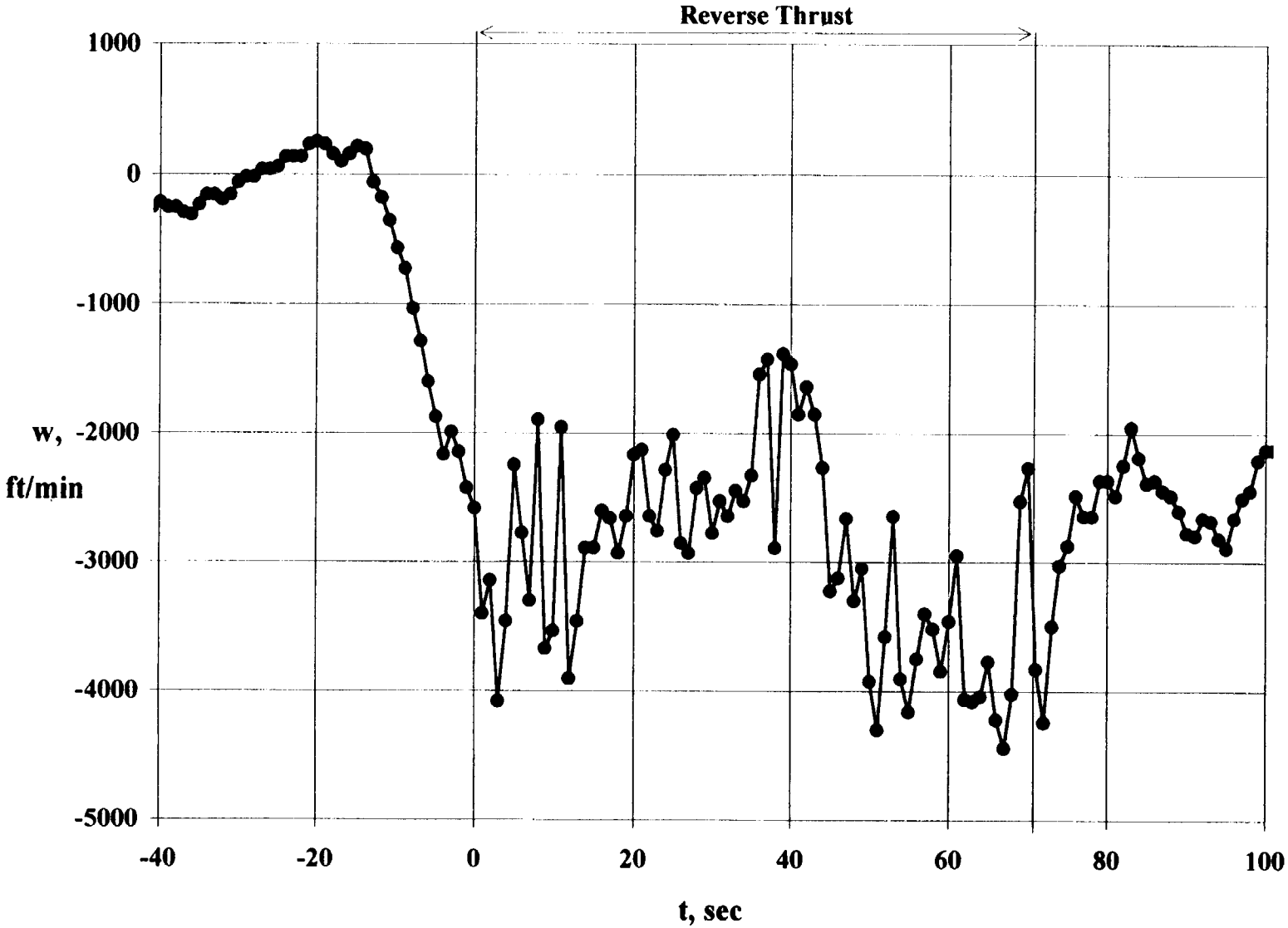

Figure 36. Vertical descent of the aircraft during the three phases of the experiment at the nominal Mach number of 0.55.

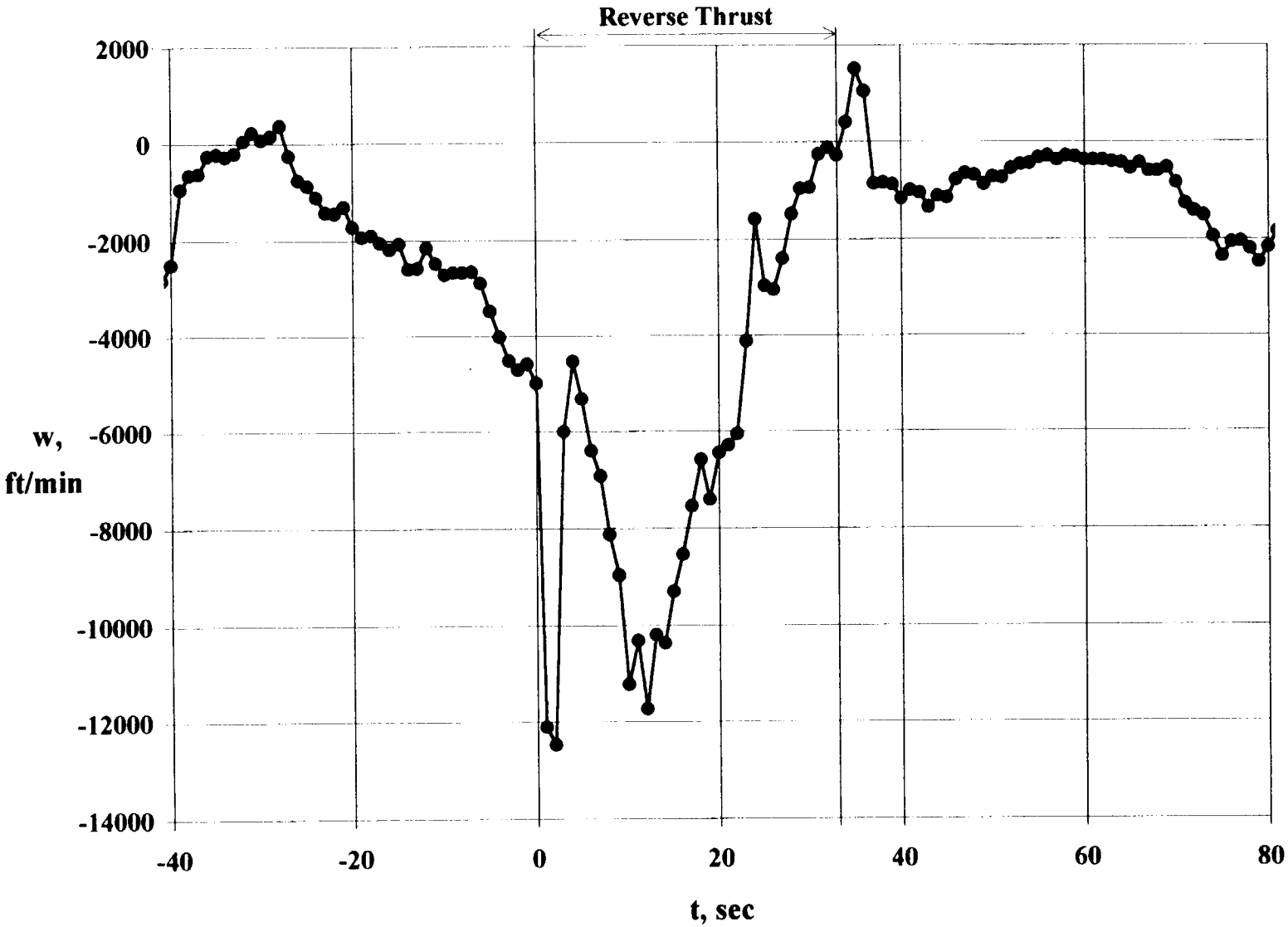

Figure 37. Vertical descent of the aircraft during the three phases of the experiment at the nominal Mach number of 0.85.

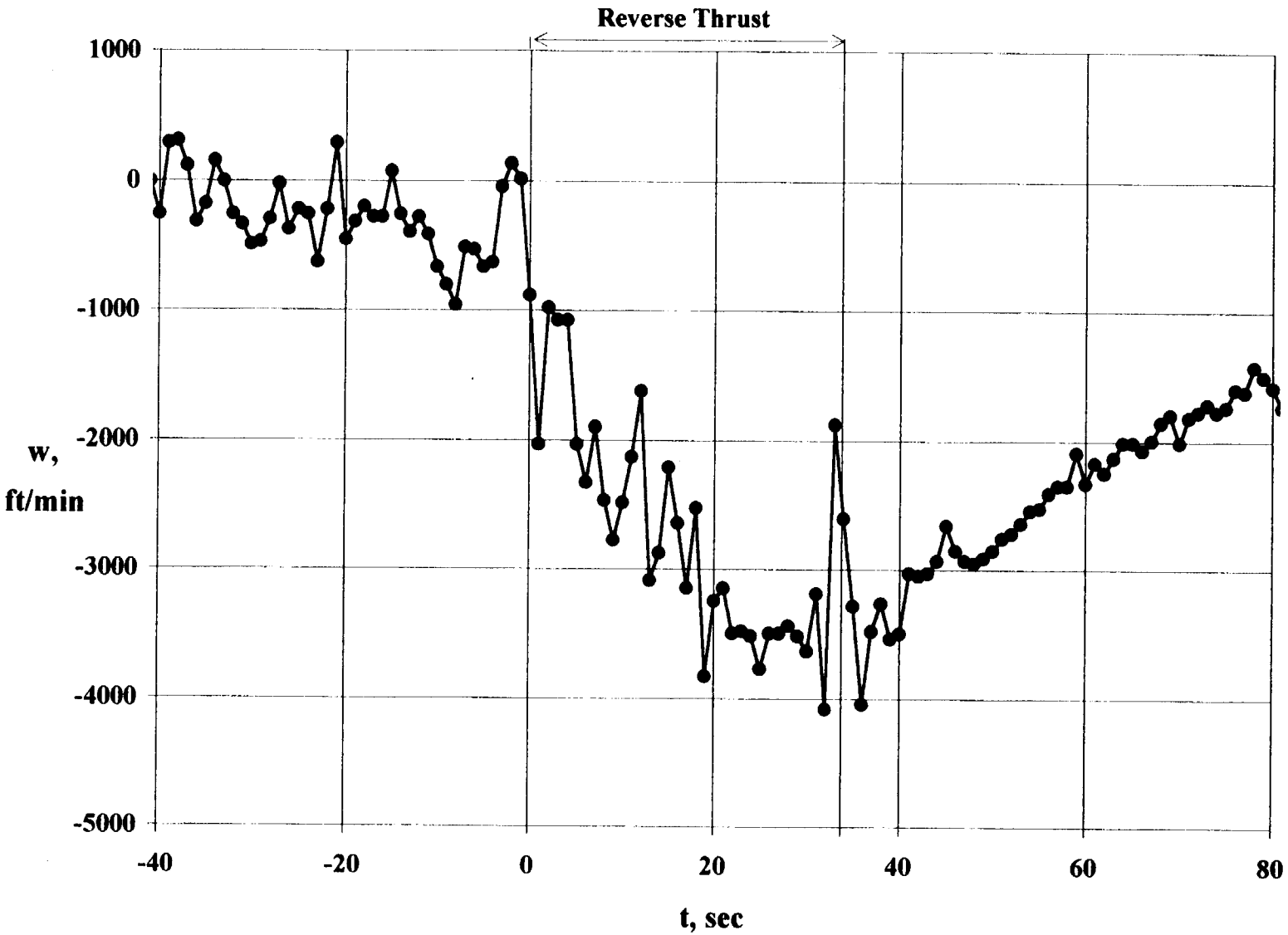

Figure 38. Vertical descent of the aircraft during the three phases of the experiment at the nominal Mach number of 0.55.

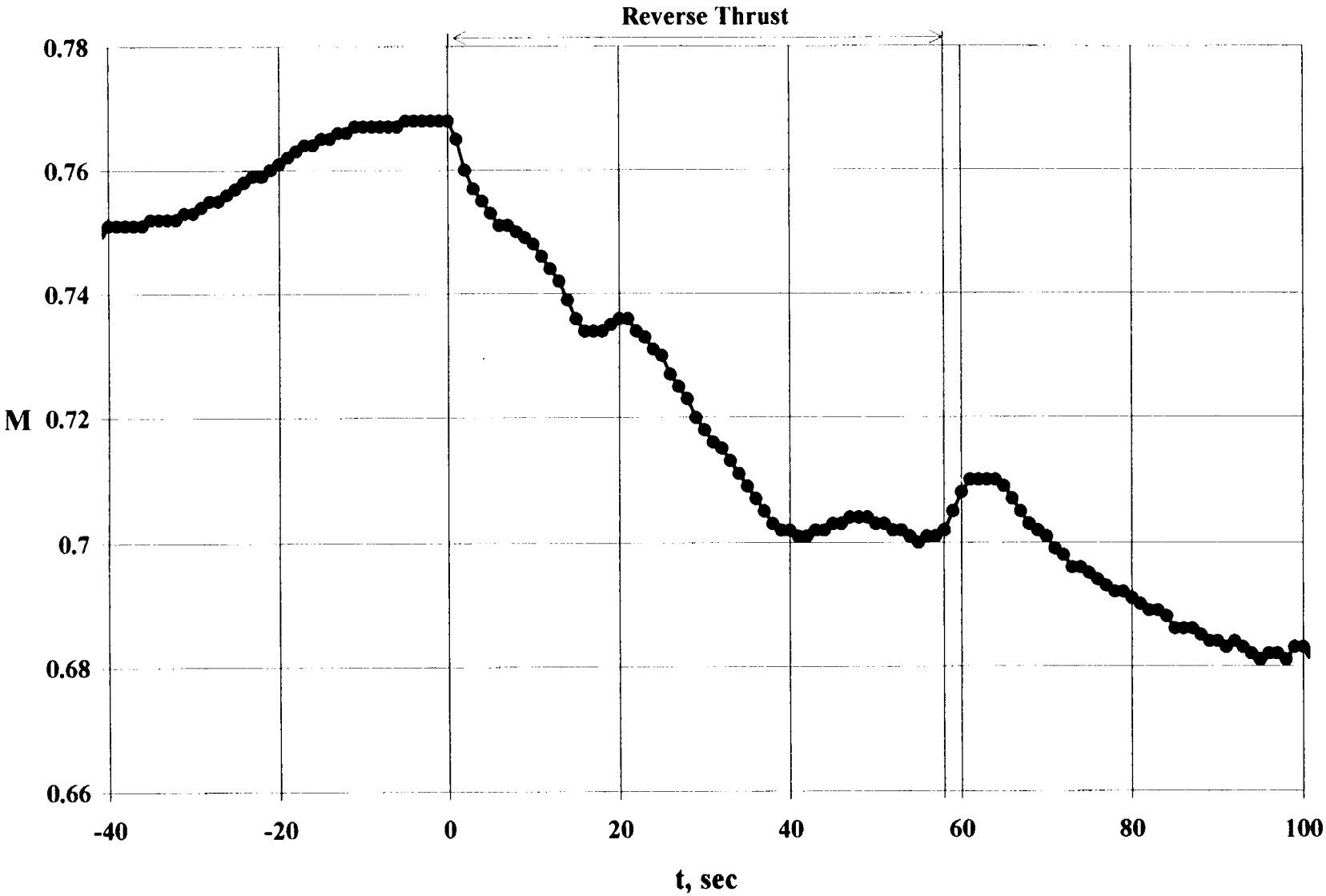

Figure 39. Mach number variations during the three phases of the experiment at the nominal Mach number of 0.70.

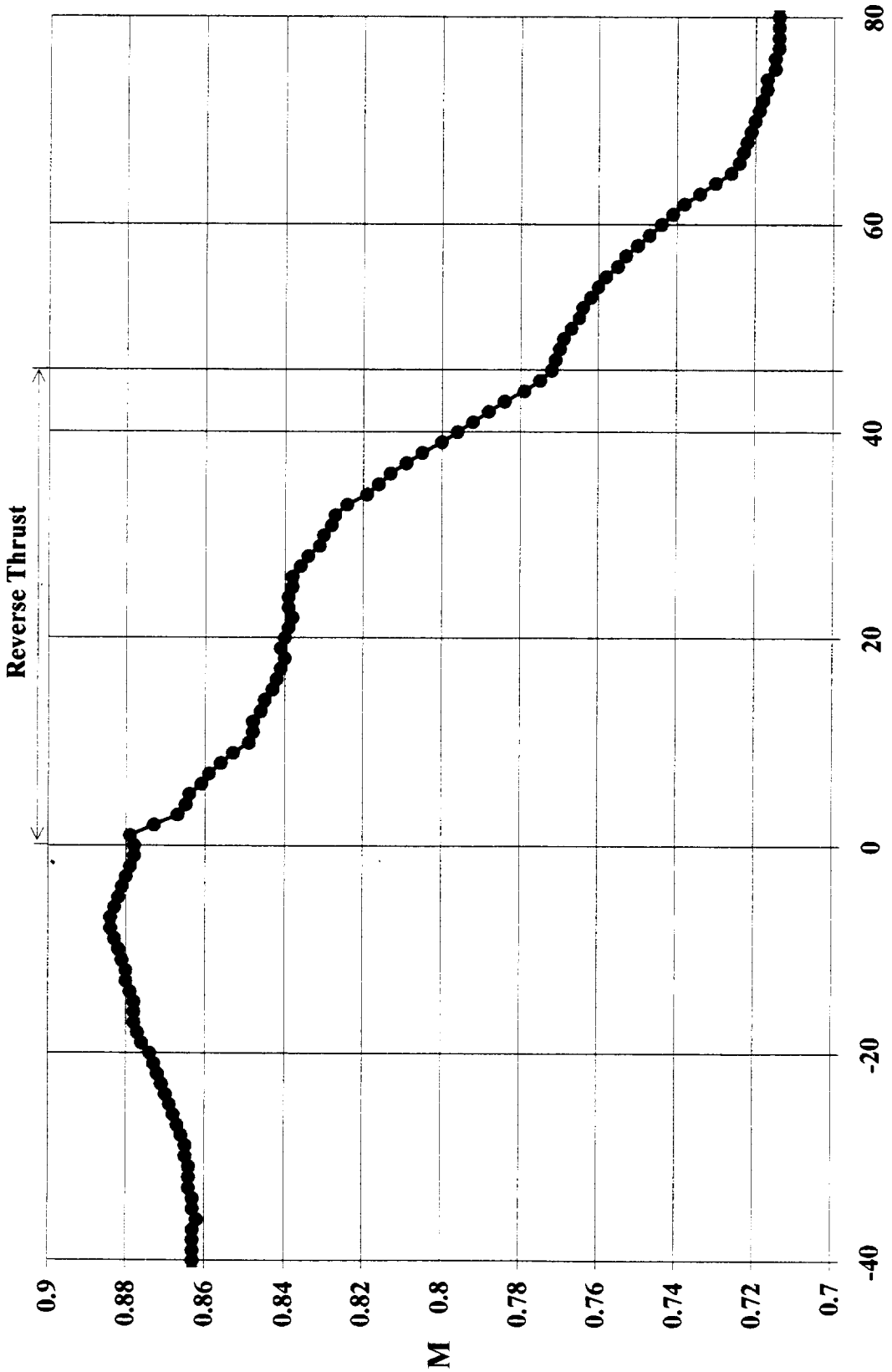

Figure 40. Mach number variations during the three phases of the experiment at the nominal Mach number of 0.85.

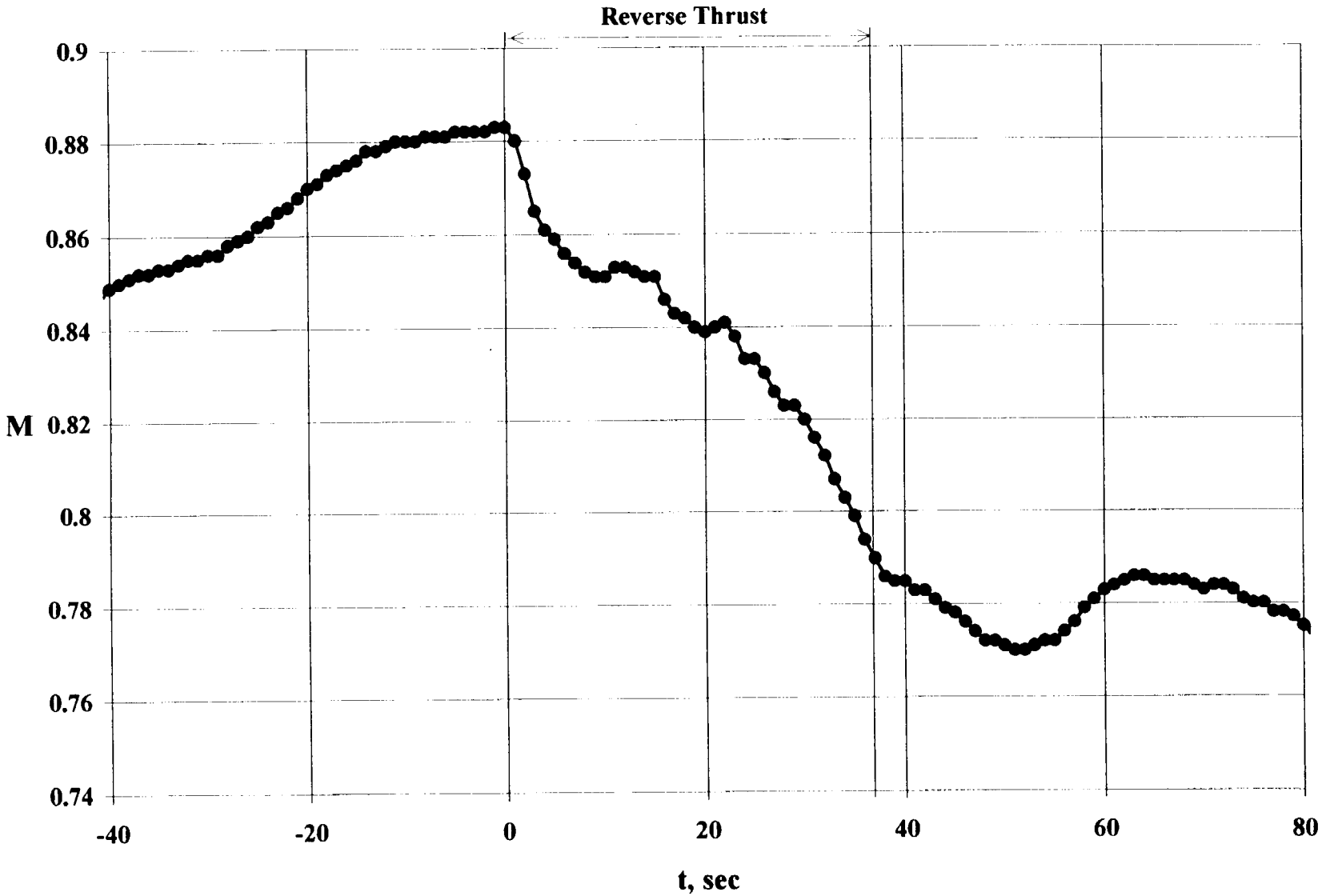

Figure 41. Mach number variations during the three phases of the experiment at the nominal Mach number of 0.85.

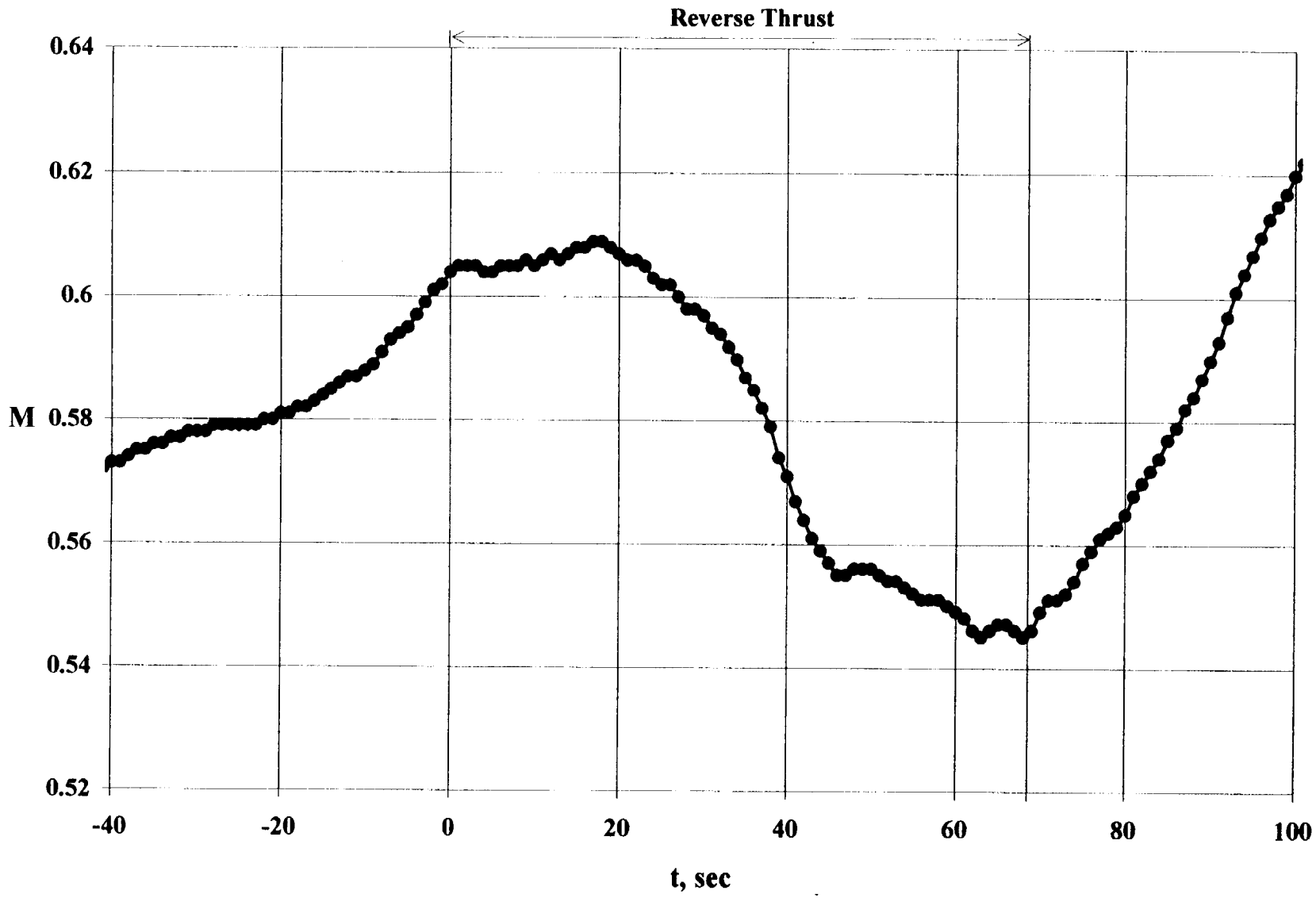

Figure 42. Mach number variations during the three phases of the experiment at the nominal Mach number of 0.55.

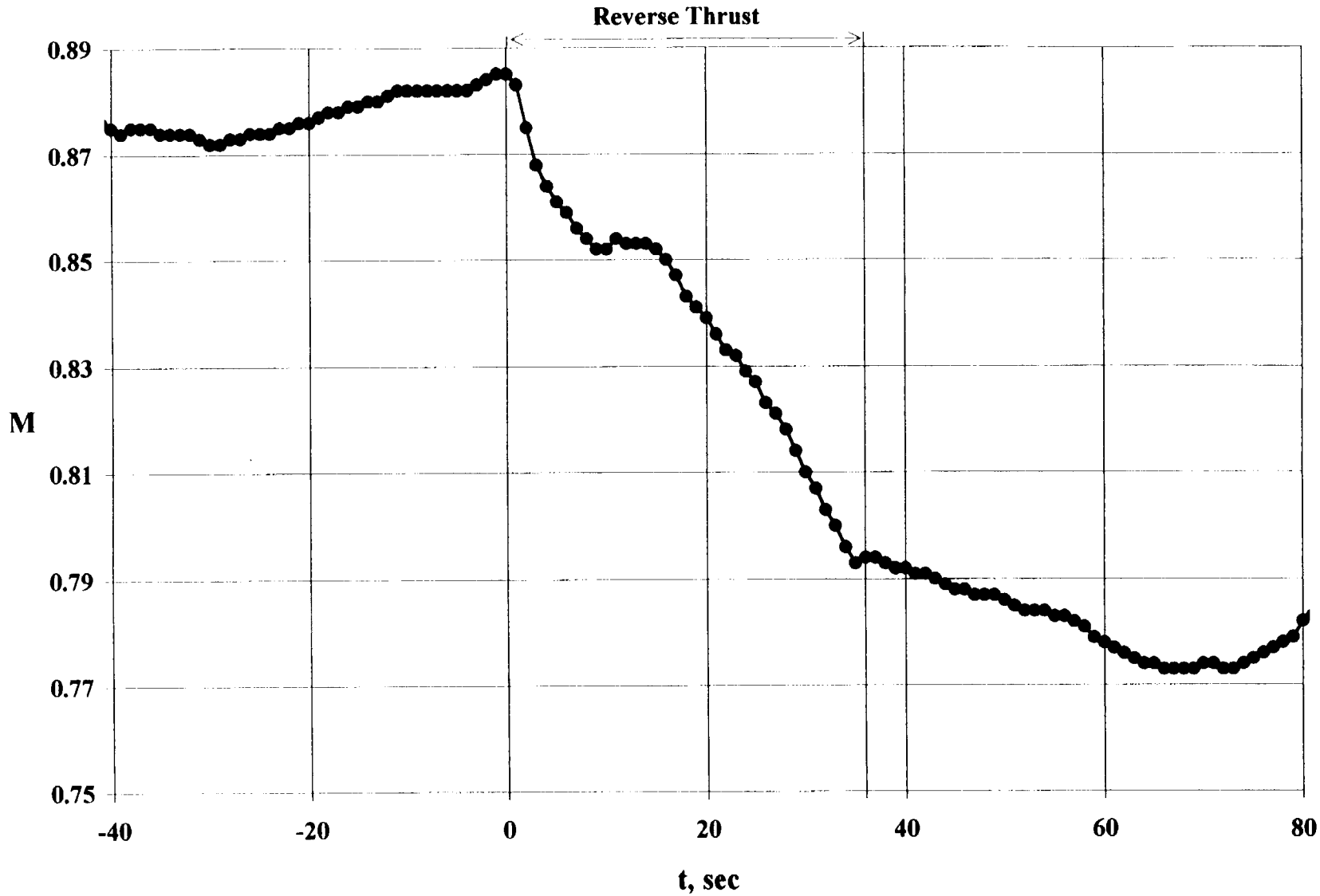

Figure 43. Mach number variations during the three phases of the experiment at the nominal Mach number of 0.85.

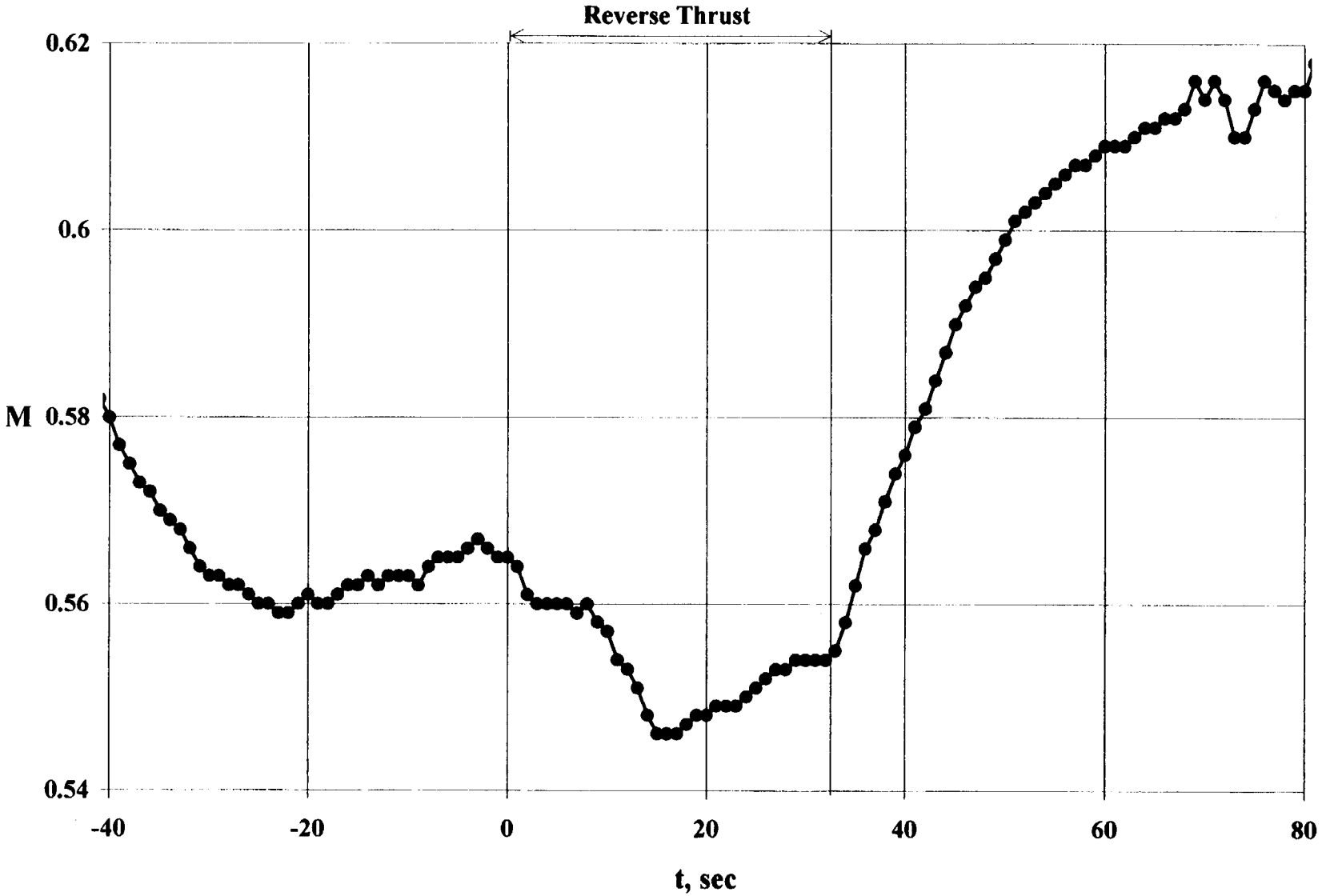

Figure 44. Mach number variations during the three phases of the experiment at the nominal Mach number of 0.55.

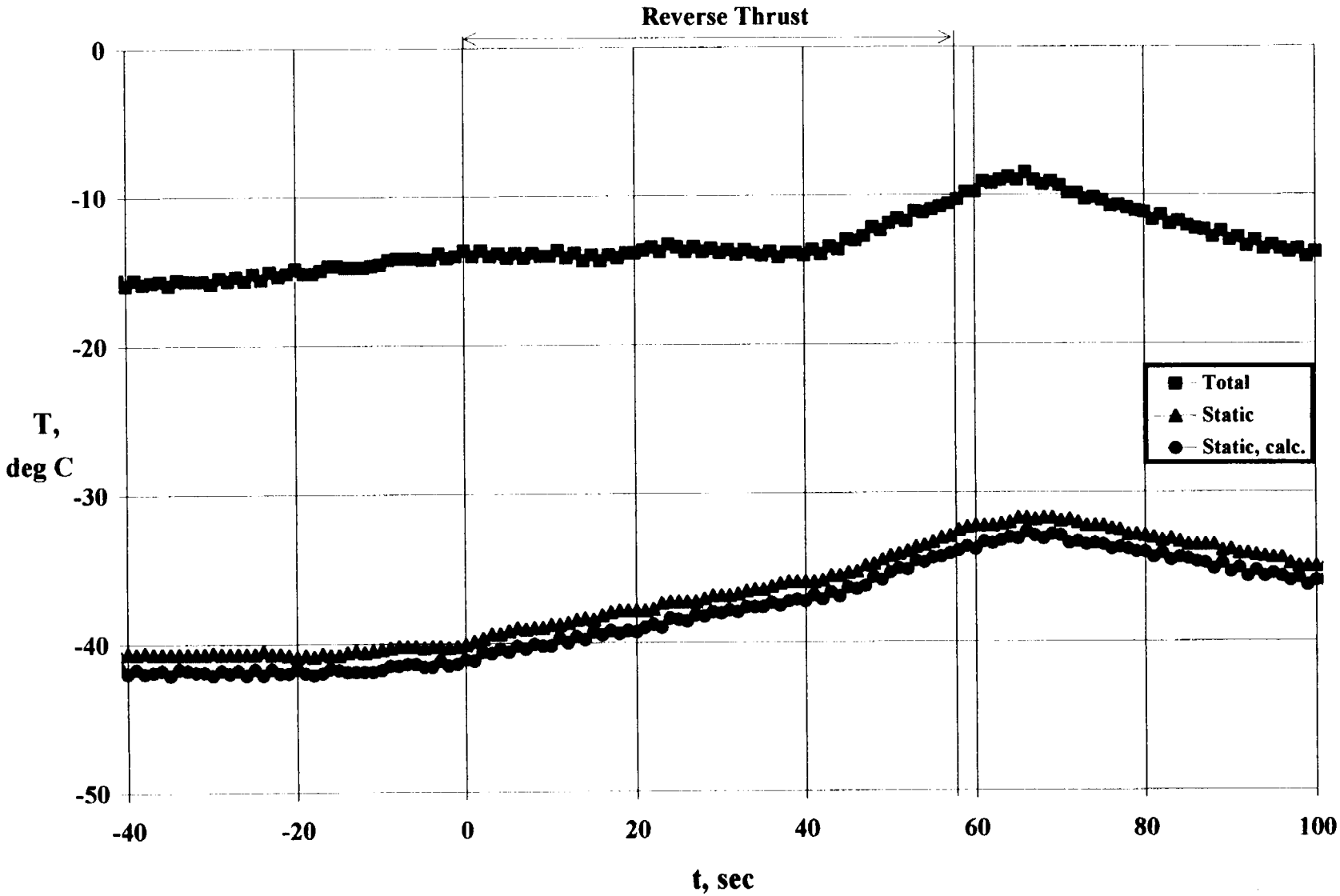

Figure 45. Temperature variations during the three phases of the experiment at the nominal Mach number of 0.70.

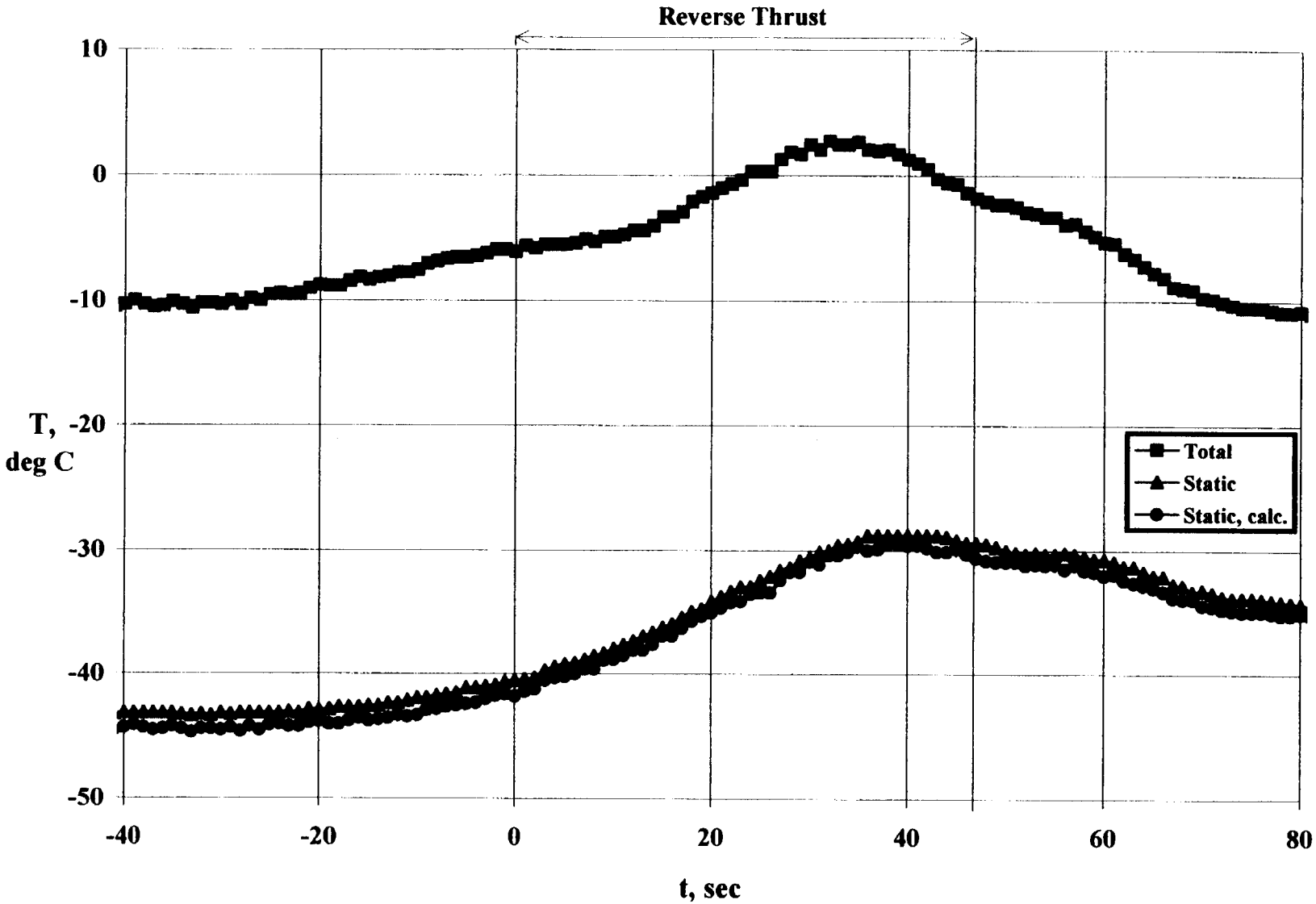

Figure 46. Temperature variations during the three phases of the experiment at the nominal Mach number of 0.85.

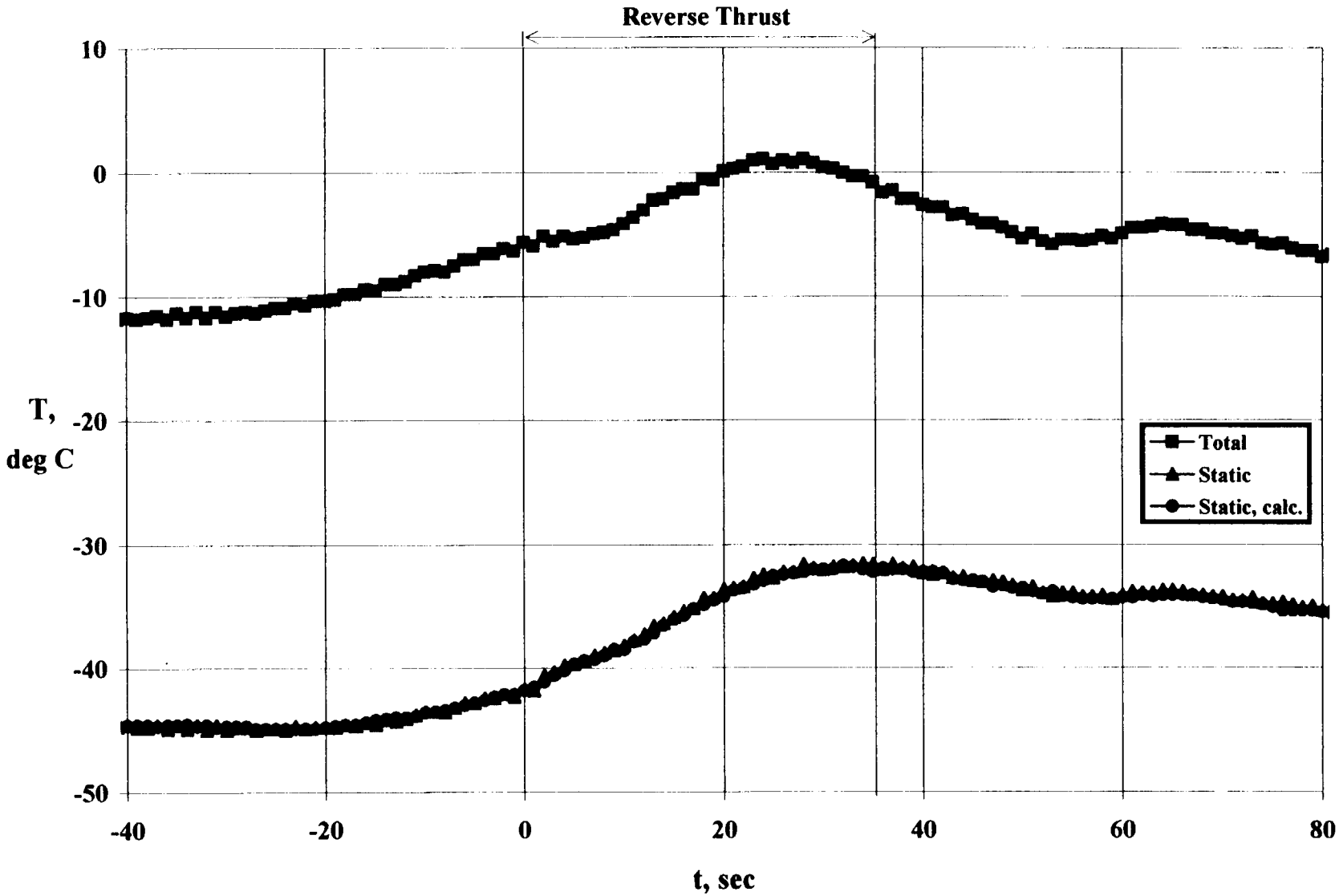

Figure 47. Temperature variations during the three phases of the experiment at the nominal Mach number of 0.85.

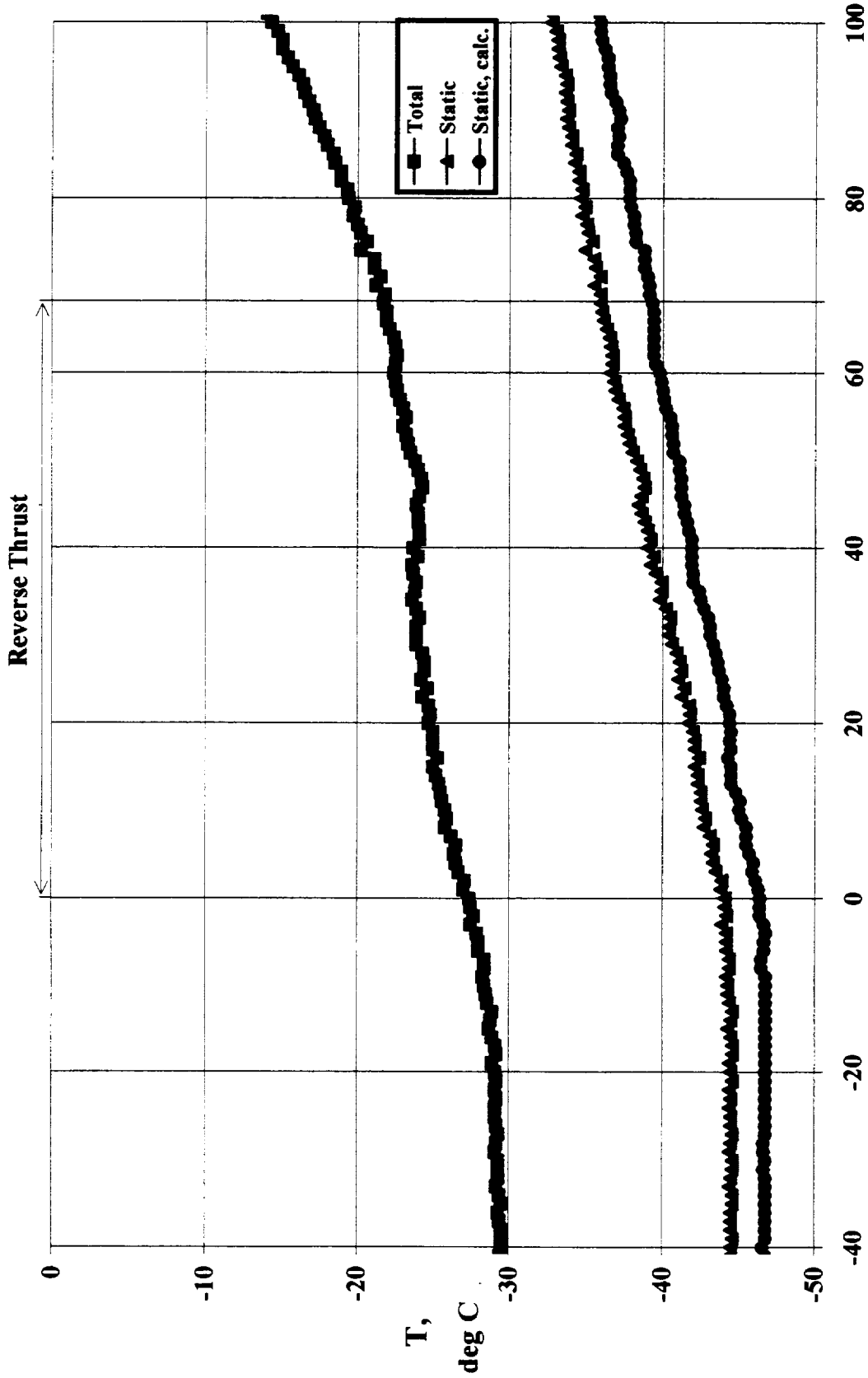

Figure 48. Temperature variations during the three phases of the experiment at the nominal Mach number of 0.55.

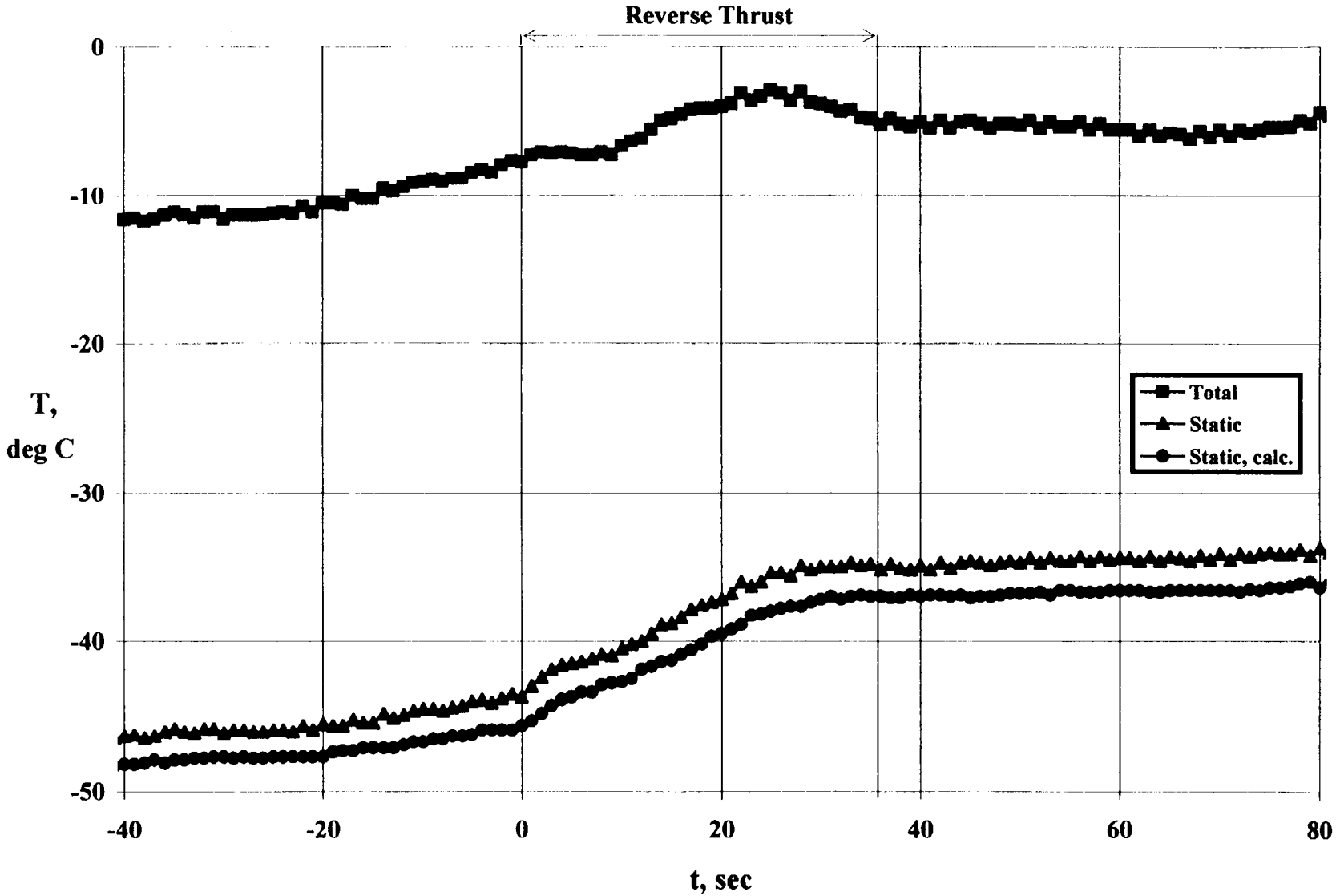

Figure 49. Temperature variations during the three phases of the experiment at the nominal Mach number of 0.85.

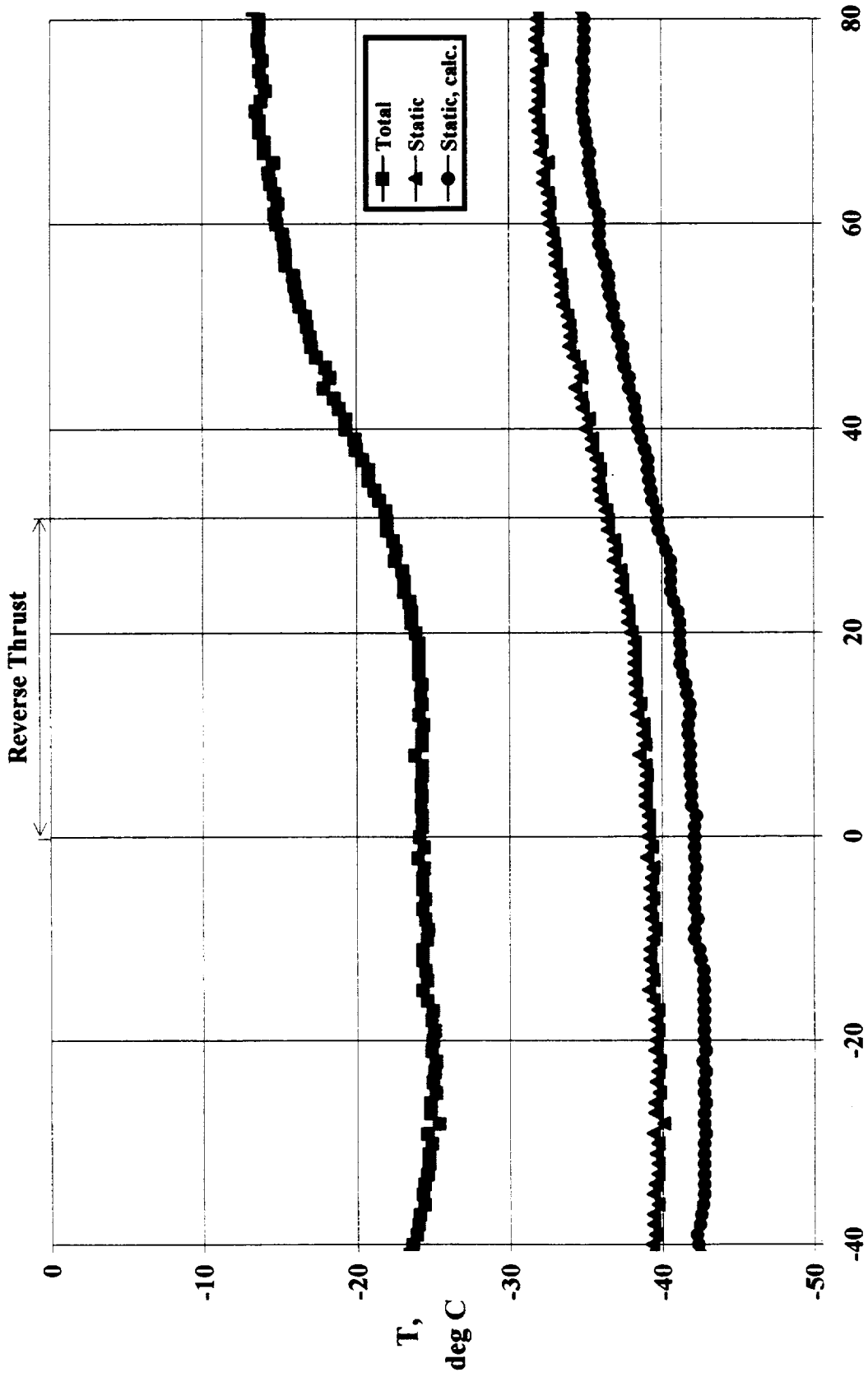

Figure 50. Temperature variations during the three phases of the experiment at the nominal Mach number of 0.55.

REPORT DOCUMENTATION PAGE

Form Approved
OMB No. 0704-0188

1. AGENCY USE ONLY *(Leave blank)*	2. REPORT DATE	3. REPORT TYPE AND DATES COVERED
	June 1995	Technical Memorandum

4. TITLE AND SUBTITLE

Investigation of Wing Upper Surface Flow-Field Disturbance Due to NASA DC-8-72 In-flight Inboard Thrust-Reverser Deployment

5. FUNDING NUMBERS

505-59-53

6. AUTHOR(S)

Hedayat U. Hamid, Richard J. Margason, and Gordon Hardy

7. PERFORMING ORGANIZATION NAME(S) AND ADDRESS(ES)

Ames Research Center
Moffett Field, CA 94035-1000

8. PERFORMING ORGANIZATION REPORT NUMBER

A-950060

9. SPONSORING/MONITORING AGENCY NAME(S) AND ADDRESS(ES)

National Aeronautics and Space Administration
Washington, DC 20546-0001

10. SPONSORING/MONITORING AGENCY REPORT NUMBER

NASA TM-110351

11. SUPPLEMENTARY NOTES

Point of Contact: Hedayat U. Hamid, Ames Research Center, MS 247-2, Moffett Field, CA 94035-1000; (415) 604-5033

12a. DISTRIBUTION/AVAILABILITY STATEMENT

Unclassified-Unlimited
Subject Category – 01

12b. DISTRIBUTION CODE

13. ABSTRACT ***(Maximum 200 words)***

An investigation of the wing upper surface flow-field disturbance due to in-flight inboard thrust reverser deployment on the NASA DC-8-72, which was conducted cooperatively by NASA Ames, the Federal Aviation Administration (FAA), McDonnell Douglas, and the Aerospace Industry Association (AIA), is outlined and discussed in detail. The purpose of this flight test was to obtain tufted flow visualization data which demonstrates the effect of thrust reverser deployment on the wing upper surface flow field to determine if the disturbed flow regions could be modeled by computational methods. A total of six symmetric thrust reversals of the two inboard engines were performed to monitor tuft and flow cone patterns as well as the character of their movement at the nominal Mach numbers of 0.55, 0.70, and 0.85. The tufts and flow cones were photographed and video-taped to determine the type of flow field that occurs with and without the thrust reversers deployed. In addition, the normal NASA DC-8 onboard Data Acquisition Distribution System (DADS) was used to synchronize the cameras.

Results of this flight test will be presented in two parts. First, three distinct flow patterns associated with the above Mach numbers were sketched from the motion videos and discussed in detail. Second, other relevant aircraft parameters, such as aircraft's angular orientation, altitude, Mach number, and vertical descent, are discussed. The flight test participants' comments were recorded on the videos and the interested reader is referred to the video supplement section of this report for that information.

14. SUBJECT TERMS

DC-8, Thrust reverser, Thrust induced flow

15. NUMBER OF PAGES

63

16. PRICE CODE

A04

17. SECURITY CLASSIFICATION OF REPORT	18. SECURITY CLASSIFICATION OF THIS PAGE	19. SECURITY CLASSIFICATION OF ABSTRACT	20. LIMITATION OF ABSTRACT
Unclassified	Unclassified		